UCSF
UC San Francisco Electronic Theses and Dissertations

Title
The role of neuroligins in synapse formation, maintenance, and plasticity

Permalink
https://escholarship.org/uc/item/9r49x66z

Author
Shipman, Seth

Publication Date
2012

Peer reviewed|Thesis/dissertation

eScholarship.org Powered by the California Digital Library
University of California

The Role of Neuroligins in Synapse Formation, Maintenance, and Plasticity

by

Seth Lawler Shipman

DISSERTATION

Submitted in partial satisfaction of the requirements for the degree of

DOCTOR OF PHILOSOPHY

in

Neuroscience

in the

For Emily

Acknowledgments

It is impossible to overstate the amount of gratitude I owe my mentor, Roger Nicoll, for his support and guidance over the last five years. Our conversations will forever shape my approach to science. Roger's advice has been sagely, his insights poignant, and his support unwavering. My time in his lab has been defining in a way that few things are. In those years, Roger bestowed on me timeless gifts: a firm grounding in basic science, the trade of electrophysiology, and a deep appreciation for rigor and integrity. At the same time, he fostered an amazing scientific environment – the voraciousness with which he devoured data was the best motivator I could ask for.

The members of my thesis committee – Robert Edwards, Anatol Kreitzer, and Peter Sargent – have provided invaluable advice on the work that forms this thesis, as has Grae Davis, who served on my major committee and has continued to offer counsel. I was first introduced to molecular biology in Rob's lab as a rotation student, for which I am incredibly grateful. His insights into my projects over the years have been pointed and accurate, and his bright disposition always leaves me feeling like success is possible. Anatol has been a wonderful source of new ideas, always offering a fresh perspective. Peter taught me the basics of electrophysiology when I was a first-year; discussing the finer technical points of it with him over the years has been a highlight of my graduate career. Grae's ideas have always been unexpected and pushed me to consider questions from different angles.

One of the intangibles of a lab is the people in it. The dynamic can be hard to predict because it is based on personalities and the group is always changing. Without a doubt, my fellow lab mates were one of the major reasons that my time in graduate school has been outstanding. I joined one lab, which became another. Early on, Aaron Milstein, Tasso Tzingounis, Karen Menuz, and Geoff Kirchner helped me get started and were each fantastic. Conversations with Aaron, in particular, really informed my thinking

and formulation of questions targeted at the synapse. Very soon after I joined the lab there was a flux, with people leaving and many new ones joining. It is this second group that I will think of as the Nicoll lab when I look back on it.

Adam Granger and Jon Levy joined the lab with me and I cannot imagine it without them. They pushed me to be better and were there for me when things were tough. Granger has been a great friend since the very beginning of graduate school. Having him right there in step with me at every phase of this adventure has been one of my favorite parts. Levy, on the other hand, I really did not know well when we both joined the lab and began sharing an eight-by-fifteen-foot windowless room – a room in which we would both spend nearly half our waking hours for the next four years. It could have gone terribly. Instead, it has been one of the best things to happen to me. Levy is the recipient of all my pure, unfiltered thoughts. Nearly everything I have put out in the world in the last four years has been bounced off him first. He is the first person I turn to when I need to troubleshoot a problem and is a constant source of new ideas.

All the graduate students in the Nicoll lab have made me look forward to coming in every day. I am grateful for their support, creativity, and friendship. Carleton Goold has been and continues to be a great source of inspiration. His unconventional style and attitude taught me there is no one way to be a scientist. Kate Lovero's enthusiasm is infectious. Her passion for science always reminds me of what I love about doing this. Knowing that Quynh-Anh Nguyen will carry the lab forward to the next generation makes me proud.

The Nicoll lab is not just made of graduate students, of course, and the post-docs are a huge part of what makes the environment so invigorating and collaborative. Alex Jackson, Wei Lu, and Yun Shi (Stone) have been there from the beginning and I hope to take what I learned of their work ethic and inquisitiveness with me into my own post-doc. John Gray has also been a friend and mentor and a great source of both medical and

career advice. Over the years, I have shared many good times with Bruce Herring – over slice cultures and Highland Scotch alike. The moment he joined the lab it seemed like he had been a part of the team forever. Newcomers Nengyin Sheng and Maya Yamazaki are valuable new assets for the lab and I am sorry I will not get to spend more time collaborating with them.

I never could have accomplished all the work presented in this thesis without the exceedingly capable technical assistance of Kirsten Bjorgan and Manuel Cerpas. Kirsten made every slice culture and dissociated culture that I used, which was no small number, and Manuel largely handled the *in utero* electroporations. These techniques do not often garner much glory, but they are fundamental to almost every result that comes out of the Nicoll lab. I owe both Kirsten and Manuel a huge debt of gratitude.

Over the years I have also had a number of great collaborators. Eric Schnell, a Nicoll lab alumni himself, really made an impact on me. He set me down the path of neuroligin and gave me the advice to study big effects, both of which have paid off tremendously and I am quite thankful to him. His mentorship through our correspondence was and continues to be incredibly edifying. Bo-Shiun Chen and Taka Hirai – both in Katherine Roche's lab – did all the biochemistry on neuroligin. Conversations with Katherine over the years have provided a valuable biochemical counterpoint to Roger's physiological slant. Dan Johnston was nice enough to allow me to visit his lab early on where Darrin Brager and Rishi Narayanan took the time to show me how they patched dendrites.

I am grateful to Lou Reichardt, Pat Veitch, and Lucita Nacionales for running the Neuroscience program at UCSF and to my first-year class, especially Brad Colquitt, Sarah Fischbach, Carolyn Johnson, Gabe McKinsey, Dana Robertson, and Meg Younger for making the first and subsequent years stimulating both scientifically and socially. I also have a wonderful extended support network in San Francisco, which has

made these years some of the best in my life. I would like to thank in particular Emma Sherwood-Forbes, Jon Stynes, Gabe Prager, and Ashley Hodge, as well as Sam Myers for the levity he brought to Genentech Hall and for his indispensable artistic abilities.

I owe a huge debt to my family for their support. My Dad taught me to ask questions and the value of looking for answers at the source. My sister introduced me to the music that played during countless days of recording, and has always supported me in more ways than she knows. My Mom, the consummate guidance counselor, first suggested that I had the skills and interest to go into neuroscience when I was 17 and has supported me in that endeavor ever since. Her belief in me is what made me the scientist I am today.

Finally, Emily, who has been there for all my success and all my frustration throughout this entire experience deserves and is the recipient of my unending devotion. I could never have done it without her. She provides the perfect counterpoint to my life in science and keeps me from losing perspective. She has additionally contributed directly to this thesis by copyediting basically everything I have ever written.

Contributions

The work in Chaper 4 was done in collaboration with other authors. The information in Chapter 2 includes a description of the methods used by other authors as well those used by Seth. All other work was conceived of and carried out by Seth. Chapters 3-5 have been previously published or accepted for publication.

The work presented in Chapter 3 has been accepted for publication in Proceedings of the National Academy of Sciences.

Takaaki Hirai and Bo-Shiun Chen, from the laboratory of Katherine Roche, contributed the biochemistry that appears in Chapter 4. In that same chapter, Takaaki Hirai additionally contributed the imaging in dissociated neurons. Eric Schnell contributed preliminary data that influenced the direction of this project. This work was published in Nature Neuroscience and is reproduced with permission:

> Shipman SL, Schnell E, Hirai T, Chen BS, Roche KW, Nicoll RA. Functional dependence of neuroligin on a new non-PDZ intracellular domain. Nature Neuroscience. 14(6): 718-726. (2011)

The work presented in Chapter 5 was published in Neuron is reproduced with permission (Copyright 2012, Elsevier):

> Shipman SL, Nicoll RA. A subtype-specific function for the extracellular domain of neuroligin 1 in hippocampal LTP. Neuron. 76: 309-315. (2012)

The role of neuroligins in synapse formation, maintenance, and plasticity

Seth Lawler Shipman

Abstract

Possession of a nervous system endows an organism with a substantial range of behavioral abilities owing to a diverse class of excitatory cells in the brain termed neurons and, more importantly, the connections between them. Primary sensory information flows through neural circuits, being shaped and processed as it does, resulting in perception, thought, decision, and action. The processing power of any individual neuron, while considerable, cannot account for such complex behavior. Rather, it is an emergent property of an interconnected system of neurons, the primary unit of connection being the chemical synapse. These synapses permit fast, moment-to-moment transmission of information between cells without compromising the electrical integrity of an individual cell, allowing integration of information can take place at both a cellular and circuit level. Healthy connections allow for split-second decisions, breathtaking insights, and incredible feats of coordination, whereas disrupted transmission can lead to devastating diseases such as schizophrenia and autism. These synaptic sites of connection between neurons are anatomical as well as functional – requiring an initial physical interaction between cells in the process of establishing a meaningful connection. This thesis begins with an inquiry into these anatomical aspects of a synapse. Specifically, I present evidence for the requirement of synaptic adhesion molecules in the formation and plasticity of synapses. I take one family of postsynaptic adhesion molecule, neuroligin, as a model for the class to test its specific function with regard to synaptogenesis and plasticity. I identify and describe three major functions of the protein, each dependent on a specific structural component: one, differentiation of

the presynaptic terminal, dependent on dimerization, achieved via the trans-synaptic clustering of the presynaptic adhesion molecule neurexin; two, recruitment of postsynaptic components during synaptic assembly, dependent on a previously uncharacterized region of the postsynaptic intracellular domain, achieved via the scaffolding of the postsynaptic site; and three, specification of synaptic subtype, dependent on alternative splicing of the extracellular domain, achieved via a trans-synaptic protein binding code. Finally, I examine the distribution of synapses along a dendritic arbor and the determination of relative synaptic weight as it relates to the electrical integrative properties of a cell.

Table of Contents

Acknowledgments iv
Contributions viii
Abstract ix
List of Tables xiv
List of Figures xv

CHAPTER 1: General Introduction 1
The synapse as a processing unit 3
An integrated molecular view of the synapse 4
The case for synaptic adhesion molecules in the genesis of a synapse 5
Post-adhesive molecular assembly of a synapse 8
Synaptic adhesion molecules and the generation of synaptic diversity 9
Synaptic adhesion molecules and disease 10
Synaptic plasticity 11
The cell as a computational unit 12

CHAPTER 2: Methods 15
Experimental constructs 16
Slice culture and biolistic transfection 20
Acute slice preparation 20
Dissociated culture preparation and transfection 21
Lentivirus production 21
Stereotaxic injection 21
In utero electroporation 22
Immunoblotting 22
Co-immunoprecipitation 22
Biotinylation of cell surface protein 23
Quantitative RT-PCR 24
Anatomy and imaging 24
Electrophysiological recording 26
Coefficient of variation analysis 28
Statistical analysis 28

CHAPTER 3: Dimerization of postsynaptic neuroligin drives synaptic assembly via trans-synaptic clustering of neurexin 29
Introduction 30
Results 32
Functional neuroligin requires an intact dimerization domain 32

Dimerization of neuroligin is required for its trans-synaptic effects 34
A rigorous test of neuroligin dimerization-driven synaptic assembly 36
Discussion 40

CHAPTER 4: Functional dependence of neuroligin on a new non-PDZ intracellular domain 54
Introduction 55
Results 58
Neuroligin c-tail is critical for functional replacement 58
Neuroligin AMPAR effect is independent of established motifs 60
Novel intracellular region required for synaptic effect 61
Effect of mutations is specific to excitatory synapses 63
Neuroligin effect remains after synaptic blockade 64
Neuroligin induces the assembly of new functional synapses 65
Discussion 67

CHAPTER 5: A subtype specific function for the extracellular domain of neuroligin 1 in hippocampal LTP 98
Introduction 99
Results 101
NLGN1 is exclusively required for LTP in the adult dentate gyrus 101
Reduction of NMDA currents by NLGN1 knockdown is due to a loss of synapses 102
Subtype specific synaptic phenotype of NLGN1 expression is dependent on a region in the extracellular domain 105
In vivo molecular replacement demonstrates a dependence of LTP in young CA1 on the B site in the extracellular domain of NLGN1 108
Discussion 110

CHAPTER 6: Distance-dependent scaling of AMPARs is cell-autonomous and GluA2-dependent 133
Introduction 134
Results 136
Verification of a distance-dependent synaptic AMPAR gradient in CA1 pyramidal neurons 136
Evidence for cell-autonomous scaling of AMPAR currents 138
A sufficient supply of AMPARs is necessary for the expression of distance-dependent scaling 140
Distance-dependent scaling additionally requires the GluA2 subunit 141
GluA2 is an organizer of synaptic location 142
Maintenance of proper synapse density over long periods of time requires action potentials 143

Discussion 145

CHAPTER 7: General Conclusions 160

Neuroligins are distinctly synaptogenic 161
Overexpression or knockdown of neuroligin results in all-or-none changes in the number of synapses 163
From structure to function of neuroligin 164
The post- and trans-synaptic effects of neuroligin are largely separable 165
The effect of experimental preparation on neuroligin phenotypes 166
Future directions for the study of neuroligin 167
Is distance-dependent scaling conceptually or mechanistically similar to homeostasis? 169

CHAPTER 8: References 180

List of Tables

CHAPTER 2

Table 1: Expression Vectors..... 18
Table 2: Experimental Constructs 18

List of Figures

CHAPTER 3

Figure 1: Mutations of neuroligin affecting dimerization abolish the synaptogenic effects of postsynaptic expression 44
Figure 2: Trafficking of the dimerization-null mutants 46
Figure 3: Dimerization-null neuroligin mutant retains the ability to enhance the postsynaptic site in the absence of presynaptic enhancements 48
Figure 4: Additional analysis of immunostained puncta 50
Figure 5: Chemically-induced dimerization and monomerization can acutely alter the synaptic phenotype of neuroligin expression 53

CHAPTER 4

Figure 6: Knockdown of neuroligin family is necessary for functional study of the c-tail 75
Figure 7: Heterodimerization of endogenous and exogenous neuroligin 77
Figure 8: Replacement of endogenous NLGNs with wild-type and mutated NLGN3 reveals AMPAR enhancement dependent on a single residue in the c-tail 79
Figure 9: Retained surface expression of point-mutant NLGN3 and lack of an effect on a wild-type background 81
Figure 10: Critical novel region identified in NLGN3 is also crucial for the function of NLGN1 and NLGN4 83
Figure 11: Dependence of neuroligin expression effects on the knockdown background 85
Figure 12: Mutation of the critical residue does not affect inhibitory synapses 87
Figure 13: Enhancement of inhibitory currents by NLGN3 is dependent on the presence of other neuroligins 89
Figure 14: The effects of neuroligin on excitatory synapses are independent of excitatory synaptic activity 91
Figure 15: Enhancement of excitatory currents by NLGN3 is not blocked by APV 93
Figure 16: Mechanism of synaptic enhancement by neuroligins and specific deficits of the mutant 95
Figure 17: Enhancement of spine density by NLGN3 does not require a c-tail domain other than the critical region 97

CHAPTER 5

Figure 18: Role of neuroligin in the expression of adult hippocampal LTP 115
Figure 19: Quantification of knockdown efficiency by microRNA constructs and baseline effects of knockdown on excitatory currents in adult hippocampus 118
Figure 20: Knockdown of NLGN1 results in a reduction in the number of functional synapses in the dentate gyrus 121

Figure 21: Knockdown of NLGN3 in the dentate gyrus results in a reduction in the number of functional synapses 123
Figure 22: Differences in expression phenotype between NLGN1 and NLGN3 are due to a specific difference in the extracellular domain 126
Figure 23: Disruption of the B site insertion in NLGN1 impairs the enhancement of NMDAR-mediated currents 128
Figure 24: Role of NLGN1 and the B site insertion in its extracellular domain in young hippocampal LTP 130
Figure 25: Baseline effects of NLGN1 knockdown and replacement by NLGN1-3 chimeras in young CA1 pyramidal neurons 132

CHAPTER 6

Figure 26: Distance-dependent scaling of AMPARs 149
Figure 27: AMPAR gradient is referenced to the soma in PLP cells 151
Figure 28: Cornichon 2 knockdown selectively reduces distal mEPSCs 153
Figure 29: GluA2 knockdown reverses the distance-dependent scaling of AMPARs 155
Figure 30: GluA2 knockdown alters the organization of spine density..... 157
Figure 31: Spine density is affected by the presence of action potentials 159

CHAPTER 7

Figure 32: Activity dependence of neuroligin 1 phenotype at a reduced expression level .. 173
Figure 33: Differential phenotype of neuroligin 1 knockdown in culture versus acute slices 175
Figure 34: Mutation of gephyrin-binding site does not alter enhancement of inhibitory currents by neuroligin 2 177
Figure 35: Enhancement of inhibitory currents by neuroligin 3 is dependent on the presence of other neuroligins 179

CHAPTER 1:

General Introduction

Perception, thought, decision, and action all arise as emergent properties of the brain and the billions of neurons contained within. These incredible capabilities cannot be explained solely through the additive properties of individual neurons. Rather, they are due to the interconnected nature of the neurons in the brain. Information moves through the system carried by electrical and chemical signals. This information travels through both time and space and is shaped and processed by each individual cell and synapse that it touches. In the same way that human society requires interpersonal communication through language, thought depends on the synaptic connections between neurons. Just as the presence of billions of people without communication does not make a civilization, the presence of billions of neurons without communication does not make a brain. The vast connections between neurons in our brain refine our experience of the world, allow us to learn new relationships, and enable associations between ideas that form the basis for all thought and culture – even explaining our ability to understanding the analogy presented in the previous sentence.

Discussing the connections between neurons does not require abstraction. These connections occur at a physical point in space: the chemical synapse, a highly regulated molecular structure that allows for incredibly precise transmission of information. This anatomical structure and its molecular components are what endow each connection of the brain with the power to not just be a relay but rather a processing unit. In this way, each synapse contributes to the encoding and decoding of information based on an immense history that at once reflects momentary fluctuations of activity within the cell, experiential changes that have occurred throughout the life of an organism, and even the entirety of the genetic evolution that has endowed each synapse with a particular molecular composition.

Indeed, the processing that occurs at a given synapse depends on the exact complement of molecules present, with different synapses specialized for different

computational tasks. Although there is some individual variation, the overall pattern of synapses with different stereotyped molecular identities must be preserved from individual to individual, this pattern having been honed by evolution to allow a species-specific range of behavioral abilities. Assembly of the molecular components of a synapse in a way that is adherent to this overarching plan is not a trivial problem. Each synapse requires coordinated assembly at the interface of (at least) two cells. An emerging model to explain the formation of synapses relies on an initial molecular adhesive interaction between neurons. The properties of this interaction may specify both the initial synapse type as well as its potential for change.

The synapse as a processing unit

The basic function of a synapse is quite straightforward: to transfer information contained in the electrical potential of one cell across space and time to another cell. At chemical synapses, this occurs when an action potential invades the presynaptic terminal, opening voltage-gated calcium channels. A local increase in calcium, acting thought the SNARE complex, stimulates the release of a vesicle of neurotransmitter. This neurotransmitter diffuses across the extracellular space of the synaptic cleft, where it binds to postsynaptic receptors. In response to transmitter binding, ion channels open, allowing charged ions to flow across the membrane, altering the electrical potential of the postsynaptic cells and completing the transfer of information.

In some cases, the function of a synapse is to faithfully recapitulate the activity of a presynaptic cell in the activity of a postsynaptic cell, such as occurs in the transmission of auditory information at the Calyx of Held (Trussell, 1999). Yet, this is not always the case. Synapses can be sign-inverting, like those between photoreceptors and ON bipolar cells in the retina (Stell et al., 1977), so that a negative response at one level of processing becomes a positive response at the next. They can perform gain-modulation

to alter the sensitivity to a given stimulus, as occurs via shunting inhibition in cerebellar granule cells (Mitchell and Silver, 2003). They can be low-fidelity, so that a given presynaptic response only generates a postsynaptic response on a random minority of instances, as occurs at the Schaffer Collateral synapse in the hippocampus (Hjelmstad et al., 1997). They can also perform coincidence detection so that the response to given input depends on whether it occurs in isolation or in combination with other inputs, as occurs in NMDAR-mediated plasticity (Malenka and Nicoll, 1993).

In this way, each synapse is a computational processor; information is altered as it moves from one cell to another, shaped by the unique properties of the synapse. The diversity of synapses defines the range of computations that are possible. The properties of each individual synapse – encoded through unique molecular composition – then are paramount to the function of a brain. Yet, how can such specialization be reliably achieved in a way that is stereotyped between individuals?

An integrated molecular view of the synapse

The classical view of communication across a chemical synapse is much like that of two shipwrecked sailors inhabiting two closely separated yet out-of-sight deserted islands. They send messages to one another via floated bottles, but have no concept of what is happening on the other island on a moment-to-moment basis and no stable infrastructure to rely on. In this view, messages between neurons move back-and-forth between cells carried by transmitter and retrograde signals, but the pre- and posysynaptic compartments are entirely independent, two communicating units separated by physical space. The only evidence for the existence of the other side is the occasional reception of a chemical message.

This view, however, may not reflect the biology of the system. In fact the space between neurons – the synaptic cleft – is not an empty void, waiting to be crossed by

chemical transmitter. There exist stable molecular bridges in the form of adhesion molecules that physically connect the two sides of a synapse (Yamagata et al., 2003). These trans-synaptic adhesive interactions unite the two dense molecular structures of the presynaptic and the postsynaptic cell into one grand molecular matrix that spans the entirety of the synapse and ties into the cytoskeletal core of both cells. This new view of a synapse is then of two separate cellular compartments built on one protein ultrastructure, like bridges and telephone wires installed to connect the two islands of our shipwrecked sailors. The two cells can communicate at the same time in discrete packets of information sent by chemical means as well as through direct, stable molecular interactions.

The case for synaptic adhesion molecules in the genesis of a synapse

What is the function of a molecular interaction between cells that can communicate chemically? It could be to simply hold the two sides of a synapse in close proximity so as to permit reliable chemical transmission of information. Alternately, the molecular interaction could transmit information itself, in parallel to the information carried by chemical transmission. One function that has been proposed for molecular adhesive interactions between neurons is the initiation of a synaptic site (Washbourne et al., 2004). The concept is that an initial molecular interaction mediated by adhesion molecules on the axon of one cell and the dendrite of another forms the heart of a nucleating reaction around which the protein components of the pre- and postsynaptic sides of a synapse form.

By far the most studied synaptic adhesion complex is that of postsynaptic neuroligin and presynaptic neurexin. Neuroligin and neurexin are both single pass transmembrane proteins with short intracellular domains and longer extracellular domains that interact to form a trans-synaptic complex (Lise and El-Husseini, 2006). Let

us first consider the evidence that this complex is instructive in the formation of a synaptic site. Aggregation of neuroligin into clusters using oligomerized neurexin applied to dissociated neurons results in the accumulation of postsynaptic molecules at the site of aggregated neuroligin (Barrow et al., 2009). Likewise, aggregation of neurexin using oligomerized antibody in dissociated neurons leads to accumulation of presynaptic molecules around the aggregated neurexin (Dean et al., 2003). Thus, each half of the complex has the ability to recruit the appropriate molecules to build opposing sides of a synapse.

Evidence for the sufficiency of this complex in the formation of a synaptic site comes from a series of co-culture experiments. Non-neuronal cell lines do not express neuroligin or neurexin and do not make synaptic contacts. If, however, neurexin is expressed in fibroblasts that are co-cultured with neurons, the neurons will form postsynaptic specializations at sites of contact with the neurexin-expressing fibroblasts (Graf et al., 2004). The reverse works as well. If neuroligin is expressed in HEK cells that are co-cultured with neurons, the neurons will form presynaptic specializations at sites of contact with the neuroligin-expressing HEK cells (Fu et al., 2003). Even further, these presynaptic sites are functional. If neuroligin is co-expressed in HEK cells with a fast excitatory synaptic receptor – AMPA or NMDA receptors – postsynaptic currents in the HEK cells can be recorded due to synaptic release of glutamate by co-cultured neurons onto those cells (Fu et al., 2003). Thus, it is clear that the presence of the neuroligin/neurexin complex is able to induce the formation of both sides of an excitatory synapse in this artificial situation, but the question remains: is that sufficient in a neuron?

Overexpression of postsynaptic neuroligin in neurons leads to increases in dendritic spines, the anatomical aspect of an excitatory synapse (Boucard et al., 2005; Chih et al., 2005). This increase in spines is accompanied by an increase in synaptic currents, suggesting that the expression of neuroligin is not merely sufficient to induce

the anatomical but also the functional components of a synapse (Levinson et al., 2005; Prange et al., 2004). Furthermore, these increases in spines and postsynaptic currents are accompanied by increases in staining for the presynaptic marker VGLUT1, indicating that expression of postsynaptic neuroligin is able to recruit components of the presynaptic machinery trans-synaptically (Chih et al., 2005).

The neuroligin/neurexin complex is therefore sufficient for synaptogenesis, but what of its necessity? First, we require a bit more background. Neuroligin and neurexin are both protein families comprised of multiple subtypes. There are four neuroligins, each expressed from separate genes, termed neuroligins 1-4. Neuroligin 1 is found exclusively at excitatory synapses (Song et al., 1999), neuroligin 2 is found exclusively at inhibitory synapses (Varoqueaux et al., 2004), and neuroligin 3 is found at both excitatory and inhibitory synapses (Budreck and Scheiffele, 2007). Neuroligin 4 has been less well studied, is not well conserved in rodents (Bolliger et al., 2008), and localizes to glycinergic synapses in the retina and spinal cord (Hoon et al., 2011). Removal of any one subtype of neuroligin by either knockout or knockdown has relatively subtle effects, whereas a triple knockout of neuroligins 1-3 is lethal at birth, suggesting some functional redundancy (Varoqueaux et al., 2006).

Triple knockdown of neuroligins 1-3 reduces the density of spines suggesting a necessary role in either the formation or maintenance of synapses (Chih et al., 2005). However, although the triple knockout of neuroligin 1-3 is not viable, neurons cultured embryonically from those animals are able to make synapses (Varoqueaux et al., 2006). This discrepancy may well be explained by the presence of other synaptic adhesion molecules that can compensate for the absence of neuroligin in the case of complete genetic deletion (Tallafuss et al., 2010).

Deletion of the presynaptic adhesion molecule neurexin presents significant technical difficulties, as neurexins are expressed from three separate genes, each with

two functional promoters generating a longer (α) and shorter (β) isoform at each locus, all of which undergo extensive alternative splicing (Tabuchi and Sudhof, 2002; Ushkaryov et al., 1992). A triple knockout of α-neurexins, like the triple knockout of neuroligins, results in lethality soon after birth combined with decreased evoked synaptic responses due to reductions in presynaptic calcium influx through voltage-gated calcium channels, linking this adhesion complex to the functional aspects of synaptic transmission at the presynaptic terminal (Missler et al., 2003). However, also like the triple neuroligin knockout, cultured neurons from these mice make synapses that are ultrastructurally normal (Missler et al., 2003). As this deletion only removes the α-, and not the β-form of neurexin, however, it is not possible to make definitive judgments about the necessity of neurexins in synaptogenesis.

Post-adhesive molecular assembly of a synapse

The evidence in support of a role for the neuroligin/neurexin complex in synaptogenesis is quite strong. Yet, much is still unknown about how exactly this complex functions. For instance, after the initial interaction between neuroligin and neurexin at the future site of a synapse, what molecular interactions are necessary for the recruitment of the pre- and postsynaptic components? On the postsynaptic side of an excitatory synapse, it has been suggested the neuroligin may serve to scaffold other postsynaptic proteins through intracellular interactions with the MAGUK family (PSD-95, PSD-93, etc.) via a PDZ-binding domain on its extreme c-terminus (Irie et al., 1997) and S-SCAM via a WW-binding domain (Iida et al., 2004). At inhibitory synapses, neuroligin may interact with gephyrin in a similar way to scaffold the inhibitory postsynaptic site (Poulopoulos et al., 2009).

On the presynaptic side, neurexins have been shown to bind the intracellular scaffolding molecule CASK though a c-terminal PDZ ligand (Hata et al., 1996), which

has the potential to couple neurexin to synaptic vesicle exocytosis though a tripartite complex of CASK, Mint1, and Velis (Butz et al., 1998). It is important to note, however, that none of these specific intracellular interactions have yet been shown to directly affect the physiological function of either neuroligin or neurexin in neurons.

Synaptic adhesion molecules and the generation of synaptic diversity

This chapter began with a discussion of the enormous computational power generated by having a diversity of synapses, each accomplishing a separate computational process. Might synaptic adhesion molecules contribute to the establishment of synaptic diversity? There are already a large number of different presynaptic and postsynaptic adhesion molecules known and more are continuously being discovered (Siddiqui and Craig, 2011). The specificity of synapse type could, therefore, be dictated by a trans-synaptic code of adhesion molecules; the properties of a particular synapse being determined based on the specific interaction between the adhesion molecules expressed in the presyanptic cell and the adhesion molecules expressed in the postsynaptic cell on which the synapse is built.

As already mentioned, there are multiple subtypes of neuroligin with differential expression based on synapse type. Most notably, neuroligin 1 is found at excitatory synapses and neuroligin 2 at inhibitory synapses (Song et al., 1999; Varoqueaux et al., 2004). Moreover, neuroligins are only one of an expanding family of postsynaptic neurexin ligands that now includes LRRTMs, cerebellins, and CL1 (Boucard et al., 2012; de Wit et al., 2009; Ko et al., 2009; Linhoff et al., 2009; Uemura et al., 2010). On the presynaptic side, there are also multiple genes encoding subtypes of neurexin (Rowen et al., 2002). This diversity is further augmented by extensive alternative splicing, which has the potential to generate thousands of different neurexin isoforms (Ullrich et al., 1995). There is additionally evidence that these different isoforms have a partially non-

overlapping distribution in the brain (Ullrich et al., 1995) and different isoforms bind preferentially to different subtypes of neuroligin (Boucard et al., 2005). Thus, it is tempting to speculate that differential expression of postsynaptic neurexin ligands combined with the regulated alternative splicing of neurexin itself could generate a trans-synaptic code around which a diverse set of synapses are created.

Moving beyond the neurexin-containing adhesion complexes, there are yet more types of synaptic adhesion molecules including cadherins (Arikkath and Reichardt, 2008), SynCAMs (Biederer et al., 2002), netrin-G ligand-3 and receptor protein tyrosine phosphatases (Woo et al., 2009), and teneurins (Mosca et al., 2012). Based on this range, it is entirely conceivable that the synaptic diversity found in the brain could well be a consequence of a combinatorial code of differentially expressed synaptic adhesion molecules.

Synaptic adhesion molecules and disease

Given the role of synaptic adhesion molecules at the synapse, it is not surprising that their dysfunction can lead to human disease (Sudhof, 2008). Multiple rare familial forms of autism have been ascribed to mutations in neuroligin genes (Daoud et al., 2009; Jamain et al., 2003; Lawson-Yuen et al., 2008; Yan et al., 2005) with subsequent experimental evidence suggesting pathogenic loss-of-function as the causative factor in these cases (Comoletti et al., 2004; Etherton et al., 2011). Copy-number variations of neurexin have also been linked to autism (Ching et al., 2010; Gauthier et al., 2011; Vaags et al., 2012) and schizophrenia (Gauthier et al., 2011; Ikeda et al., 2010; Rujescu et al., 2009). Moreover, the superfamily of synaptic adhesion molecules linked to neuropsychiatric disease additionally includes cadherins (Redies et al., 2012) and LRRTMs (Sousa et al., 2010; Wang et al., 2009)

Synaptic plasticity

Not all properties of a synapse are determined at the time of its initial formation. Development and ongoing activity at a given synapse can alter the synapse molecularly to affect its subsequent response to activation. This is broadly termed synaptic plasticity. One particular form of synaptic plasticity is long-term potentiation, in which a synapse that is co-activated with other synaptic inputs undergoes a rapid strengthening of response that is maintained over time (Bliss and Lomo, 1973). This phenomenon has been the recipient of much study because it is widely believed to be a cellular correlate of memory (Bliss and Collingridge, 1993) and, indeed, follows the general principles first postulated by Hebb to explain associative learning (Hebb, 1949).

In the mammalian central nervous system, long-term potentiation has been most thoroughly studied at the Schaffer Collateral synapse in the hippocampus. There, excitatory synapses contain two subtypes of fast glutamatergic postsynaptic receptors: AMPA receptors (AMPARs) and NMDA receptors (NMDARs). AMPARs at this synapse are permeable only to the monovalent cations Na^+ and K^+, whereas NMDARs are additionally permeable to divalent Ca^{2+}. At the resting potential of a neuron, NMDARs are blocked by Mg^{2+} driven into their pore by the hyperpolarized potential of the cell (Ascher and Nowak, 1988). Thus, activation of a single synapse in isolation will lead to ion flux through the AMPAR, which serves to drive the cell toward threshold potential for an action potential, but no flux through the NMDAR. If, however, the cell is depolarized prior to the activation of a synapse, as might occur due to coordinated activation of multiple inputs or the repeated activation of a single input, the Mg^{2+} block of NMDARs will be relieved and Ca^{2+} will flow into the cell. This influx of Ca^{2+}, acting primarily through CamKII (Silva et al., 1992), leads to an increase in the number of AMPARs at the synapse through a yet-unresolved mechanism, which effectively strengthens the synapse on subsequent activation.

The cell as a computational unit

As outlined above, each synapse contributes to the processing power of the brain. If we move up one level, we can think of each individual cell then as an interpreter of this processed information, generating the massive computational power of the brain. A given pyramidal neuron, for instance, might receive as many as 30,000 unique synaptic inputs (Ahmed and Mehta, 2009). Yet the sole output of these cells is an all-or-none action potential, this output being affected by the integration of all inputs occurring over both time and space. The fact that the neuron occupies space introduces a number of computational complexities. Propagation of dendritic potentials is passive, in contrast to the regenerative axonal potentials that are maintained by voltage-gated sodium channels. This means that dendritic potentials decline in amplitude as they travel due to a leak of current through channels in the membrane. In cells with complex dendritic arbors, not all synapses can be the same distance from the axon initial segment and therefore synaptic currents arising from different locations along a dendrite will be filtered by differing amounts before contributing to the spiking output of a cell. In order to compensate for this filtering over distance, pyramidal neurons of the hippocampus display distance-dependent scaling of AMPAR-mediated responses (Magee and Cook, 2000). Synapses that are further from the soma contain more AMPARs than synapses that are close to the soma so that currents are normalized over the length of the dendrite and each synapse may contribute equally to the spiking output of the cell (Smith et al., 2003).

This problem is different than but related to the issue of generating synapse diversity or changing the synaptic strength in response to activity discussed above. Here the properties of individual synapses must be weighted, with the cell somehow performing the complex computation of electrotonic distance so as to appropriately scale the input strength of each synapse to counteract intrinsic cable properties of the

dendrite, yielding a democratization of synaptic contribution to the spiking output of the cell.

In the following thesis, I begin by addressing a number of issues related to the role of synaptic adhesion molecules, specifically neuroligin, in synaptogenesis, synaptic maintenance, and synaptic plasticity and end with an investigation into the mechanisms of distance-dependent scaling. In chapter three, I examine one aspect of postsynaptic neuroligin with regard to its synaptogenic properties: its basal state as a constitutive dimer. I show that dimerization is required for the synaptogenic properties of neuroligin and likely serves to induce presynaptic differentiation via a trans-synaptic clustering of neurexin. Further, I introduce chemically-inducible, exogenous dimerization domains to the neuroligin molecule, effectively bestowing chemical control of neuroligin dimerization. This allows me to identify the acute requirements of neuroligin dimerization by chemically manipulating the monomeric-to-dimeric conversion of neuroligin. Based on the results of the inducible dimerization experiments, I propose a model in which dimerized neuroligin induces the mechanical clustering of presynaptic molecules as part of a requisite step in the coordinated assembly of a chemical synapse.

In chapter four, I investigate the assembly of the postsynaptic components of a synapse by neuroligin. Neuroligins are thought to drive postsynaptic assembly via binding of their intracellular domain to PSD-95. However, there is little direct evidence to support the functional necessity of the neuroligin intracellular domain in postsynaptic development. I find that the presence of endogenous neuroligin can obscure the study of exogenous mutated neuroligin. Therefore, I use chained microRNAs in rat organotypic hippocampal slices to generate a reduced background of endogenous neuroligin. On this reduced background, I find that neuroligin function is critically dependent on its cytoplasmic tail. However, surprisingly, this function requires neither the PDZ ligand nor

any other previously described cytoplasmic binding domain, but rather requires a novel conserved region. Mutation of a single critical residue in this region inhibits neuroligin-mediated excitatory synaptic potentiation. Finally, I report a novel functional distinction between neuroligins 1 and 3.

In chapter five, I follow up on the distinction between neuroligins 1 and 3. These subtypes have roles in synaptogenesis and synaptic maintenance that appear largely overlapping. I combine electrophysiology with molecular deletion and replacement of these proteins to identify similarities and differences between these subtypes. In doing so, I identify a subtype specific role in LTP for neuroligin 1 in young CA1, which persists into adulthood in the dentate gyrus. As neuroligin 3 showed no requirement for LTP, I constructed chimeric proteins of the two excitatory neuroligin subtypes to identify the molecular determinants particular to the unique function of neuroligin 1. Using *in vivo* molecular replacement experiments, I find that these unique functions depend on a region in the neuroligin 1 extracellular domain containing the B site splice insertion previously shown to determine specificity of neurexin binding.

Finally, in chapter six, I undertake an investigation into the molecular mechanisms of distance-dependent scaling. Using dendritic recordings, I am able to independently reproduce the basic phenomenon. I extend the cellular understanding of this phenomenon by showing that it is expressed cell-autonomously by exploiting a rare cell type in the hippocampus. I then manipulate it cell-autonomously to show that it depends on the presence of a reserve pool of AMPARs and also requires the AMPAR subunit GluA2. Finally, I look at the cellular location of excitatory synapses onto pyramidal cells and report a dependence on both GluA2 and postsynaptic spiking.

CHAPTER 2:

Methods

Experimental Constructs

The triple microRNA construct to knockdown neuroligins 1, 2, and 3 (NLmiRs) was constructed using targeting sequences based on those which have been previously characterized (Chih et al., 2005). Specifically, sequences ggaaggtactggaaatctata (*NLGN1*), atggagcaagttcaacagcaa (*NLGN2*), and gcagcgttcttgcaagttatg (*NLGN3*) were cloned into a chained microRNA format immediately following GFP using BLOCK-iT miR RNAi (Invitrogen). The resulting GFP and chained microRNAs were subsequently subcloned into pCAGGS for biolistic expression or pFUGW for lentiviral production. Sequences targeting NLGN1 (NLGN1 miR) and NLGN3 (NLGN3 miR) were individually expressed in a microRNA format following GFP in the lentiviral vector FUGW. A version of pCAGGS with GFP but no microRNAs was used to visualize control spines. A version of the NLmiRs in pCAGGS with mCherry instead of GFP was used when co-transfecting GFP-tagged neuroligins to determine localization. Neuroligin overexpression constructs were based on mouse *NLGN1* containing an HA-tag (gift of AM Craig), rat *NLGN2* containing an HA-tag (gift of F Varoqueaux), human *NLGN3* (accession number BC051715), and human *NLGN4* (accession number BC034018). Truncations of NLGN3 were made by PCR and cloned into pCAGGS using In-Fusion (Clontech), while deletions, point-mutations and RNAi-proofing of all neuroligins were made using overlap-extension PCR followed by In-Fusion cloning. RNAi-proofing was accomplished with degenerate changes to five (*NLGN1*) or six (*NLGN2*) nucleotides in the target region. Overexpression constructs were cloned into a pCAGGS vector containing IRES mCherry for biolistic expression except where noted. The chemically-inducible dimerization construct (NLGN3$^{D\text{-}N}$-iDmr) was created using NLGN3$^{D\text{-}N}$ with the addition of an FKBP derivative DmrB domain (Clontech) inserted at the extreme c-terminus via overlap extension PCR followed by In-Fusion cloning into pCAGGS. For the induced-dimerization experiments, both NLGN3$^{D\text{-}N}$-iDmr and wild-type NLGN3 were expressed in

pCAGGS following the IRES, rather than ahead of the IRES, to reduce expression due to a low level of constitutive dimerization of the chemically-inducible domain at high levels of expression. The artificial dimer/chemically-inducible monomer (NLGN3$^{D\text{-}N}$-revDmr) was constructed in an identical fashion with the substitution of the DmrD reverse dimerization domain (Clontech) for the DmrB domain. GFP fusion constructs of NLGN3 full-length and NLGN3 E740N were created by cloning the neuroligins into pEGFP-N1 and subsequently transferring the neuroligins, fused at the c-terminus to GFP, into pCAGGS. A version of NLGN1* to be expressed virally as well as a GFP control viral plasmid were created by cloning the genes into pFUGW following the Ubiquitin promoter. Specific chimeras of the extracellular domain were made at crossover points of shared homology and are named according to the first amino acid difference that matches NLGN3, with amino acid numbering referenced to untagged NLGN1 (including both A and B splice insertions). Knockdown constructs targeting *GluA1* (shGluA1, target sequence: ggaatccgaaagattggttac), *GluA2* (shGluA2, target sequence: ggagcactccttagcttga), and *CNIH2* (shCNIH2, target sequence: gatgcggtctctatcatga) were expressed from an H1 promoter in pFHUGW along with GFP expressed from the Ubiquitin promoter to mark the transfected cell. GFP-IRES-Kir2.1 (*KCNJ2*) was expressed in pFUGW from the Ubiquitin promoter. Molecular graphics of dimerization mutations are based on structures from Araç et al. (2007) and were produced using UCSF Chimera package from the Resource for Biocomputing, Visualization, and Informatics at the University of California, San Francisco (Pettersen et al., 2004).

Table 1: Expression Vectors

Expression Vector	Promoter(s)
pCAGGS	hybrid chicken β-actin/rabbit β-globin promoter with a CMV enhancer
FUGW	Ubiquitin
FHUGW	Ubiquitin/H1

Table 2: Experimental Constructs

Expression Construct	Description	Species	Vector	Fluorophore	Chapters Used
NLGNmiRs	Triple miR construct to knockdown NLGNs 1-3	Rat	pCAGGS	GFP	4, 5
NLGNmiRs	Triple miR construct to knockdown NLGNs 1-3	Rat	FUGW	GFP	4, 5
NLGNmiRs	Triple miR construct to knockdown NLGNs 1-3	Rat	pCAGGS	mCherry	4
NLGN1 miR	Single miR to knockdown NLGN1	Rat	FUGW	GFP	5
NLGN3 miR	Single miR to knockdown NLGN3	Rat	FUGW	GFP	5
HA-NLGN1	Neuroligin 1, containing insertions at both A and B splice sites and extracellular HA tag	Mouse	pCAGGS	-IRES-mCherry	3, 4, 5
HA-NLGN1*	RNAi-proof neuroligin 1	Mouse	pCAGGS	-IRES-mCherry	4, 5
HA-NLGN1* E747N	Contains mutation in critical region of c-tail	Mouse	pCAGGS	-IRES-mCherry	4
HA-NLGN1*-GFP	GFP-tagged at extreme c-terminus	Mouse	pCAGGS	GFP	4
HA-NLGN1^{DM1}	1st dimerization-null mutant of NLGN1: F458A/M459A/W463A	Mouse	pCAGGS	-IRES-mCherry	3
HA-NLGN1^{DM2}	2nd dimerization-null mutant of NLGN1: E628A/L629A	Mouse	pCAGGS	-IRES-mCherry	3
HA-NLGN1^{DM3}	3rd dimerization-null mutant of NLGN1: K622A/V623A	Mouse	pCAGGS	-IRES-mCherry	3
HA-NLGN1* ΔB	NLGN1 lacking 8 amino acids of the B site	Mouse	pCAGGS	-IRES-mCherry	5
HA-NLGN2	Neuroligin 2, containing an extracellular HA tag	Rat	pCAGGS	-IRES-mCherry	4
HA-NLGN2*	RNAi-proof neuroligin 2	Rat	pCAGGS	-IRES-mCherry	4
HA-NLGN2* E740N	Contains mutation in critical region of c-tail	Rat	pCAGGS	-IRES-mCherry	4
NLGN3	Neuroligin 3	Human	pCAGGS	-IRES-mCherry	3, 4, 5
NLGN3	Neuroligin 3	Human	pCAGGS	mCherry-IRES-	3
NLGN3 Δ4	Lacks last 4 amino acids	Human	pCAGGS	-IRES-mCherry	4
NLGN3 Δ25	Lacks last 25 amino acids	Human	pCAGGS	-IRES-mCherry	4
NLGN3 Δ46	Lacks last 46 amino acids	Human	pCAGGS	-IRES-mCherry	4
NLGN3 Δ77	Lacks last 77 amino acids	Human	pCAGGS	-IRES-mCherry	4
NLGN3 Δ90	Lacks last 90 amino acids	Human	pCAGGS	-IRES-mCherry	4
NLGN3 Δ99	Lacks last 99 amino acids	Human	pCAGGS	-IRES-mCherry	4
NLGN3 Δ109	Lacks last 109 amino acids	Human	pCAGGS	-IRES-mCherry	4

NLGN3 Δ77-90	Lacks amino acids 77-90, from the c-terminus	Human	pCAGGS	-IRES-mCherry	4
NLGN3 E740N	Contains mutation in critical region of c-tail	Human	pCAGGS	-IRES-mCherry	4
NLGN3-GFP	GFP-tagged at extreme c-terminus	Human	pCAGGS	GFP	4
NLGN3^{DM1}	1st dimerization mutant of NLGN3: F437A/M438A/W442A	Human	pCAGGS	-IRES-mCherry	3
NLGN3^{DM2}	2nd dimerization mutant of NLGN3: H606A/L607A Also referred to as NLGN3^{D-N}	Human	pCAGGS	-IRES-mCherry	3
NLGN3^{DM3}	3rd dimerization mutant of NLGN3: K600A/V601A	Human	pCAGGS	-IRES-mCherry	3
NLGN3^{D-N}-iDmr	Dimerization null NLGN3 containing an inducible dimerization domain at the extreme c-terminus	Human	pCAGGS	mCherry-IRES-	3
NLGN3^{D-N}-revDmr	Dimerization null NLGN3 containing an inducible monomerization domain at the extreme c-terminus	Human	pCAGGS	-IRES-mCherry	3
NLGN-TM-NLGN3	Chimera containing the extracellular domain of NLGN1* and intracellular domain of NLGN3	Mouse/ Human	pCAGGS	-IRES-mCherry	5
NLGN1-418-NLGN3	Chimera containing 418 n-terminal amino acids of NLGN1*	Mouse/ Human	pCAGGS	-IRES-mCherry	5
NLGN1-390-NLGN3	Chimera containing 390 n-terminal amino acids of NLGN1*	Mouse/ Human	pCAGGS	-IRES-mCherry	5
NLGN1-326-NLGN3	Chimera containing 326 n-terminal amino acids of NLGN1*	Mouse/ Human	pCAGGS	-IRES-mCherry	5
NLGN1-254-NLGN3	Chimera containing 254 n-terminal amino acids of NLGN1*	Mouse/ Human	pCAGGS	-IRES-mCherry	5
NLGN1-211-NLGN3	Chimera containing 211 n-terminal amino acids of NLGN1*	Mouse/ Human	pCAGGS	-IRES-mCherry	5
NLGN1-166-NLGN3	Chimera containing 166 n-terminal amino acids of NLGN1*	Mouse/ Human	pCAGGS	-IRES-mCherry	5
NLGN4	Neuroligin 4	Human	pCAGGS	-IRES-mCherry	4
NLGN4 N726E	Contains mutation in critical region of c-tail	Human	pCAGGS	-IRES-mCherry	4
shGluA1	shRNA targeting GluA1	Rat	FHUGW	GFP	6
shGluA2	shRNA targeting GluA2	Rat	FHUGW	GFP	6
shCNIH2	shRNA targeting CNIH2	Rat	FHUGW	GFP	6
Kir2.1	Inwardly rectifying potassium channel	Human	FUGW	GFP-IRES-	6
GFP	Green Fluorescent Protein		FUGW		3
GFP	Green Fluorescent Protein		pCAGGS		4
mCherry	Monomeric Cherry		pCAGGS		3

Slice Culture and Biolistic Transfection

Hippocampal organotypic slice cultures were prepared from 6- to 8-day-old rats as described (Stoppini et al., 1991). All experiments were performed in accordance with University of California San Francisco guidelines for animal use. Transfections were carried out 24 hours after culturing using a Helios Gene Gun (Bio-Rad) with 1μm DNA-coated gold particles. When biolistically expressing two plasmids, gold particles were coated with equal amounts of each plasmid and plasmids always expressed different fluorescent markers. Observed frequency of coexpression was nearly 100%. Slices were maintained at 34^{o} C with media changes every other day.

Acute Slice Preparation

Acute hippocampal slices were prepared from adult rats 10-12 days after virus injection or young rats from p11 to p15 after *in utero* electroporation. Adult rats were anesthetized through intraperitoneal injection of a ketamine/xylazine combination and transcardially perfused with an ice-cold (4ºC) cutting solution (210 mM sucrose, 2.5 mM KCl, 0.5 mM $CaCl_2$, 7 mM $MgCl_2$, 1.25 mM NaH_2PO_4, 25 mM $NaHCO_3$, 7 mM glucose, 1.3 mM ascorbic acid, 3 mM pyruvic acid saturated with 95% O_2/5% CO_2) prior to decapitation. Young rats were anesthetized with isoflourane and decapitated. While submerged in cutting solution, brains were removed and sliced into 350μm near-horizontal sections using a vibratome (D.S.K.). Slices were then transferred to a holding chamber containing ACSF (125 mM NaCl, 2.5 mM KCl, 1.25 mM NaH_2PO_4, 25 mM $NaHCO_3$, 11 mM glucose, 1 mM $MgSO_4$, 2 mM $CaCl_2$ saturated with 95% O_2/5% CO_2) and incubated for 30 minutes at 34ºC.

Dissociated Culture Preparation and Transfection

Dissociated cultures were prepared from E18-19 rats. Hippocampi were surgically isolated, then dissociated by 0.25% trypsin followed by gentle mechanical trituration. Cells were plated on poly-D-lysine treated glass coverslips at an approximate density of 20,000 cell/cm^2 and maintained in neurobasal (Invitrogen)-based media supplemented with B27, penicillin-streptomycin, and L-glutamine at 37^oC/5% CO_2. Transfections were achieved using Lipofectamine 2000 (Invitrogen). Cells were transfected at DIV 10 and analyzed 3 to 4 days later.

Lentivirus Production

For the production of lentiviral particles, HEK293T cells were cotransfected with either the expression construct (in FUGW along with psPAX2 and pVSV-G using FuGENE HD (Roche). Forty hours later supernatant was collected, filtered, and concentrated by ultracentrifugation (80,000g for 2h at 4° C) or precipitated using PEG-it (Systems Biosciences) and collected via centrifugation. The resulting viral pellet was resuspended in Opti-Mem and stored at –80^o C until use.

Stereotaxic Injection

Concentrated lentiviruses were injected bilaterally into the medial hippocampi of isoflourane anesthetized 4-5 week old rats using a stereotaxic apparatus (Kopf). 500nl per hemisphere was delivered at 500nl/min via a Hamilton (88011) syringe driven by a Micro4 microsyringe pump controller (WPI). All experiments were performed in accordance with established protocols approved by the University of California San Francisco Institutional Animal Care and Use Committee.

In Utero Electroporation

In utero electroporations were performed as previously described with minimal adjustments to achieve hippocampal expression (Walantus et al., 2007). Expression constructs were introduced via intraventricular injection into E16 rat embryos. Immediately after DNA injection, electroporations were performed using an Electro Square Porator ECM830 (BTX Genetronics) (5 pulses, 50 V, 50 ms, 1 s interval). Electroporation tweezertrodes (BTX Genetronics) were placed with the negative pole over the left hemisphere.

Immunoblotting

Primary cultured neurons (DIV6) were infected with Lentivirus containing NLmiRs or control shRNA. Neurons (DIV12) were harvested in PBS buffer with 2mM EDTA and protease inhibitor mixture (Roche Applied Science). The cell lysate was sonicated briefly, sedimented by centrifugation (100,000g for 20 min) and solubilized in PBS containing 1% SDS for 15 min at 37° C. Ten volumes of PBS containing 1% Triton X-100 were added to the lysate resulting in a final concentration of 0.1% SDS. Insoluable material was removed by centrifugation at 100,000g for 20 min. Proteins were resolved by SDS-PAGE and analyzed by Western blot with NLGN1 (Synaptic Systems), NLGN2 (Synaptic Systems) or NLGN3 (Abcam) antibody.

Co-immunoprecipitation

In COS cells, plasmids encoding Flag-tagged NLGN1 (gift of T Sudhof), NLGN3, myc-tagged NLGN3, and myc-tagged NLGN3 Δ90 were co-transfected into COS cells with a plasmid encoding HA-tagged NLGN1. After 48 hrs, cells were harvested in buffer A (25 mM Tris-HCl pH7.4, 137 mM NaCl, 2 mM EDTA, and EDTA-free complete protease

inhibitor), lysed with buffer A supplemented with 1% Triton X-100, and then centrifuged at 13,000g for 10 min. In neurons, primary cortical neuronal cultures were infected with lentivirus expressing HA-tagged NLGN1* or GFP on DIV7 and harvested in buffer A on DIV10, then centrifuged at 13,000g for 5 minutes. The resulting pellets were resuspended in buffer A supplemented with 1% Triton X-100, incubated at 4° C for 30 minutes, then centrifuged at 100,000g for 20 minutes. In each case, HA-tagged NLGN1 in the supernatant was immunoprecipitated using anti-HA antibody (Abcam) conjugated protein A-sepharose at 4° C for overnight. After washing four times, immunoprecipitants were denatured in SDS-sample buffer at 65° C for 5 min and then subjected to immunoblot analysis.

Biotinylation of Cell Surface Protein

HEK cells, cultured in 10cm dishes, were transfected with 20μg of cDNA using Calphos transfection system (Clontech). After 48 hrs, cells were washed three times with ice-cold wash buffer A (PBS containing 1 mM $MgCl_2$ and 0.1 mM $CaCl_2$), then incubated with 1 mg/ml EZ-Link Sulfo-NHS-LC-biotin (Thermo Scientific) in cold wash buffer for 10 min at 4°C with gentle agitation. Cells were then washed twice with ice-cold quenching buffer (100 mM glycine in wash buffer A) and lysed (25 mM Tris-HCl, pH 7.4, 137 mM NaCl, 2 mM EDTA, 1% SDS, EDTA-free complete protease inhibitor) (Roche) for 15 min at 37° C with gentle shaking. Lysate was neutralized with 1% TritonX-100 and centrifuged at 100,000g for 20 min. 10% of the supernatant was saved for use as input, while the remaining supernatant was incubated with neutravidin beads (30μl) (Thermo Scientific) for 2h at 4°C. Beads were pelleted by centrifugation, and washed four times with wash buffer B (25 mM Tris-HCl, pH 7.5, 137 mM NaCl, 1 mM EDTA, and 0.1% TritonX-100).

Biotinylated proteins were denatured with SDS-sample buffer at 65°C for 5 min and analyzed by immunoblotting as described above.

Quantitative RT-PCR

To assess the efficiency of knockdown, dissociated hippocampal neuronal cultures were prepared from E18-19 rats. Hippocampi were surgically isolated, then dissociated by 0.25% trypsin followed by gentle mechanical trituration. Cells were plated on poly-D-lysine treated glass coverslips and maintained in a neurobasal (Invitrogen)-based media supplemented with B27, penicillin-streptomycin, and L-glutamine at 37ºC/5% CO_2. Lentiviruses containing the miR constructs were introduced one day after plating. Ten days later, RNA was harvested by lysis and reverse transcribed to synthesize cDNA using a Cells-to-CT kit (Life). Amplification of cDNA by real-time PCR was quantified using SYBR Green in a Stratagene Mx3005P with the following sequence specific primers: NLGN1, forward CTGGAAATCTATATGATGGGAGTG, reverse TGCTCAAGAAGCCAAGTACC; NLGN3, forward GGCTCTTACATGGAAGGAACAG, reverse GTGCTCAGGAAACCTAGCAC.

Anatomy and Imaging

Spine images of biolisitically transfected neurons in live hippocampal organotypic cultures were acquired on DIV 7-9 using an upright confocal microscope (Zeiss LSM5 Pascal) from cells expressing either GFP alone (control condition) or GFP plus $NLGN^{D-N}$. Slices were submerged in HEPES buffered ACSF containing 140 mM NaCl, 2.5 mM KCl, 1 mM $MgCl_2$, 2 mM $CaCl_2$, 10 mM HEPES, and 10 mM glucose. Localization of GFP-tagged neuroligins was carried out in live organotypic slices with neurons biolistically transfected with NLmiRs (with mCherry to visualize the dendrite) plus the

relevant neuroligin construct, fused to GFP at the c-terminus. Imaging was carried out using a confocal microscope (Zeiss LSM5 Pascal). Neurons were imaged along their primary apical dendrite for a length of 100µm, starting 100µm from the cell body. For spine density as a function of distance, cells were imaged over the entire length of their primary apical dendrite and spines were counted in 30µm bins starting from the cell body.

For spine density analysis in acute slices, control and tranduced dentate granule cells were filled with an intracellular solution containing Alexa Fluor 568 (Invitrogen) for 5-10 minutes. Slices were fixed with 4% paraformaldehyde in sodium-phosphate buffered saline (PBS) additionally containing 4% sucrose. Slices were mounted on glass coverslips in SlowFade Gold (Invitrogen) and stored at 4ºC until imaging. Images were acquired on an inverted confocal microscope (Zeiss LSM510 Meta). For each neuron, three 50 µm sections of dendrite (from separate branches) were imaged starting 60 µm from the cell body. Cells were imaged and analyzed blind to condition.

Images of immunostained synaptic proteins in dissociated culture were acquired on an inverted confocal microscope (Zeiss LSM510 Meta). All images in a series were collected with identical settings for laser power, pinhole diameter, detector gain, amplifier gain and amplifier offset. Images were analyzed using ImageJ using maximum intensity z-projections. Three 50 µm sections of dendrite were analyzed for each cell. For the puncta analysis, an identical threshold was applied to all images in a series and a mask was created from which all puncta greater than 0.15 μm^2 were selected and analyzed for punta density and size. This mask was applied to the original image to collect puncta intensity.

Electrophysiological Recording

Electrophysiological recordings were carried out on an upright Olympus BX51WI microscope using a Multiclamp 700B amplifier (Molecular Devices). For organotypic slices, transfected and control neurons were recorded simultaneously on DIV 7-9 at 20-25^{o}C using glass patch electrodes filled with an internal solution containing (in mM): 120 $CsMeSO_4$, 20 CsCl, 10 HEPES, 4 NaCl, 0.5 EGTA, 0.3 $CaCl_2$, 4 Mg-ATP, 0.3 Na-GTP, and 5 QX-314 and an external solution containing: 125 NaCl, 2.5 KCl, 1.25 NaH_2PO_4, 25 $NaHCO_3$, 11 glucose, 4 $MgSO_4$, and 4 $CaCl_2$, bubbled continuously with 95% O_2-5% CO_2. CA1 pyramidal neurons were identified visually, while transfected neurons were identified using fluorescence. Excitatory synaptic responses were recorded in the presence of 100μM picrotoxin and 10μM gabazine to block inhibition and 50nM NBQX was added to reduce epileptiform activity. 2-Cl-Adenosine (at 5μM) was used during some early recordings to reduce epileptiform activity. However, it was determined that the addition of 2-Cl-Adenosine exaggerated the difference in release probability seen between control neurons and those expressing neuroligin so NBQX was used instead. Inhibitory synaptic responses were recorded in the presence of 50μM APV and 10μM NBQX to block excitatory currents. In all experiments, transfected and neighboring control cells were recorded simultaneously and synaptic currents were evoked by Schaffer collateral stimulation. Typically each pair of neurons is from a separate slice, while on rare occasions two pairs may come from one slice. For all paired recordings, number of experiments (n) reported in figure legends refers to the number of pairs. Peak AMPAR EPSCs were recorded at –70mV and NMDAR EPSCs were recorded at +40mV and were measured 100ms after the stimulus. Paired-pulse ratio was determined by delivering two pulses separated by 40ms. The ratio was defined as the peak current of the second EPSC over the peak current of the first EPSC. IPSCs were recorded at 0mV and peak current was used. mEPSCs were recorded in the presence of 0.5μM

TTX, 100μM picrotoxin, and 10μM gabazine with 0–100mM sucrose added to increase the frequency of events. mEPSCs were analyzed off-line with customized software (IGOR). For the chemically-induced dimerization/monomerization experiments, the small molecules B/B Homodimerizer (AP20187) or D/D Solubilizer (Clontech) were added to slice media at 100 nM for the specified duriation prior to recording.

Acute slices were maintained in ACSF (125 mM NaCl, 2.5 mM KCl, 1.25 mM NaH_2PO_4, 25 mM $NaHCO_3$, 11 mM glucose saturated with 95% O_2/5% CO_2) containing 1 mM $MgSO_4$, 2 mM $CaCl_2$. Paired recordings were carried out as described in organotypic slices without the addition of 50nM NBQX. The internal solution used during the recording of LTP varied slightly (135 mM $CsMeSO_3$, 10 mM HEPES, 8 mM NaCl, 0.3 mM EGTA, 4 mM Mg-ATP, 0.3 mM Na-GTP, 5 mM QX-314, and 0.1 mM spermine). When recording from CA1 pyramidal cells, synaptic currents were elicited by stimulation of the Schaffer collaterals with a bipolar electrode (Micro Probes). Synaptic responses were evoked by stimulation of the perforant path when recording from dentate granule cells. LTP was induced via a pairing protocol of 2 Hz stimulation for 90 seconds at a holding potential of 0 mV. For LTP graphs, AMPAR-mediated current amplitudes were normalized to baseline amplitudes prior to LTP induction on a cell-by-cell basis. Recordings of spontaneous EPSCs were carried out at -70 mV with no external Mg^{2+} so as to record the NMDAR component. Dendritic recordings were obtained using thick-walled glass recording pipettes containing (in mM): 120 K-methylsulphate, 20 KCl, 10 HEPES, 4 NaCl, 0.5 EGTA, 0.3 $CaCl_2$, 4 Mg-ATP, 0.3 Na-GFP, and 5 QX-314 in the presence of 1μM TTX. Lucifer yellow was added to the internal to allow tracing of the dendrite from the recording location to the cell body for measurements of distance. Hyperosmotic solution to elicit local mEPSCs was composed of external solution with the addition of 300mM sucrose and 0.5μM TTX and was puffed locally via a patch pipette.

Coefficient of Variation Analysis

Coefficient of variation was calculated as standard deviation over mean EPSC amplitude for simultaneously recorded evoked current sweeps from paired control and experimental cells. Based on theoretical calculations and experimental measurements, changes in the ratio of CV^{-2} (expt/ctrl) will vary linearly along the 45º line with the ratio of mean amplitudes (expt/ctrl) when the effect is due to a change in N or P_r and vary along the horizontal when the effect is due to a change in q as given by the equation $CV^{-2} = NP_r/(1-P_r)$ (notice that q does not contribute to CV^{-2}) (Bekkers and Stevens, 1990; Del Castillo and Katz, 1954; Manabe et al., 1993).

Statistical Analysis

Statistical significance of paired whole-cell recordings was determined by a Wilcoxon signed-rank test, while statistical comparisons between sets of paired data were performed using a Mann-Whitney U test on the ratios of experimental to control amplitudes. Paired-pulse ratios were statistically analyzed using a student's t-test. Statistical significance of spine density, immunostaining intensity, mEPSC amplitude and mEPSC frequency was determined by a Mann-Whitney U test.

CHAPTER 3:

Dimerization of postsynaptic neuroligin drives synaptic assembly via trans-synaptic clustering of neurexin

Introduction

The synapse is among the most complex of cellular structures, dense with highly organized protein interactions. Although our knowledge of this molecular matrix is expanding rapidly, the precise dynamics that govern the formation of a synapse, with its matched asymmetric sides, are still not fully understood. Yet, some particularly important interactions are beginning to emerge. For instance, the trans-synaptic complex of presynaptic neurexin and postsynaptic neuroligin has been proposed to lie at the heart of an emerging synapse (Craig and Kang, 2007; Sudhof, 2008).

Independent manipulations of either neuroligin or neurexin can result in modifications of both pre- and postsynaptic assembly, suggesting an instructive trans-synaptic role for the neuroligin/neurexin complex in synaptic formation. Most strikingly, in experiments using a co-culture system of neurons and non-neuronal cells, neuroligin expressed the non-neuronal cells is able to induce the formation of functional presynaptic terminals onto those cells from co-cultured neurons (Fu et al., 2003), while neurexin expression in non-neuronal cells supports the formation of postsynaptic specializations at the junctions of those non-neuronal cells and co-cultured neurons (Graf et al., 2004). Whether or not the neuroligin/neurexin complex is absolutely required for synapse formation is not clear, given that dissociated hippocampal and cortical cultures from triple-knockout mice lacking neuroligins 1, 2, and 3 display normal synapse density, although these mice do die at birth from respiratory failure as a consequence of reduced synaptic transmission in the brainstem (Varoqueaux et al., 2006). While this finding certainly suggests that the neuroligin family is not essential for synaptic formation, it remains possible that compensation by another family of postsynaptic adhesion molecules such as the LRRTMs (de Wit et al., 2009; Ko et al., 2009a; Linhoff

et al., 2009) or the cerebellin/GluRD complex (Uemura et al., 2010) could be masking the effects of a germ-line knockout of the three major neuroligin subtypes.

Like the synapse, the neuroligin/neurexin complex is itself asymmetric. Neuroligin exists natively as a dimer, while neurexin, in an unbound state, is monomeric (Arac et al., 2007). The complex, then, is an asymmetric tetramer consisting of a neuroligin dimer and two neurexin molecules – the neurexin molecules brought in close proximity to each other via their interaction with the neuroligin dimer (Arac et al., 2007; Comoletti et al., 2007; Fabrichny et al., 2007). As stated above, *in vitro* evidence suggests that neurexin clustering may be an early step in the differentiation of an axon segment into a presynaptic terminal (Dean et al., 2003). Such clustering could be achieved by the monomeric-to-dimeric conversion of neurexin upon neuroligin binding. Importantly, this clustering would be entirely dependent on the presence of neuroligin in a dimerized state.

We set out to define the functional requirement of neuroligin dimerization with an aim to specifically test the hypothesis that the clustering of neurexin via an interaction with dimerized neuroligin is required for presynaptic assembly. We find strong evidence to support this hypothesis and propose a model whereby postsynaptic neuroligin drives presynaptic differentiation via the clustering of neurexin, while also being required for some, but not all, aspects of postsynaptic assembly.

Results

Functional neuroligin requires an intact dimerization domain

To directly test the physiological requirement for neuroligin dimerization we constructed mutants of neuroligin that have been previously shown to eliminate dimerization (Dean et al., 2003; Ko et al., 2009b). We tested three separate mutants that each contain alanine substitutions at the interface of the neuroligin dimer (Fig . 1A,B). These mutants have been shown to retain surface localization and neurexin binding and, indeed, have been shown in one case to result in increases in synapse density when expressed in neurons. However, the mutants also display deficits in function as compared with wild-type neuroligin, including the lack of aggregation of neurexin-expressing cells in a non-neuronal cell-adhesion assay and the lack of an increase in synaptic cluster size when expressed in neurons (Dean et al., 2003; Ko et al., 2009b).

The postsynaptic expression of wild-type neuroligin results in a profound enhancement of excitatory synaptic currents (Chubykin et al., 2007; Futai et al., 2007). Therefore, we evaluated the effect of expressing exogenous, dimerization-null mutants of neuroligin on this enhancement of postsynaptic currents. To do so we expressed wild-type or mutated neuroligin using sparse biolistic transfection of organotypic hippocampal slice cultures. This resulted in transfection of only one to a few hippocampal pyramidal cells per slice, allowing for the simultaneous recording of whole-cell currents from a transfected neuron and a neighboring control cell. Evoking action potentials in the Schaffer axon collaterals with an extracellular stimulating electrode resulted in simultaneous excitatory synaptic currents in both the experimental and control cell, the relative magnitude of which serves as a readout of the effect of the manipulation on synaptic strength. We found that the introduction of dimerization-null mutations into NLGN1 eliminated the neuroligin-induced enhancement of synaptic currents (Fig. 1C).

To test the generality of this requirement for dimerization in neuroligin function, we made homologous mutations in neuroligin 3 (NLGN3). These dimerization-null mutants of NLGN3 also completely lacked the synapse promoting effects of wild-type NLGN3, with their expression instead resulting in a depression of synaptic strength (Fig. 1D). We conclude that dimerization is essential for the normal physiological function of neuroligin.

Although the original characterizations of dimerization-null mutants of NLGN1 reported preserved surface expression (Dean et al., 2003; Ko et al., 2009b), a more recent study found evidence for endoplasmic reticulum retention of dimerization-null mutants (Poulopoulos et al., 2012). In order to assess whether a trafficking deficit could explain our findings, we examined surface expression of wild-type and dimerization-null mutants of both NLGN1 and NLGN3 in neurons by staining for the presence of an HA-tag in the extracellular domain of the proteins under non-permeabilizing conditions. In all cases, we found evidence for surface expression of the protein (Fig. 2A-B) indicating that the dimerization-null mutants are competent for trafficking.

Nonetheless, it is possible that there exists a trafficking deficit in the mutants that is simply overwhelmed by the relatively long duration or high degree of our overexpression but that still influences our findings. In the same study that found intracellular retention of the dimerization-null mutants, a single amino acid substitution in the transmembrane domain was shown to mitigate this retention (Poulopoulos et al., 2012). To directly test whether a subtle trafficking deficit may be contributing to the synaptic phenotype that we observe, we introduced this single amino acid substitution (N702L) into wild-type and dimerization-null NLGN3, which we expressed in individual neurons in slice culture to assess the effect on synaptic currents. We found that this N702L substitution had no effect on the synaptic phenotype of either wild-type or dimerization-null mutants of neuroligin – wild-type neuroligin still enhanced currents and two different dimerization-null mutants still depressed currents (Fig. 2C). Based on the

combination of surface staining and the lack of any effect of this mutation, we conclude that the synaptic phenotype of the dimerization-null neuroligin is likely due to an effect at the cell surface rather than a trafficking effect.

Dimerization of neuroligin is required for its trans-synaptic effects

Neuroligin has been implicated in the formation (Chih et al., 2005), validation (Ko et al., 2009b), and maintenance (Kim et al., 2008) of synapses. The overexpression of neuroligin in particular has been shown to result in an increase in the number of synapses as evidenced by an increase in mEPSC frequency (Levinson et al., 2005; Prange et al., 2004), an increase in the density of spines (Boucard et al., 2005; Chih et al., 2005), and an increase in both pre- and postsynaptic markers by immunostaining (Chih et al., 2005; Levinson et al., 2005). We sought to determine which aspects of neuroligin-induced synaptogenesis are dependent on dimerization. For the remainder of the experiments we chose to use NLGN3, owing to the more severe effects of dimerization-null mutations and less variable effects of overexpression. We used just one dimerization-null mutant for consistency ($NLGN3^{DM2}$ in Figure 1, hereafter referred to as $NLGN3^{D-N}$), although we saw no differences between different dimerization mutants on any test of function. Based on the evidence that dimerization-null mutants of neuroligin can still induce spinogenesis (Ko et al., 2009b), but that clustering of neurexin has been shown to induce presynaptic differentiation (Dean et al., 2003), we hypothesized that there may be a differential requirement for neuroligin dimerization with regard to post- and trans-synaptic effects. Indeed, we were able to replicate the previous finding that expression of a dimerization-null mutant of neuroligin can increase the density of spines (Fig. 3A), even though we showed that this same mutant does not retain the ability to enhance synaptic currents. To further investigate the synaptic deficit

of the dimerization-null mutant, we moved to dissociated hippocampal cultures to allow for immunostaining of the pre- and postsynaptic components of a synapse.

Neuroligin has been shown to increase immunostaining for the postsynaptic scaffolding molecule PSD-95 (Chih et al., 2005), consistent with its enhancement of postsynaptic currents and spine density. We confirmed this enhancement of PSD-95 upon the expression of wild-type NLGN3 (Fig. 3B) and additionally found an increase in PSD-95 staining following expression of the dimerization mutant (Fig. 3B) – again, not surprisingly given our prior finding of an increase in spine density. However, the relative magnitude of PSD-95 enhancement by wild-type and dimerization-null NLGN3 was different, with wild-type inducing a significantly larger postsynaptic effect. This could indicate a postsynaptic impairment in the dimerization-null mutant, or that this postsynaptic effect is secondary to the trans-synaptic effects presented below.

Typically, postsynaptic expression of neuroligin results in an increase in the presynaptic marker VGLUT1 (Chih et al., 2005; Levinson et al., 2005) via a trans-synaptic interaction with presynaptic neurexin. We could clearly show this presynaptic enhancement of VGLUT1 following the overexpression of wild-type NLGN3, but not with the dimerization-null mutant of NLGN3 (Fig. 3C). Rather, expression of the dimerization-null neuroligin actually reduced the amount of VGLUT1. Thus, the trans-synaptic effects of neuroligin would seem to depend on intact dimerization. A closer examination of the PSD-95 immunostaining reveals an increase in PSD-95 puncta density following expression of dimerization-null NLGN3 with no significant change in puncta size or intensity (Fig. 4A-D), while the VGLUT1 immunostaining shows a similar, but opposite effect. That is, a reduction in VGLUT1 puncta density with no change in puncta size or intensity (Fig. 4E-H). While not entirely conclusive, this finding is consistent with all-or-none effects on both pre- and postsynaptic assembly, rather than modifications of synaptic strength. It would appear, then, that the ability of neuroligin to induce the

assembly of postsynaptic components of a synapse remains largely intact in the absence of dimerization, whereas its ability to induce the clustering of the functional presynaptic components of a synapse is compromised. Further, the dominant-negative effect of the NLGN3 dimerization mutants on synaptic currents must have a primarily presynaptic locus of origin.

A rigorous test of neuroligin dimerization-driven synaptic assembly

Given the remarkable dependence of neuroligin on dimerization for its trans-synaptic effects, we wondered how exactly the mutations that we introduced were exerting their effects on the protein. One possibility may be that there are protein interaction sites near the dimerization domain that mediate interactions other than dimerization, which could have been inadvertently affected by our dimerization mutations, or that there exist specific protein interaction sites that occur only in an uncompromised native neuroligin dimer. An alternative explanation would be that simple mechanical clustering of the interacting partners of neuroligin is the driving force behind neuroligin-induced synaptogenesis, and that such clustering is dependent on the presence of dimerized neuroligin.

We decided to test the mechanical clustering hypothesis by introducing chemically-inducible dimerization domains into dimerization-null mutants of NLGN3. In this way, we can artificially cluster the monomeric NLGN3 mutants acutely. If this chemically-induced dimerization is able to rescue the function of the dimerization-null mutants, we can conclude that there is a simple mechanical clustering requirement for neuroligin-induced synaptogenesis, whereas, conversely, a lack of rescue upon chemical-induced dimerization would suggest that the effect of these dimerization mutations is more complex. We used a chemically inducible dimerization domain initially

based on FKBP12 and its small molecule ligand FK506 (Spencer et al., 1993), modified to induce dimerization in the absence of endogenous interactions (Clackson et al., 1998). We tested inclusion of the inducible dimerization domain in numerous positions along the length of neuroligin, including several near the original dimerization domain and several in more distant regions of the protein.

In a wild-type NLGN3, only inclusion of the chemically inducible dimerization domain at the extreme intracellular C-terminus of neuroligin resulted in a functional protein, as evidenced by retention of the synaptogenic overexpression phenotype. Insertion of the dimerization domain in membrane-proximal regions of the intracellular tail or in any position in the extracellular domain resulted in elimination of endogenous function of the protein. We have previously shown that the extreme end of the cytoplasmic tail is not required for neuroligin function, explaining the tolerance to the inclusion of this artificial domain at that position (Shipman et al., 2011). However, as the C-terminus is quite distant from the endogenous dimerization domain and, indeed, is in the intracellular rather than extracellular compartment, we believe that this represents a rigorous test of the clustering hypothesis. Thus, the aim of this experiment was to express a monomeric NLGN3 by mutating the endogenous dimerization domain, and then chemically induce dimerization in these expressed proteins through an artificial dimerization domain to test the synaptogenic effects of neuroligin clustering (Fig. 5A).

We found that, as expected, mutation of the endogenous dimerization domain in a NLGN3 construct containing the artificial inducible dimerization domain ($NLGN3^{D\text{-}N}$-iDmr) resulted in decreased excitatory synaptic currents rather than the increased currents that are evident upon expression of wild-type NLGN3 (Fig. 5B). We then exposed slices containing cells that expressed the $NLGN3^{D\text{-}N}$-iDmr construct to the dimerizing compound. We found that, over the course of 48 hours, the synaptogenic phenotype of neuroligin expression in the dimerization-null mutant was recovered by

artificial dimerization. Specifically, in cells expressing the NLGN3$^{D\text{-}N}$-iDmr construct, the amplitude of evoked excitatory synaptic currents as compared with those currents in neighboring control cells was enhanced by the addition of the dimerizing compound, such that after 48 hours the phenotype was indistinguishable from wild-type expression (Fig. 5B). Given that this inducible, artificial dimerization does not recapitulate the endogenous site, but rather induces dimerization via an independent domain, we conclude that dimerization of neuroligin is required for its synaptogenic phenotype due to a simple clustering mechanism. We did not see evidence for further enhancement with longer exposure to the dimerizing compound.

Given the ability of chemically-induced dimerization to rescue function, we next tested whether chemically-induced monomerization would acutely recapitulate the phenotype of expressing a monomeric neuroligin. This experiment was designed to distinguish between two alternative possibilities: first, that monomeric neuroligin is an ineffective synaptogenic molecule; or second, that the presence of monomeric neuroligin acutely inhibits synaptic function. To do this we employed a strategy similar to that of the chemically induced dimerization. Using a dimerization-null NLGN3 as our starting point, we added a domain to the extreme c-terminus, which natively forms a dimer but is converted into a monomer in the presence of a solubilizing compound, based on the same principles as the inducible dimerization domain (Fig. 5C). Similar to a wild-type neuroligin, expression of this artificially dimerized neuroligin (NLGN3$^{D\text{-}N}$-revDmr, for reverse dimerization) resulted in enhanced excitatory synaptic currents, in stark contrast to the dimerization-null mutant (Fig. 5D) – once again confirming that the requirement for neuroligin dimerization is simple clustering rather than a special property of the endogenous dimerization domain. Furthermore, incubation of cells expressing the NLGN3$^{D\text{-}N}$-revDmr construct in the solubilizing compound for 24 hours resulted in an elimination of the enhancement of synaptic currents as compared with the currents in

neighboring control cells (Fig. 5D). Given the timeframe and magnitude of reduction in synaptic currents in the presence of the solubilizer, we believe that this result is consistent with the model that monomeric neuroligin actively inhibits the occurrence of fully functional synapses and suggests a lasting role for the neuroligin/neurexin complex at existing synapses.

Discussion

We set out to test the specific requirements of neuroligin dimerization for the formation and maintenance of synapses. Our results indicate that dimerization is required for the synaptogenic effects of neuroligin, but that this requirement is primarily due to a trans-synaptic effect on the presynaptic site. Moreover, we find that the synaptogenic effects of the neuroligin dimer are achieved via a simple clustering mechanism. Thus, we put forward a model whereby postsynaptic neuroligin, in its native dimerized state, binds previously monomeric, axonal neurexin and induces differentiation into a functional presynaptic site (Fig. 5E). These conclusions largely confirm the hypothesis originally presented by Dean et al. (Dean et al., 2003) with respect to the clustering of neurexin.

We cannot state with absolute certainty whether the postsynaptic function of dimerization-null neuroligin is entirely unaffected. While we saw evidence for increases in PSD-95 staining and spine density upon expression of the dimerization-null neuroligin, indicating retention of at least some postsynaptic function, the enhancement of PSD-95 staining by the dimerization-null mutant was of a smaller magnitude than was seen with expression of wild-type neuroligin. It is, therefore, possible that monomeric neuroligin is less effective at inducing the assembly of the postsynaptic components of a synapse. Alternatively, it could be that the postsynaptic sites induced by the dimerization-null neuroligin are less mature or are functionally stunted due to the lack of an opposing glutamate release site.

It should be noted that, although our interpretation of the results of this study has contrasted the function of monomeric versus dimeric neuroligin, we cannot rule out the formation of higher-order assemblies occurring downstream of neuroligin dimerization – though weaker dimer-dimer interactions or though intermediate proteins. Dean et al.

(Dean et al., 2003) found recruitment of synaptic vesicles following the clustering of neurexin with multimerized, but not dimerized, antibody suggesting that higher-order complexes of neuroligin might be necessary to exert a trans-synaptic effect. Moreover, there is structural evidence in support of lateral neuroligin/neurexin sheets at the synapse (Tanaka et al., 2012). Acute dimerization of our expressed constructs via the chemically-inducible dimerization could, therefore, be permissive for the assembly of higher-order complexes, which may be required for the synaptic effects that we observe.

It would seem, from the bulk of our results, that the presence of monomeric neuroligin actively excludes the presence of a functional presynaptic terminal through a trans-synaptic action. That is, a diffuse arrangement of neurexin when bound to monomeric neuroligin – as opposed to the aggregated arrangement that normally occurs when bound to dimerized neuroligin – can inhibit the formation of presynaptic terminals. This may be a fundamental principle underlying neuroligin physiology with ramifications even outside the central nervous system; in fact, a recent study found that clustered neuroligin stimulates trans-cellular insulin release from pancreatic β cells (acting through an unknown partner other than neurexin) whereas diffuse neuroligin does not (Suckow et al., 2012). Within the CNS, neuroligins are only one class of what is an emerging superfamily of postsynaptic neurexin ligands, including LRRTMs (de Wit et al., 2009; Ko et al., 2009a; Linhoff et al., 2009), cerebellins (Uemura et al., 2010), and the G-protein-coupled receptor CIRL1/Latrophlin-1 (Boucard et al., 2012), which, together with neurexin, are situated within an even larger class of synaptic adhesion complexes, including those formed by cadherins (Arikkath and Reichardt, 2008), SynCAMs (Biederer et al., 2002), netrin-G ligand-3 and receptor protein tyrosine phosphatases (Kwon et al., 2010; Woo et al., 2009), and teneurins (Mosca et al., 2012). Given the apparent mechanistic requirement of neurexin clustering for neuroligin-induced synaptogenesis, it

will be of considerable interest to explore the extent to which this is a shared function among neurexin ligands and synaptic adhesion complexes in general.

Figure 1. Mutations of neuroligin affecting dimerization abolish the synaptogenic effects of postsynaptic expression.

(A) Structure of the neuroligin 1/neurexin 1beta extracellular domains viewed side-on looking through the synaptic cleft. Schematic to the left (neuroligin in blue, neurexin in purple) indicates the viewing angle. To the right, two neuroligin molecules, shown in dark and light blue, form a dimer with each neuroligin molecule bound to neurexin, shown in purple. Calcium ions at the neuroligin/neurexin interface are shown in grey. Locations of the dimerization-inhibiting mutations are indicated in orange. Structure from Araç et al. (Arac et al., 2007). **(B)** As in A, but viewed from the presynaptic side of the synapse, looking toward the postsynaptic side. **(C)** Postsynaptic expression of wild-type NLGN1 results in increased AMPAR-mediated EPSCs as compared to control ($p<0.01$, $n=11$), while the expression of dimerization-null mutants do not ($NLGN1^{DM1}$ $p>0.05$, $n=15$; $NLGN1^{DM2}$ $p>0.05$, $n=10$; $NLGN1^{DM3}$ $p>0.05$, $n=8$). Open circles represent individual pairs, closed circles indicate mean ±SEM. **(D)** Postsynaptic expression of wild-type NLGN3 also results in increased AMPAR-mediated EPSCs as compared to control ($p<0.001$, $n=12$), while expression of dimerization-null mutants result in decreased AMPAR-mediated EPSCs ($NLGN3^{DM1}$ $p<0.005$, $n=9$; $NLGN3^{DM2}$ $p<0.05$, $n=11$; $NLGN3^{DM3}$ $p<0.05$, $n=9$). As in C, open circles represent individual pairs, closed circles indicate mean ±SEM. Expression of wild-type NLGN1 and NLGN3, previously shown in Shipman et al. (Shipman et al., 2011) are repeated here for clarity. Sample traces in C and D show individual paired recordings with control AMPAR-mediated currents in black and experimental in green (scale bar: 20pA/20ms).

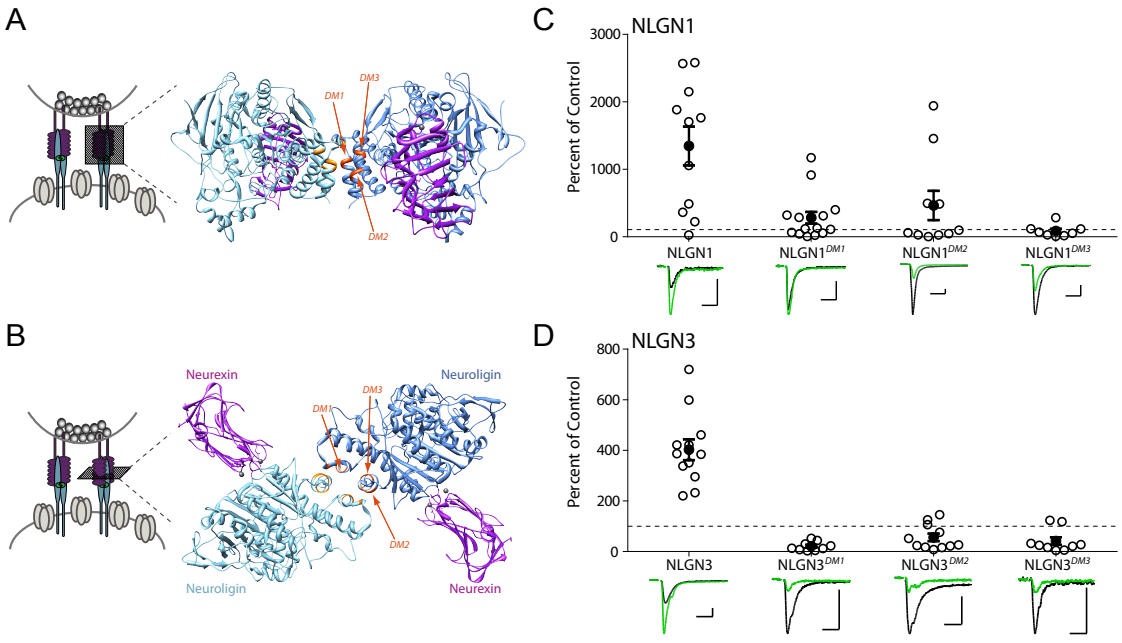

A
DM3
DM1
DM2
B
Neurexin
Neuroligin
DM3
DM1
DM2
Neuroligin
Neurexin
C
NLGN1
Percent of Control
3000
2000
1000
0
NLGN1
NLGN1DM1
NLGN1DM2
NLGN1DM3
D
NLGN3
Percent of Control
800
600
400
200
0
NLGN3
NLGN3DM1
NLGN3DM2
NLGN3DM3

Figure 2. Trafficking of the dimerization-null mutants.

(A) Surface staining against an HA-tag in the extracellular domain of wild-type NLGN1, NLGN1^{DM1}, NLGN1^{DM2}, or NLGN1^{DM3} (far left, in green) expressed in dissociated hippocampal neurons. Soluble mCherry marks the transfected cell (middle, red). Merged image is shown to the far right. **(B)** As in A, but for HA-tagged NLGN3, NLGN3^{DM1}, NLGN3^{DM2}, or NLGN3^{DM3}. **(C)** Addition of the N702L mutant to wild-type NLGN3, NLGN3^{DM1}, or NLGN3^{DM2} does not change the synaptic phenotype of postsynaptic expression in hippocampal neurons. Expressed as percent of control, comparing transfected neurons in organotypic slice culture to neighboring control neurons. Sample traces to the right show individual paired recordings with control AMPAR-mediated currents in black and experimental in green (scale bar: 20pA/20ms).

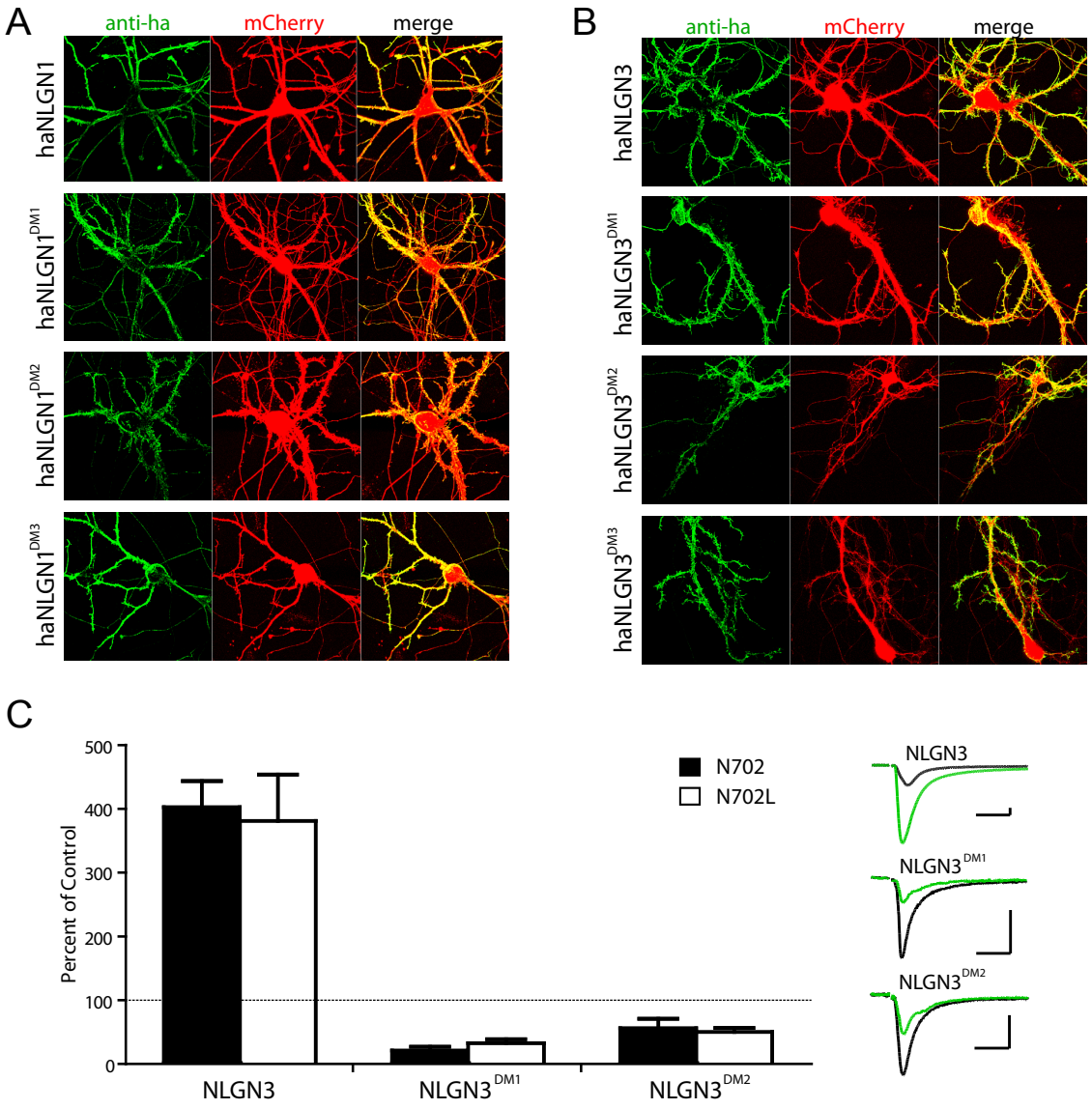

A
anti-ha
mCherry
merge
haNLGN1
haNLGN1DM1
haNLGN1DM2
haNLGN1DM3
B
anti-ha
mCherry
merge
haNLGN3
haNLGN3DM1
haNLGN3DM2
haNLGN3DM3
C
Percent of Control
500
400
300
200
100
0
N702
N702L
NLGN3
NLGN3DM1
NLGN3DM2
NLGN3
NLGN3DM1
NLGN3DM2

Figure 3. Dimerization-null neuroligin mutant retains the ability to enhance the postsynaptic site in the absence of presynaptic enhancements.

(A) Postsynaptic expression of $NLGN3^{D-N}$ results in an increased spine density along the apical dendrite of CA1 pyramidal neurons in organotypic hippocampal cultures as compared to control neurons ($p<0.0001$, n=8 ctrl, 8 expt). Circles represent individual cells, horizontal bars indicate mean ±SEM. Sample images show individual sections of dendrite (scale bar: 5μm). **(B)** Postsynaptic expression of either wild-type or dimerization-null NLGN3 increases PSD-95 immunofluorescence intensity in dissociated hippocampal neurons (NLGN3 $p<0.001$, n=12; $NLGN3^{D-N}$ $p<0.05$, n=12; ctrl n=13). Circles represent individual cells, horizontal bars indicate mean ±SEM. In sample images, dendrites are shown using mCherry, red (left), while PSD-95 staining is in green (right) (scale bar: 5 μm). **(C)** Postsynaptic expression of wild-type NLGN3 increases VGLUT1 staining onto the postsynaptic cell ($p<0.005$, n=7; ctrl n=7), while expression of $NLGN3^{D-N}$ decreases VGLUT1 staining onto the postsynaptic cell ($p<0.05$, n=9). Circles represent individual cells, horizontal bars indicate mean ±SEM. In sample images, dendrites are shown using mCherry, red (left), while VGLUT1 staining is in green (right) (scale bar: 5 μm).

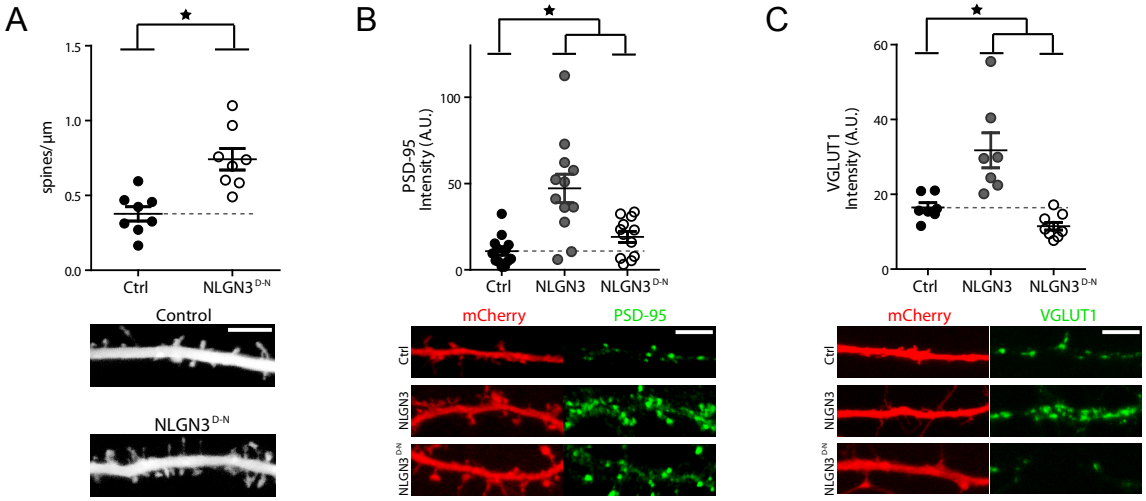

A
spines/µm
1.5
1.0
0.5
0.0
Ctrl
NLGN3D-N
Control
NLGN3D-N
B
PSD-95 Intensity (A.U.)
100
50
0
Ctrl
NLGN3
NLGN3D-N
mCherry
PSD-95
Ctrl
NLGN3
NLGN3D-N
C
VGLUT1 Intensity (A.U.)
60
40
20
0
Ctrl
NLGN3
NLGN3D-N
mCherry
VGLUT1
Ctrl
NLGN3
NLGN3D-N

Figure 4. Additional analysis of immunostained puncta.

(A) Sample images of PSD-95 immunostaining for control and $NLGN3^{D-N}$ conditions. In each case, original image is shown on top with individual puncta outlined below (scale bar: 5μm). **(B)** PSD-95 puncta density expressed as puncta/50μm showing an increase in density following the expression of $NLGN3^{D-N}$ ($p<0.05$, n=13 ctrl, 12 expt). **(C)** No change in PSD-95 puncta size (μm^2) following expression of $NLGN3^{D-N}$ ($p>0.05$, n=13 ctrl, 12 expt). **(D)** No change in PSD-95 puncta intensity following the expression of $NLGN3^{D-N}$ ($p>0.05$, n=13 ctrl, 12 expt). **(E)** Sample images of VGLUT1 immunostaining for control and $NLGN3^{D-N}$ conditions. As in *A*, original image is shown on top with individual puncta outlined below (scale bar: 5μm). **(F)** Expression of $NLGN3^{D-N}$ results in a reduction of VGLUT1 puncta ($p<0.05$, n=13 ctrl, 12 expt). **(G)** No change in VGLUT1 puncta size (μm^2) following expression of $NLGN3^{D-N}$ ($p>0.05$, n=13 ctrl, 12 expt). **(H)** No change in VGLUT1 puncta intensity following the expression of $NLGN3^{D-N}$ ($p>0.05$, n=13 ctrl, 12 expt). For all scatter plots (B-D, F-H), circles represent individual cells, horizontal bars indicate mean ±SEM.

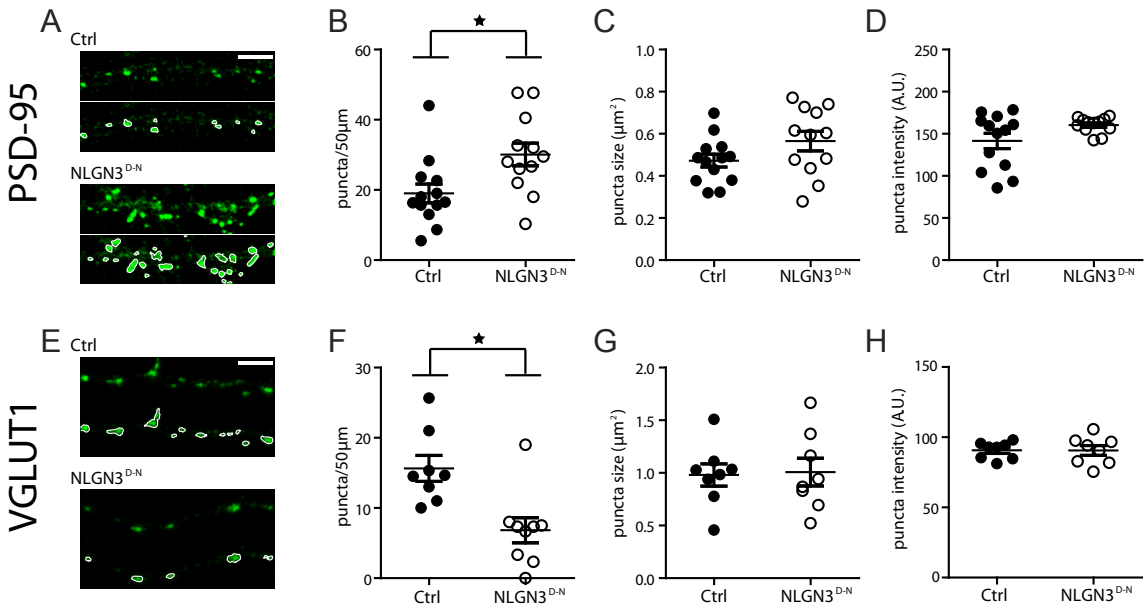
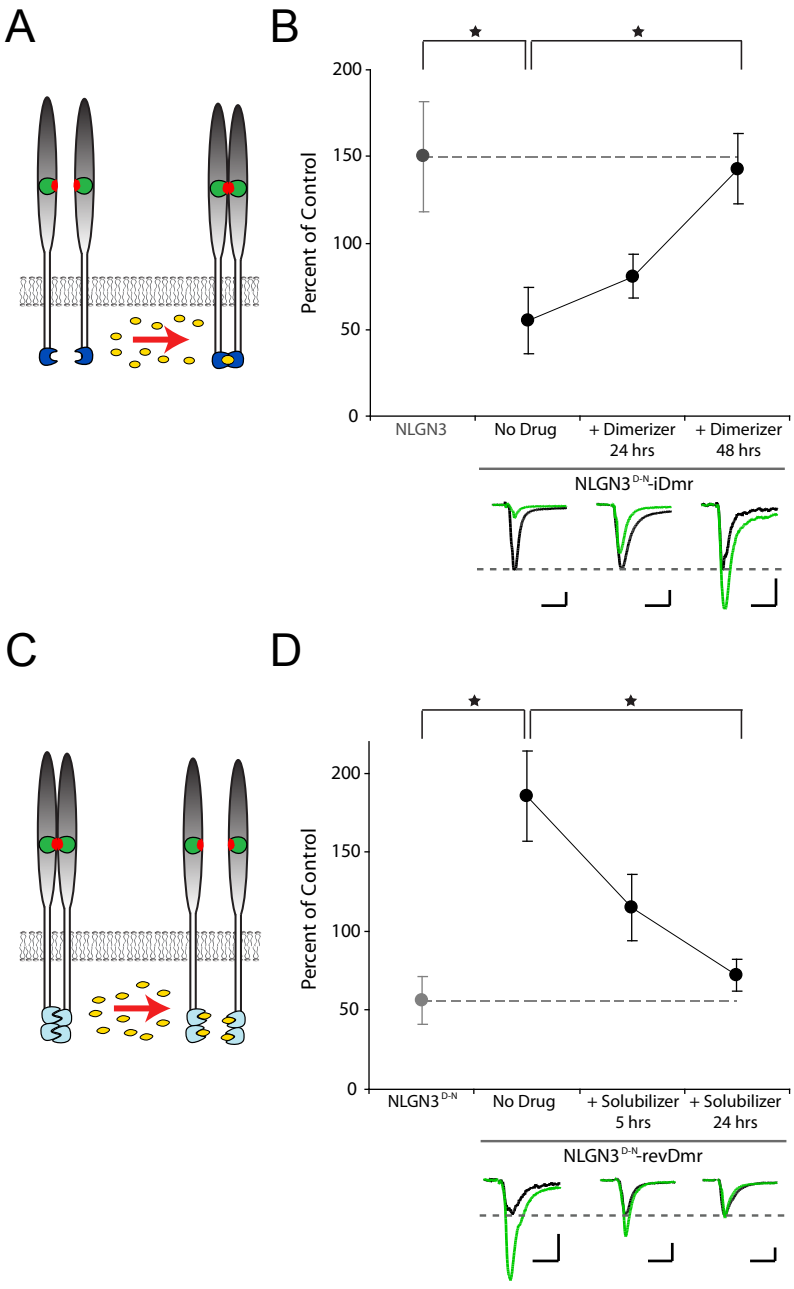

A
Ctrl
NLGN3 D-N
PSD-95
B
puncta/50µm
60
40
20
0
Ctrl
NLGN3 D-N
C
puncta size (µm²)
1.0
0.8
0.6
0.4
0.2
0.0
Ctrl
NLGN3 D-N
D
puncta intensity (A.U.)
250
200
150
100
50
0
Ctrl
NLGN3 D-N
E
Ctrl
NLGN3 D-N
VGLUT1
F
puncta/50µm
30
20
10
0
Ctrl
NLGN3 D-N
G
puncta size (µm²)
2.0
1.5
1.0
0.5
0.0
Ctrl
NLGN3 D-N
H
puncta intensity (A.U.)
150
100
50
0
Ctrl
NLGN3 D-N

Figure 5. Chemically-induced dimerization and monomerization can acutely alter the synaptic phenotype of neuroligin expression.

(A) Schematic of induced-dimerization experiments. Neuroligin monomers with a mutated endogenous dimerization domain (green/red) and an exogenous, inducible dimerization domain (blue) at the extreme c-terminus are acutely dimerized via the addition of the small molecule B/B Homodimerizer (AP20187) (yellow). **(B)** Acute dimerization rescues the synaptogenic phenotype of the dimerization-null neuroligin mutant. In the absence of the homodimerizing compound, expression of the NLGN3$^{D\text{-}N}$-iDmr construct has an inhibitory effect on evoked AMPAR-mediated EPSCs as compared to wild-type NLGN3 expression ($p<0.005$). Yet, 48 hours of exposure to the B/B Homodimerizer results in an increase in the AMPAR-mediated current amplitudes as compared to the no drug condition ($p<0.005$), rescuing the phenotype to a wild-type level (48 hour condition versus wild-type expression, $p>0.05$) (NLGN3 n=12; NLGN3$^{D\text{-}N}$-iDmr no drug condition n=9, 24 hour homodimerizer n=10, 48 hour homodimerizer n=10). Closed circles indicate mean AMPAR-mediated current amplitudes expressed as percent of control amplitudes for all paired recordings ±SEM. Example traces illustrate individual pairs, with control cells shown in black and experimental cells shown in green (scale bar: 20pA/20ms) **(C)** Schematic of the induced-monomerization experiments. Dimerization-null mutant neuroligin is artificially dimerized via an exogenous domain (light blue) that, in the presence of the small molecule D/D Solubilizer (yellow), is converted to monomeric state. **(D)** Artificial dimerization via the exogenous dimerization domain rescues basal synaptogenic properties of neuroligin as evidenced by an increase in AMPAR-mediated synaptic currents upon expression of NLGN3$^{D\text{-}N}$-revDmr as compared to NLGN3$^{D\text{-}N}$ in the absence of drug ($p<0.005$). NLGN3$^{D\text{-}N}$ expression, originally shown in Figure 1D is repeated here for clarity. Monomerization of NLGN3$^{D\text{-}N}$-

revDmr by the addition of the D/D Solubilizer results in elimination of the synaptogenic phenotype as compared to the no drug condition ($p<0.005$), returning the synaptic phenotype to the dimerization-null condition (24 hour condition versus $NLGN3^{D-N}$ expression, $p>0.05$) ($NLGN3^{D-N}$ n=10; $NLGN3^{D-N}$-revDmr no drug condition n=12, 5 hour solubilizer n=8, 24 hour solubilizer n=10). Closed circles indicate mean AMPAR-mediated current amplitudes expressed as percent of control amplitudes for all paired recordings ±SEM. Example traces illustrate individual pairs, with control cells shown in black and experimental cells shown in green (scale bar: 20pA/20ms). **(E)** Model for neuroligin-induced synaptogenesis whereby postsynaptic, dimerizered neuroligin binds to and clusters presynaptic neurexin, leading to the differentiation of a presynaptic terminal.


A
B
200
150
100
50
0
Percent of Control
NLGN3
No Drug
+ Dimerizer 24 hrs
+ Dimerizer 48 hrs
NLGN3 D-N-iDmr
C
D
200
150
100
50
0
Percent of Control
NLGN3 D-N
No Drug
+ Solubilizer 5 hrs
+ Solubilizer 24 hrs
NLGN3 D-N-revDmr
E
Neurexin
Neuroligin

CHAPTER 4:

Functional dependence of neuroligin on a new non-PDZ intracellular domain

Introduction

Synaptic junctions are points of both functional and anatomical connection between neurons. The functional connection, in the form of a chemical synapse, underlies the unique ability of a neuron to relay signals, allowing any given cell to integrate information received in thousands of discrete units from distant or nearby cells. Prior to the assembly of the components necessary for functional chemical transmission, however, synaptic points of contact must be established anatomically. This initial step is thought to occur through a physical interaction between trans-acting synaptic adhesion molecules of various types (de Wit et al., 2009; Dean and Dresbach, 2006; Washbourne et al., 2004; Yamagata et al., 2003). Indeed, neuroligins – a critical family of adhesion molecules on the postsynaptic side – are able to induce the formation and maturation of synapses through an interaction with presynaptic neurexin (Chih et al., 2005; Song et al., 1999; Sudhof, 2008; Wittenmayer et al., 2009). This synapse-spanning complex is capable of inducing both pre- and postsynaptic specializations in artificial synapse assays using beads (Graf et al., 2004) as well as non-neuronal cells (Fu et al., 2003; Nam and Chen, 2005; Scheiffele et al., 2000). Furthermore, extensive evidence suggests that mutations in neuroligin genes cause cognitive impairments in humans including autism (Daoud et al., 2009; Jamain et al., 2003; Lawson-Yuen et al., 2008; Sudhof, 2008), and behavioral and memory alterations in mice (Blundell et al., 2010; Kim et al., 2008; Radyushkin et al., 2009).

Neuroligins are a family of single-pass transmembrane proteins with an extracellular acetylcholinesterase-like domain that both interacts with neurexin and is responsible for dimerization between neuroligins (Arac et al., 2007; Fabrichny et al., 2007). In addition, a short cytoplasmic tail contains a number of motifs thought to be necessary for the scaffolding of postsynaptic components; these include a PSD-95/Discs

large/zona occludens-1 (PDZ) ligand, a WW-binding domain, and a gephyrin-binding site (Iida et al., 2004; Irie et al., 1997; Poulopoulos et al., 2009). Neuroligins 1–4 (NLGN1–4) are expressed in both rodents and humans and are thought to share many of the same functions. However, some noted specializations have been described. NLGN1 is primarily localized to excitatory synapses, whereas NLGN2 is localized to inhibitory synapses and NLGN3 is found at both (Budreck and Scheiffele, 2007; Graf et al., 2004; Levinson et al., 2005; Song et al., 1999; Varoqueaux et al., 2004). The existence of such specialization is supported by single knockouts and overexpression of NLGN1 or NLGN2 individually (Chubykin et al., 2007), although, paradoxically, the individual knockdown of NLGN1 does not reduce excitatory currents (Futai et al., 2007) and overexpressed proteins of both subtypes are capable of localizing to and potentiating either type of synapse (Levinson et al., 2005; Prange et al., 2004). The presence of compensation with single knockdown, as well as the loss of synapse-type segregation with overexpression, may be due to the ability of these proteins to heterodimerize with NLGN3, which is located at both excitatory and inhibitory synapses (Budreck and Scheiffele, 2007). The fourth member of the family is less well characterized and, although it possesses a characteristic neuroligin structure in humans, is not well conserved in mice (Bolliger et al., 2008).

Though several interactions between the cytoplasmic tail of neuroligin and postsynaptic scaffolding molecules have been described biochemically, resolving the relative importance of these interactions for the function of endogenous neuroligin in neurons has proven difficult. Indeed, the overexpression of truncation mutants lacking the canonical binding domains often reveal little or no phenotypic difference from overexpressed wild-type protein (Dresbach et al., 2004; Ko et al., 2009b). These negative results could be explained by dimerization between overexpressed mutated protein and endogenous neuroligin, which may obscure the effect of the mutation.

Unfortunately, one cannot study the function of neuroligins in the absence of dimerization, because dimerization itself is required for normal neuroligin function (Dean et al., 2003). Further complication is introduced by the demonstration that neuroligins can heterodimerize (Budreck and Scheiffele, 2007), limiting the use of overexpression on the background of any single knockout. Finally, a triple knockout generated with loss of neuroligins 1–3 dies at birth, so extensive experimentation on a null background has thus far not been possible (Varoqueaux et al., 2006).

In this study, we tested the functional importance of the cytoplasmic domain of neuroligin on a background of reduced endogenous neuroligin expression, which we achieved with a novel triple knockdown strategy. Surprisingly, we find that the canonical protein binding sites previously identified in the cytoplasmic tail of neuroligin play no obvious role in its ability to potentiate synaptic transmission. Instead, we identify a single critical residue in the cytoplasmic tail that is essential for the postsynaptic functional effects of neuroligins at excitatory synapses. Given the prior consensus in the field that the PDZ motif mediates neuroligins' primary post-synaptic interactions, these new functional findings force a redirection of study on a new molecular determinant of neuroligin function.

Results

Neuroligin c-tail is critical for functional replacement

To study the postsynaptic role of neuroligin, we used a dual whole-cell recording configuration in organotypic hippocampal slice cultures (Fig. 6A) to simultaneously record evoked excitatory postsynaptic currents (EPSCs) in a transfected and a nearby control cell. We first characterized neuroligin 3 (NLGN3) because of its endogenous expression at both excitatory and inhibitory synapses and its implication in the pathogenesis of autism (Budreck and Scheiffele, 2007; Jamain et al., 2003). We introduced exogenous human NLGN3 because it is not susceptible to knockdown with RNAi targeting rat NLGN3 due to differences at the nucleotide level between the rat and human neuroligins, despite their highly conserved amino acid sequences (Chih et al., 2005). On a wild-type background, overexpression of a full-length version of NLGN3 yielded an increase in AMPA receptor- (AMPAR) evoked currents (Fig. 6G), consistent with previous studies that report increases in the number of synaptic contacts onto neuroligin expressing cells (Ko et al., 2009b; Levinson et al., 2005; Prange et al., 2004). However, surprisingly, a truncated version of NLGN3 (NLGN3Δ90) also yielded increases in AMPAR-evoked currents of comparable magnitude, despite the loss of most of the cytoplasmic tail (Fig. 6G).

One possible explanation for the lack of an effect following the severe truncation of the cytoplasmic tail would be if endogenous neuroligin were able to compensate for the deficits of the truncation mutant. Dimerization and heterodimerization, which can occur between neuroligins (Arac et al., 2007; Budreck and Scheiffele, 2007; Fabrichny et al., 2007), might complicate the interpretation of results with exogenously expressed mutants. In COS cells, we confirmed that heterodimerization can occur between our NLGN1 and NLGN3 constructs and that full-length NLGN1 can dimerize with a truncated

version of NLGN3 (NLGN3Δ90) (Fig. 7A**)**. Moreover, in dissociated neuronal cultures we demonstrated that exogenous NLGN1 can heterodimerize with endogenous NLGN3 as shown by co-immunoprecipitation of endogenous NLGN3 with virally expressed, HA-tagged exogenous NLGN1 (Fig. 7B). Such dimerization between truncated and full-length neuroligin might mask the detection of a differential effect on AMPAR-evoked currents between the full-length and truncated neuroligins.

To minimize any possible influence of endogenous neurolgins, we employed a triple knockdown strategy using three exogenous microRNAs – one each to knock down neuroligins 1, 2, and 3 – chained together and expressed in a single transcript with GFP (Fig. 6B). These chained targeting sequences, previously characterized individually (Chih et al., 2005), yield an efficient knockdown of all three neuroligins from one construct (Fig. 6C). Expression of the neuroligin microRNAs (NLmiRs) substantially reduces both AMPAR- (Fig. 6D) and NMDA receptor- (NMDAR) evoked currents (Fig. 6E), demonstrating the integral nature of this protein family at excitatory synapses. Although neuroligins are known to affect the maturation of presynaptic terminals through their interaction with neurexin (Wittenmayer et al., 2009), removal of neuroligins had no effect on paired-pulse ratio, a measure of presynaptic release probability (Fig. 6F). Critically, when the same full-length or truncated versions of NLGN3 are co-expressed with the NLmiRs, the truncated version is no longer capable of potentiating AMPAR-evoked currents (Fig. 6H), which both illustrates the confounding influence of endogenous protein and firmly demonstrates that the cytoplasmic tail is necessary for full neuroligin function.

Neuroligin AMPAR effect is independent of established motifs

Given the clear functional dependence of neuroligin on its cytoplasmic tail, we next characterized the relative importance of several previously described protein binding motifs found there. To do so, we first co-expressed the NLmiRs with wild-type NLGN3 or NLGN3 that lacked the PDZ motif (NLGN3Δ4). Expression of wild-type NLGN3 on the reduced neuroligin background yields a dramatic increase in evoked AMPAR current amplitude. Yet, surprisingly, the elimination of the canonical PDZ binding motif did not affect the enhancement of AMPAR currents compared to wild-type NLGN3 (Fig. 8A). This finding is in contrast to that of a previous study (Nam and Chen, 2005), which found reductions in AMPAR- and NMDAR-evoked currents with the expression of a CFP-tagged NLGN1 construct lacking the PDZ binding motif. However, subsequent studies have not reported such dominant-negative phenotypes with the expression of PDZ-truncated neuroligins on a wild-type background (Chen et al., 2010; Chih et al., 2005). The difference in findings may therefore result from the different constructs used and perhaps the inclusion of an extracellular cyan fluorescent protein tag.

To further characterize the role of previously described cytoplasmic binding domains, we made subsequent truncations to eliminate the WW-binding domain (NLGN3Δ46) and the gephyrin-binding domain (NLGN3Δ77) (Fig. 8A). Similarly, we saw no effect on NLGN3 function, indicating that interactions between NLGN3 and PSD-95, S-SCAM, and gephyrin mediated by these sites in the cytoplasmic tail are not required for enhancement of excitatory postsynaptic currents by neuroligin.

Novel intracellular region required for synaptic effect

As none of the previously identified binding sites affected the postsynaptic NLGN3 phenotype, we made further truncations to ascertain whether other sites on the cytoplasmic tail contribute to the postsynaptic function of this protein. Indeed, we find that removing more than 77 residues (NLGN3Δ90, NLGN3Δ99, NLGN3Δ109) from the C-terminus eliminates the enhancement of AMPAR currents by NLGN3 as compared to control cells (Fig. 8A,B), signifying the presence of a previously undescribed critical region in the cytoplasmic tail that is essential for postsynaptic potentiation. To define this critical region more narrowly, we next selectively deleted a total of 13 amino acids between amino acid 77 and 90, counting from the C-terminus (NLGN3Δ77–90). Like the truncation mutants, this deletion eliminated the enhancement of AMPAR currents on the reduced-neuroligin background (Fig. 8A,B) despite the inclusion of PDZ, WW-binding, and gephrin-binding domains. We next took advantage of a recent finding that neuroligin 4 (NLGN4), when overexpressed, causes a dominant-negative-like reduction in excitatory currents (Zhang et al., 2009), in stark contrast with the enhancement of currents that results from the overexpression of the other neuroligins. There are three amino acid differences in NLGN4 within the critical region that are conserved between NLGN1 and NLGN3, one of which is a substitution from a negatively charged glutamic acid to a polar asparagine (Fig. 10A). To test the dependence of neuroligin function on this residue, we made a NLGN3 point-mutant, switching the glutamic acid at position 740 for asparagine (NLGN3 E740N). Strikingly, this single point mutation eliminated the enhancement of AMPAR currents by NLGN3 when co-expressed with the NLmiRs (Fig. 8A,B).

As expected, overexpression of NLGN3 postsynaptically induces a presynaptic effect, as evidenced by a decrease in paired-pulse ratio, a measure of release

probability (Fig. 8C). This increase in the probability of release is seen with all of the truncation mutants that do not abolish the AMPAR enhancement, but is not present in the deletion mutant or point-mutant that lack an enhancement of AMPAR currents (Fig. 8C). This indicates that functional enhancement of the postsynaptic side is necessary for neuroligin-induced maturation of presynaptic terminals. However, this increase in release probability upon overexpression of full-length NLGN3 and near truncation mutants is not sufficient to explain the enhancement of AMPAR currents, as wild-type NLGN3 does not induce a similar enhancement of NMDAR currents, which would be expected if the effect were primarily presynaptic (Fig. 8D). Moreover, the effect of the point-mutation is not due to a deficit in surface trafficking, as surface levels of the point-mutant are identical to those of the full-length (Fig. 9A). Critically, the effects of these various mutants can only be seen on the background of reduced endogenous neuroligin expression. Indeed, expression of the point-mutant (NLGN3 E740N) on a wild-type background results in enhancements of AMPAR currents that are indistinguishable from expressing full-length NLGN3 on a wild-type background (Fig. 9B).

To test whether this site is necessary for the function of neuroligin in general or is specific to NLGN3, we made the same amino acid swap in the corresponding residue (E747) of an RNAi-proof version of NLGN1 (NLGN1* E747N) (Fig. 10A). As with NLGN3, this single point-mutation in NLGN1* dramatically reduced the enhancement of AMPAR currents induced by NLGN1* expression on the background of the NLmiRs (Fig. 10B). Interestingly, the effect of NLGN3 is primarily restricted to AMPARs and not NMDARs (Fig. 8D) – a finding consistent with a preferential increase in AMPARs at new synapses or an unsilencing of synapses that previously contained only NMDARs. However, NLGN1* enhances both AMPAR- and NMDAR-mediated EPSCs (Fig. 10D). This difference between NLGN1 and NLGN3 has not previously been reported and can be observed only on a background of reduced endogenous neuroligin, presumably due

to heterodimerization between exogenous NLGN3 and endogenous NLGN1 that occurs on a wild-type background (Fig. 11A). Introducing the point-mutation E747N to NLGN1* also reduced the enhancement of NMDAR EPSCs (Fig. 10D), indicating that the effect of this mutation is upstream of a specific enhancement of either AMPAR or NMDAR currents. Like NLGN3, the effect of the NLGN1* E747N point-mutation was only apparent on the background of reduced endogenous neuroligin (Fig. 11B). Finally, since this amino acid swap was generated based on the sequence of NLGN4, we made the opposite mutation to NLGN4 (NLGN4 N726E) in the hope of transferring the NLGN3 phenotype to NLGN4. In fact, whereas the wild-type human NLGN4, when expressed singly, reduces both AMPAR and NMDAR currents, the point-mutant, which more closely matches the other neuroligins, enhances AMPAR currents and does not affect NMDAR currents (Fig. 10C,E), demonstrating that, in fact, this critical region is sufficient for the functional enhancement of AMPAR current by neuroligin. This effect can also be seen on the reduced-neuroligin background (Fig. 11C).

Effect of mutations is specific to excitatory synapses

We next tested whether this newly identified site is specific to excitatory synapses or extends to all synapse-promoting functions of neuroligin. The knockdown of neuroligins with the NLmiRs also reduces the amplitude of IPSCs as compared with control cells (Fig. 12A,B), implicating this family of proteins in inhibitory as well as excitatory synapse function. Neuroligin 2 (NLGN2) is the member of the family most closely associated with inhibitory synapses (Varoqueaux et al., 2004). Thus, along with the NLmiRs, we co-expressed an RNAi-proof version of neuroligin 2 (NLGN2*), which dramatically enhanced evoked inhibitory post-synaptic currents (IPSCs) (Fig. 12A,C). In this case, unlike the excitatory phenotype, a mutation of the analogous amino acid in

NLGN2 (NLGN2* E740N) had no effect on the magnitude of enhancement of inhibitory currents (Fig. 12A,D). NLGN3 produced only a modest rescue of the knocked-down currents and the point-mutant NLGN3 E740N also produced a modest rescue that was indistinguishable from that achieved by expressing NLGN3 (Fig. 12A).

These results indicate that this site is critical for excitatory synaptic function, but does not extend to inhibitory synapses. It is interesting that expression of NLGN3 on the knockdown background produced only a modest rescue of inhibitory currents whereas NLGN2* expression increased currents to a dramatic degree, given that both neuroligins have been shown to localize to inhibitory synapses (Budreck and Scheiffele, 2007; Graf et al., 2004). To explore this effect further, we examined the effect of NLGN3 expression on a wild-type background and found that this expression resulted in large increases in evoked IPSCs (Fig. 13). This raises the intriguing possibility that the presence of NLGN2 may be required for the function of NLGN3 at inhibitory synapses.

Neuroligin effect remains after synaptic blockade

It was previously reported that chronic blockade of NMDARs or CaM-Kinase II in dissociated neuronal cultures mitigates the effect of NLGN1 overexpression on evoked EPSCs and synapse density (Chubykin et al., 2007). This finding of activity-dependence has been used to support a model of neuroligin function in which the role of neuroligin is confined to the maturation rather than the genesis of synapses (Sudhof, 2008). The findings presented thus far could result from changes in either synaptic maturation or synaptogenesis. The slice culture system and dual whole-cell configuration provide an excellent opportunity to study pharmacologic manipulations, as both the control and transfected cells experience identical pharmacologic conditions.

To test whether our neuroligin effects are dependent on synaptic activity we co-expressed either NLGN3 or NLGN1*, each with the NLmiRs as before, but maintained the slices in NBQX and APV to block all fast excitatory synaptic transmission for the duration of the transfection (Fig. 14A). We found that the effects of NLGN1* and NLGN3 persisted when excitatory synaptic activity was blocked. Indeed, in these experiments as in the previous experiments, NLGN3 enhanced AMPAR- but not NMDAR-mediated currents (Fig. 14B) and NLGN1* enhanced both AMPAR- and NMDAR-mediated currents (Fig. 14C). Similar results were obtained upon co-expressing NLGN3 and the NLmiRs in the presence of only APV (Fig. 15). These findings are consistent with a previous report (Heine et al., 2008), which found no change in the ability of neurexin to cluster AMPARs at sites of NLGN/neurexin contact in the presence of either APV or TTX.

Neuroligin induces the assembly of new functional synapses

Finally, we examined miniature EPSCs (mEPSCs) to further define the basis for the enhancement of excitatory transmission by neuroligins. mEPSCs were recorded in both the wild-type and point-mutant forms of NLGN3, each co-expressed with the NLmiRs. We find that the wild-type form greatly increases the frequency of mEPSCs with no effect on amplitude, whereas the point-mutant displays a modest increase in frequency, but has a significant reduction in amplitude (Fig. 16A,B). Moreover, when we image both transfected and control neurons to examine spine density – an anatomical approximation of synapse number – we find that though the NLmiRs reduce the density of spines, both the wild-type and point-mutant forms of NLGN3 increase the density of spines (although the point-mutant does so to a lesser extent) (Fig. 16C). In contrast, NLGN3Δ77, which displays the same effect as the wild-type with respect to AMPAR

currents, also induces an increase in spine density of comparable magnitude to that of the wild-type on the background of the NLmiRs (Fig. 17).

Together, these results suggest that the enhancement of AMPAR currents by neuroligin is at least in part due to the assembly of new functional synapses. Furthermore, given that mEPSC amplitude is reduced by the expression of NLGN3 E740N even though both spine density and mEPSC frequency are higher than in wild-type, it appears that the point-mutant displays a specific postsynaptic deficit with respect to the recruitment of AMPARs to functional synapses. Notably, the effect of the point mutation is not a result of a trafficking deficit as GFP fusion constructs of both the full-length and the point-mutant clearly localize to spines (Fig. 16C). In further support of a specific postsynaptic deficit imparted by the point-mutation, we found that both wild-type and point-mutant versions of NLGN1 and NLGN3 increased presynaptic VGLUT1 staining to similar magnitudes when expressed on the background of the NLmiRs in dissociated neurons (Fig. 16D). This suggests that the trans-synaptic effects of neuroligin, via the interaction with presynaptic neurexin, are unaffected by the cytoplasmic point-mutation, but rather only the ability to functionally enhance the postsynaptic site is perturbed.

Discussion

In the current study we have used a combination of powerful approaches to examine the molecular determinants of neuroligin function at the post-synaptic site. Our findings clearly confirm the integral role of the neuroligin family of proteins to the function of both excitatory and inhibitory synapses, as evidenced by reductions in AMPAR- and NMDAR-mediated EPSCs as well as IPSCs in neurons with experimentally reduced levels of neuroligins 1–3. Furthermore, we have demonstrated, on this reduced background, that the canonical postsynaptic protein binding sites thought to mediate necessary interactions between neuroligin and other postsynaptic scaffolding molecules, such as S-SCAM and the MAGUK family (including PSD-95) are not required for the potentiation of excitatory synaptic currents seen when neuroligins are overexpressed. Rather, we identify a previously uncharacterized site in the cytoplasmic tail that is indispensible for the postsynaptic function of neuroligin at excitatory synapses. Based on our findings future research should focus on this new molecular domain rather than on the PDZ-mediated interactions of neuroligin, given the lack of a functional dependence on the PDZ motif. Ideally, our extensive molecular dissection of the relative importance of regions within the cytoplasmic domain of neuroligin will allow subsequent biochemical studies to identify new protein interactions at the postsynaptic site, among them those which occur earliest during the formation and assembly of excitatory synapses.

These findings required a reduced background of endogenous neuroligin to prevent a confounding influence observed in the presence of endogenous protein, which could be occurring as the result of dimerization between mutant and endogenous protein. Indeed, we have shown here that such heterodimerization does occur. We believe that this represents the most parsimonious explanation of the effects that we observe. However, since dimerization is required for the full function of neuroligin (Dean

et al., 2003), we cannot state definitively that heterodimerization is the cause of this confounding influence, but rather only that the presence of endogenous neuroligin does not allow for accurate study of exogenous mutant neuroligin. We believe that this represents an important step forward in the study of this family, as well as other families, of partially redundant proteins. Indeed, a confounding effect in the presence of endogenous neuroligin may explain the differing results that have been reported when neuroligin is expressed in either neurons or non-neuronal cells that have no endogenous neuroligin (Ko et al., 2009b).

Our findings also shed light on the synapse-specificity of neuroligin. The critical site identified in our experiments is specifically necessary for the function of neuroligin at excitatory, but not inhibitory, synapses. The gephyrin binding site in the cytoplasmic tail of NLGN2 (Poulopoulos et al., 2009) may account for its ability to enhance IPSCs, though we have shown here that the gephyrin binding is not required for the action of neuroligin at excitatory synapses. The role of neuroligins in the balance of excitation and inhibition has been the topic of much previous research (Levinson and El-Husseini, 2005). In fact, the mutations in NLGN3 that have been found in patients with autism may exert their phenotypic effect through a shift in the ratio of excitation to inhibition (Gutierrez et al., 2009; Tabuchi et al., 2007). Yet, the critical single residue identified in this study is present both in the neuroligins found endogenously at excitatory synapses, NLGN1 and NLGN3, as well as NLGN2, found exclusively at inhibitory synapses. This is reminiscent of the finding that the gephyrin-binding domain is present in all four neuroligins even though NLGN2 appears to be specifically required for the assembly of inhibitory synapses (Poulopoulos et al., 2009). Clearly, an unknown mechanism independent of specific, identified interaction sites in the cytoplasmic tail must segregate neuroligin subtypes to their respective synapses.

In addition to the subtype specializations at excitatory and inhibitory synapses, we report a difference in phenotype between NLGN1 and NLGN3. Specifically, the overexpression of NLGN1 enhances both AMPAR- and NMDAR-mediated excitatory currents, whereas the effect of NLGN3 overexpression is relatively restricted to AMPARs. This difference may reflect a primary role for NLGN3 in the unsilencing of synapses. Indeed, its overexpression mimics the known effects of synapse unsilencing that occur during synapse development and long-term potentiation, in which the selective increase in evoked AMPAR EPSCs is accompanied primarily by an increase in mEPSC frequency (Kerchner and Nicoll, 2008; Petralia et al., 1999). Although, given that NLGN3 rescues the NMDAR current from the knockdown level and increases spine density, it is unlikely that the sole effect of NLGN3 is due to the unsilencing of synapses. Conversely, the more equivalent enhancements of both AMPAR and NMDAR currents seen with NLGN1 may reflect a role that is shifted toward the creation of new functional synapses. The striking functional segregation between NLGN1 and NLGN3 raises a number of interesting issues. For instance, matched increases in AMPARs and NMDARs, as are observed with the expression of NLGN1, are reminiscent of a developmental global increase in synapses. Whereas specific modulation of AMPARs, as is the case with the expression of NLGN3, mirrors the changes that are most often seen during long-term potentiation (Bredt and Nicoll, 2003).

In contrast to the present results, several studies have presented evidence in support of a functional interaction between neuroligin and PSD-95 or S-SCAM, either in the form of enhanced neuroligin phenotypes by co-expression of PSD-95 (Prange et al., 2004) or S-SCAM (Iida et al., 2004), or an alteration in the neuroligin overexpression phenotype by the reduction of PSD-95 (Futai et al., 2007) or S-SCAM (Stan et al., 2010). One possible scenario to explain the different conclusions is that PSD-95 and S-SCAM interact indirectly with the neuroligins during synapse formation. Indeed, it has been

shown that whereas the clustering of neuroligin induces a rapid accumulation of NMDARs, the same clustering is followed by a much slower recruitment of PSD-95 (Barrow et al., 2009). Others have also reported that neuroligin localization to synaptic sites lacks dependence on the PDZ or WW-binding domains when expressed on a wild-type background (Dresbach et al., 2004). It is important to note that, while we have found no requirement for the PDZ motif in the synaptogenic phenotype induced by neuroligin in this set of experiments, it is not our intention to categorically exclude its involvement in all aspects of synaptic function. It is possible that a PDZ-mediated interaction could be involved at other developmental stages, in other synaptic adhesion molecules, or in other aspects of synaptic function not tested in this set of experiments. While we believe that this replacement strategy and culture system provide a reasonable surrogate for CNS physiology, they do represent a particular developmental stage and may introduce peculiarities that are specific to the experimental setup. Future studies will be aimed at demonstrating the relevance of this newly defined critical region to adult CNS physiology.

In addition to its synaptogenic properties, postsynaptic neuroligin is thought to exert a maturational effect on apposing presynaptic terminals (Varoqueaux et al., 2006). In fact, differing roles have been suggested for the extracellular domain, implicated in the assembly of presynaptic terminals through an interaction with neurexin, and the intracellular domain, required for the maturation of those same terminals (Wittenmayer et al., 2009). In the present study, we describe evidence for an increase in release probability with the overexpression of neuroligin, which is consistent with a maturational effect on presynaptic terminals. Notably, the point-mutants and deletion mutants of NLGN3 that did not induce enhancements of AMPAR currents also do not have this presynaptic effect. We believe this is consistent with the previous finding that an intact cytoplasmic tail of neuroligin is required for the maturation of presynaptic terminals.

However, a change in release probability is unlikely to underlie the major increase in AMPAR currents because there is not an equivalent change in NMDAR currents with the expression of those same functional proteins. Rather, these findings suggest that the majority of the increase in AMPAR currents is due to a postsynaptic increase in AMPARs. Interestingly, the knockdown of neuroligins with the NLmiRs, which reduces both AMPAR- and NMDAR-evoked currents, does not affect the paired-pulse ratio. This finding, when viewed in combination with the reduction in spine density that accompanies expression of the NLmiRs, is consistent with a loss of synapses, rather than an alteration in maturational state at existing synapses.

The findings presented in this study contribute to the body of literature concerning the pathogenesis of autism, as mutations in NLGN3 and NLGN4 have been associated with the disease (Jamain et al., 2003). However, the loss-of-function mutations presented in this study are substantially different than those found in patients with autism. The previously described autism-related neuroligin mutations have all been localized to the extracellular domain and the most well-characterized one (NLGN3 A451C) appears to result in the ER-retention of the mutant protein (Comoletti et al., 2004). Thus, patients with these mutations may exhibit a total loss of synaptic NLGN3 or NLGN4. In contrast, the cytoplasmic mutation presented here imparts a specific deficit in postsynaptic function, while the protein retains synaptic targeting and trans-synaptic function. We therefore cannot directly relate the findings presented here to the pathogenesis of autism, but believe this represents a step forward in the understanding of neuroligin function at the synapse and thus indirectly may contribute to our understanding of autism.

The triple knockdown of neuroligins 1–3 dramatically reduced, but did not eliminate, excitatory and inhibitory transmission. We do not know if the remaining current is due to residual neuroligin expression or rather neuroligin-independent synaptic

assembly. There is certainly evidence that the neuroligin/neurexin complex is not the only mechanism of synaptic assembly, since neurons cultured from neuroligin triple knockout animals have synapses present in a density comparable to wild-type as determined by electron microscopy (Varoqueaux et al., 2006). Other families of postsynaptic adhesion molecules, most notably the LRRTMs, have also been shown capable of inducing the formation of synapses in neurons (de Wit et al., 2009; Ko et al., 2009a; Linhoff et al., 2009). Regardless of the nature of the remaining current, the triple knockdown was clearly sufficient to allow us to measure the functional importance of the neuroligin cytoplasmic tail in mammalian neurons.

There is a notable difference between the effect of an acute knockdown of NLGNs 1–3, presented here, and the previous characterization of the triple NLGN1–3 knockout mouse. Whereas we find that the acute reduction of NLGNs 1–3 results in decreased AMPAR- and NMDAR-evoked EPSCs as well as decreased IPSCs, the triple knockout did not appear to affect excitatory currents and did not change the total number of synapses in cultured neurons (Varoqueaux et al., 2006). It is possible that there may be compensation by other synaptic adhesion molecules, such as the LRRTM family, when endogenous neuroligin is absent throughout the embryonic development of an animal. Indeed, the fact that knockout of NLGN1 alone results in decreased NMDAR currents (Chubykin et al., 2007), but the triple knockout does not affect NMDAR currents suggests that such compensation is possible.

The findings presented here significantly advance our understanding of the family of neuroligins. At an experimental level, our results emphasize the importance of performing experiments that target this family of proteins on a background of reduced endogenous expression. Using this approach we have shown that the postsynaptic role of neuroligins does not depend on binding to S-SCAM and PSD-95, as was previously believed. Instead we define a new region and critical residue in the intracellular domain.

This shift in focus, away from PDZ-mediated neuroligin interactions and toward a new molecular site of importance in the cytoplasmic domain should redirect the course of future research into this family of proteins. It will be interesting to explore the nature of this new domain as it may regulate the function of neuroligin with respect to known components of the postsynaptic site or may mediate new, unexpected interactions between neuroligin and other proteins that play a yet-to-be described role in the assembly or maintenance of a postsynaptic site. A number of interesting candidates for a possible interaction at this site may be found in the results of a yeast 2-hybrid screen using the cytoplasmic tail of NLGN2 lacking the terminal PDZ motif (Poulopoulos et al., 2009). Moreover, given the relevance of neuroligins to human disease, with specific mutations of NLGN3 and NLGN4 associated with autism (Jamain et al., 2003), understanding the molecular determinants of neuroligin function has implications for clinical, as well as basic science research.

Figure 6. Knockdown of neuroligin family is necessary for functional study of the cytoplasmic tail.

(A) Dual whole-cell recording configuration. Leftmost pipette is stimulating electrode. Dashed lines indicate Schaffer collaterals. **(B)** CAG promoter driving GFP expression and chained microRNAs targeting neuroligins 1–3. **(C)** Western blot analysis of knockdown. **(D)** AMPAR-mediated EPSC scatter plots showing reductions in amplitude in NLmiR-transfected neurons compared with control, untransfected neurons ($p < 0.005$, n=18). Open circles are individual pairs, filled circle is mean ±SEM. Black sample trace is control, green is transfected (scale bar: 10pA, 50ms). Bar graph plots transfected amplitude normalized to control ±SEM. **(E)** NMDAR-mediated EPSC scatter plots and normalized amplitude showing reductions in amplitude in NLmiR-expressing cells ($p < 0.005$, n=19, scale bar: 20pA, 100ms). **(F)** Paired-pulse ratio (PPR), second EPSC over first EPSC, ±SEM for consecutive stimuli separated by 40ms ($p > 0.05$, n=10). Example traces normalized at first EPSC (scale bar: 20ms). **(G)** AMPAR-mediated EPSCs showing no difference in phenotype between full-length NLGN3 ($p < 0.0005$, n=12) and truncated NLGN3 ($p < 0.0005$, n=18) when overexpressed alone. Bar graph and scatter plot are as described for D, full-length in black, truncation mutant in red. Schematic to the right illustrates truncation with previously described domains (PDZ; WW: WW-binding; GB: gephyrin-binding; TM: transmembrane). **(H)** AMPAR-mediated EPSCs showing a clear phenotypic difference between full-length NLGN3 ($p < 0.0005$, n=40) and truncated NLGN3 ($p > 0.05$, n=19) when co-expressed with NLmiRs. Bar graph and scatter plot are as described for D, schematic is as described for G.

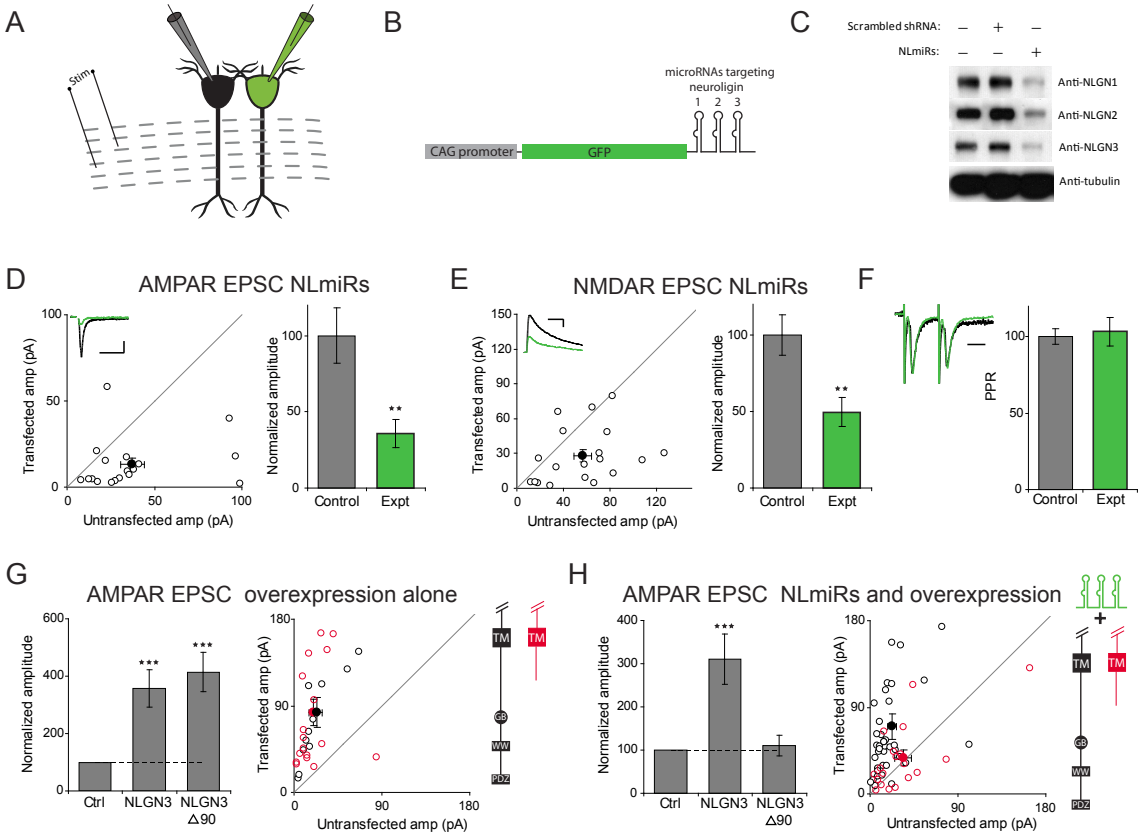

A
Stim
B
microRNAs targeting neuroligin
1 2 3
CAG promoter
GFP
C
Scrambled shRNA: – + –
NLmiRs: – – +
Anti-NLGN1
Anti-NLGN2
Anti-NLGN3
Anti-tubulin
D
AMPAR EPSC NLmiRs
Transfected amp (pA)
Untransfected amp (pA)
Normalized amplitude
Control
Expt
E
NMDAR EPSC NLmiRs
F
PPR
G
AMPAR EPSC overexpression alone
Normalized amplitude
Ctrl
NLGN3
NLGN3 Δ90
Transfected amp (pA)
Untransfected amp (pA)
TM
PB
WW
PDZ
H
AMPAR EPSC NLmiRs and overexpression

Figure 7. Heterodimerization of endogenous and exogenous neuroligin.

(A) Immunoblot analysis showing homo- and heterodimers of NLGN following co-immunoprecipitation with an HA antibody. Specifically, HA-tagged NLGN1 co-immunoprecipitates with Flag-tagged NLGN1 (lane 7), wild-type NLGN3 (lane 8), myc-tagged NLGN3 (lane 9), and a myc-tagged ∆90 truncation mutant of NLGN3 (lane 10). NLGN3 antibody is against the cytoplasmic tail of the protein and thus does not recognize the ∆90 truncation mutant. **(B)** HA-tagged NLGN1 was expressed via a virus in primary cortical neuronal cultures. This exogenous HA-NLGN1 forms heterodimers with endogenous NLGN3 (lane 4) in primary cortical neurons.

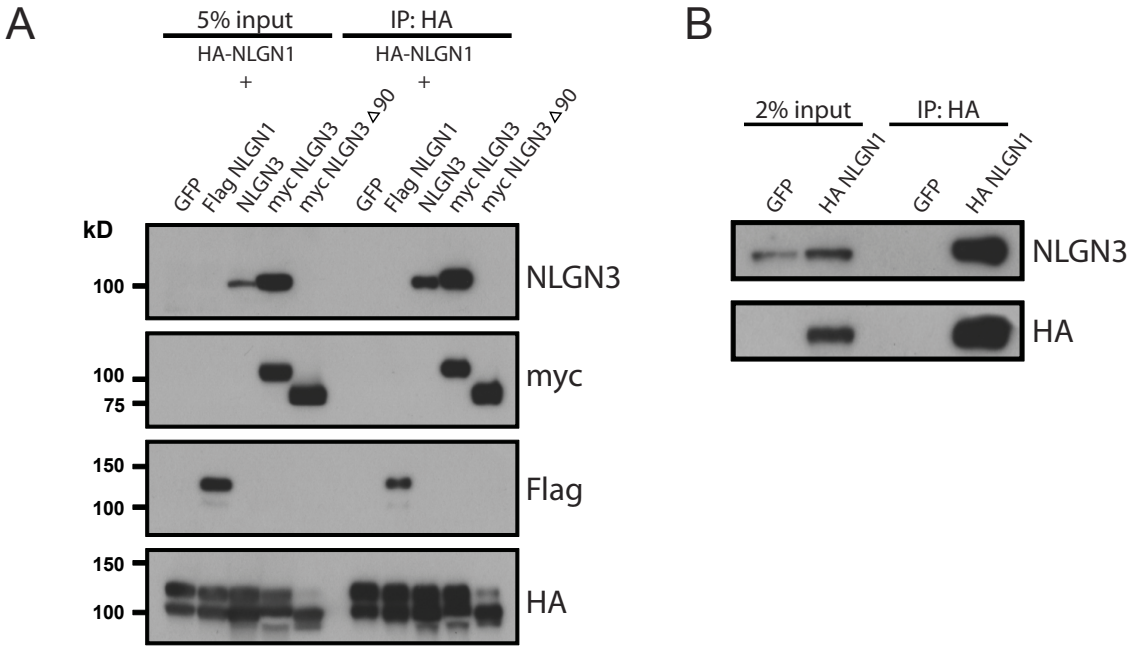

A
5% input
IP: HA
HA-NLGN1
HA-NLGN1
+
+
GFP
Flag NLGN1
NLGN3
myc NLGN3
myc NLGN3 Δ90
GFP
Flag NLGN1
NLGN3
myc NLGN3
myc NLGN3 Δ90
kD
100
NLGN3
100
75
myc
150
100
Flag
150
100
HA
B
2% input
IP: HA
GFP
HA NLGN1
GFP
HA NLGN1
NLGN3
HA

Figure 8. Replacement of endogenous NLGNs with wild-type and mutated NLGN3 reveals AMPAR enhancement dependent on a single residue in the c-tail.

(A) Evoked AMPAR EPSC amplitudes as percent of control ±SEM for each NLGN3 construct co-expressed with the NLmiRs (NLGN3 Full, $p<0.0001$, n=40; NLGN3 ∆4, $p<0.005$, n=14; NLGN3 ∆25, $p<0.05$, n=9; NLGN3 ∆46, $p<0.05$, n=11; NLGN3 ∆77, $p<0.0001$, n=26; NLGN3 ∆90, $p>0.05$, n=19; NLGN3 ∆99, $p>0.05$, n=7; NLGN3 ∆109, $p>0.05$, n=10; NLGN3 ∆77–90, $p>0.05$, n=19; NLGN3 E740N, $p>0.05$, n=19). Delta number indicates number of truncated amino acids from C-terminus. Schematic below graph represents cytoplasmic tail of NLGN3 (TM: transmembrane; GB: Gephyrin-binding; WW: WW-binding; PDZ). Bar graphs for NLGN3 Full and NLGN3 ∆90 are same as those in Figure 1G. **(B)** AMPAR EPSC scatter plots for notable replacements. Open circles are individual pairs, filled are mean ±SEM. Black sample traces are control, green are transfected (scale bar: 20pA, 50ms). Scatter plot for NLmiRs plus NLGN3 Full, originally shown with NLGN3 ∆90 in Figure 1H, repeated here for clarity. **(C)** Paired-pulse ratios – second EPSC over first EPSC – for notable replacements, normalized to control ±SEM (NLGN3 full, $p<0.05$, n=26; NLGN3 ∆77, $p<0.05$, n=16; NLGN3 ∆77–90, $p>0.05$, n=14; NLGN3 E740N, $p>0.05$, n=15). **(D)** Normalized NMDAR EPSC amplitudes for NLGN3 full-length ($p>0.05$, n=19) and NLGN3 E740N ($p>0.05$, n=19) expression on background of triple NLGN knockdown ±SEM. Black sample traces are control, green are transfected (scale bar: 20pA, 100 ms).

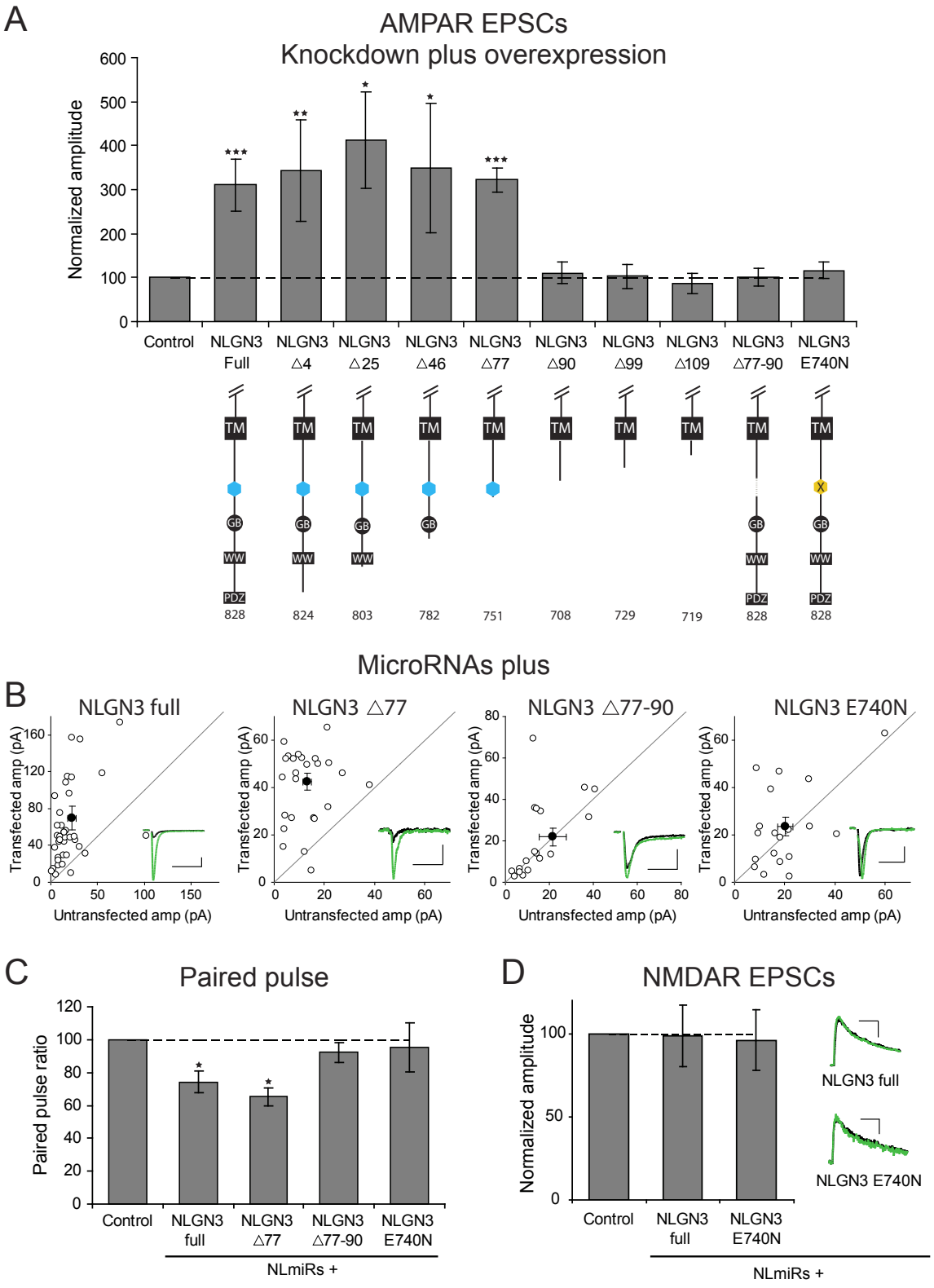
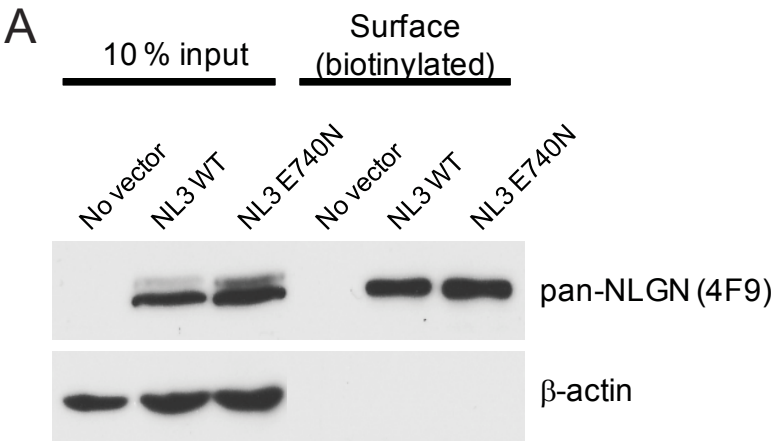

A
AMPAR EPSCs
Knockdown plus overexpression
Normalized amplitude
600
500
400
300
200
100
0
Control
NLGN3 Full
NLGN3 △4
NLGN3 △25
NLGN3 △46
NLGN3 △77
NLGN3 △90
NLGN3 △99
NLGN3 △109
NLGN3 △77-90
NLGN3 E740N
TM
GB
WW
PDZ
X
828
824
803
782
751
708
729
719
828
828
MicroRNAs plus
B
NLGN3 full
NLGN3 △77
NLGN3 △77-90
NLGN3 E740N
Transfected amp (pA)
Untransfected amp (pA)
C
Paired pulse
Paired pulse ratio
Control
NLGN3 full
NLGN3 △77
NLGN3 △77-90
NLGN3 E740N
NLmiRs +
D
NMDAR EPSCs
Normalized amplitude
NLGN3 full
NLGN3 E740N
Control
NLGN3 full
NLGN3 E740N
NLmiRs +

Figure 9. Retained surface expression of point-mutant NLGN3 and lack of an effect on a wild-type background.

(A) Blot of biotinylated proteins showing no difference in surface expression between the full-length and E740N forms of NLGN3. **(B)** Evoked AMPAR EPSC amplitudes expressed as percent of control for NLGN3 full-length ($p < 0.0005$, n=12) and NLGN3 E740N ($p < 0.005$, n=9) when expressed alone.


A
10 % input
Surface
(biotinylated)
No vector
NL3 WT
NL3 E740N
No vector
NL3 WT
NL3 E740N
pan-NLGN (4F9)
β-actin

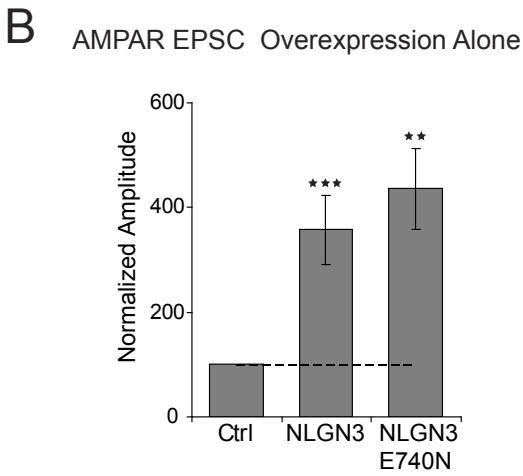

B
AMPAR EPSC Overexpression Alone
Normalized Amplitude
600
400
200
0
***
**
Ctrl
NLGN3
NLGN3
E740N

Figure 10. Critical novel region identified in NLGN3 is also crucial for the function of NLGN1 and NLGN4.

(A) Alignment of the transmembrane domain and C-tails of NLGNs 1 (mouse), 3 (human), and 4 (human). Critical region identified in NLGN3 is highlighted with a star indicating the position of the single AA swap. The PDZ domain is highlighted in green. **(B)** AMPAR EPSC scatter plots and normalized amplitudes for NLGN1*(RNAi-Proof) and NLGN1* E747N on the background of the triple knockdown demonstrating a significant difference ($p < 0.005$, n=14 NLGN1*, n=8 NLGN1* E747N). **(C)** AMPAR EPSC scatter plots and normalized amplitudes for NLGN4 and NLGN4 N726E on a wild-type background demonstrating the gain-of-function by this mutation ($p < 0.0001$, n=13 NLGN4, n=15 NLGN4 N726E). Open circles are individual pairs, filled circles are mean ±SEM. Black sample traces are control, green are transfected (scale bars: 20pA, 50ms). Bar graphs plot transfected amplitude normalized to control ±SEM. **(D)** NMDAR EPSC scatter plots and normalized amplitudes for NLGN1*(RNAi-Proof) and NLGN1* E747N on the background of the triple NLGN knockdown also demonstrating a significant reduction in current amplitude ($p < 0.005$, n=13 NLGN1*, n=8 NLGN1* E747N, scale bars: 40pA, 100ms). **(E)** NMDAR EPSC scatter plots and normalized amplitudes for NLGN4 and NLGN4 N726E on a wild-type background ($p < 0.005$, n=12 NLGN4, n=15 NLGN4 N726E, scale bars: 20pA, 100ms). Open circles are individual pairs, filled circles are mean ±SEM. Black sample traces are control, green are transfected. Bar graphs plot transfected amplitude normalized to control ±SEM.

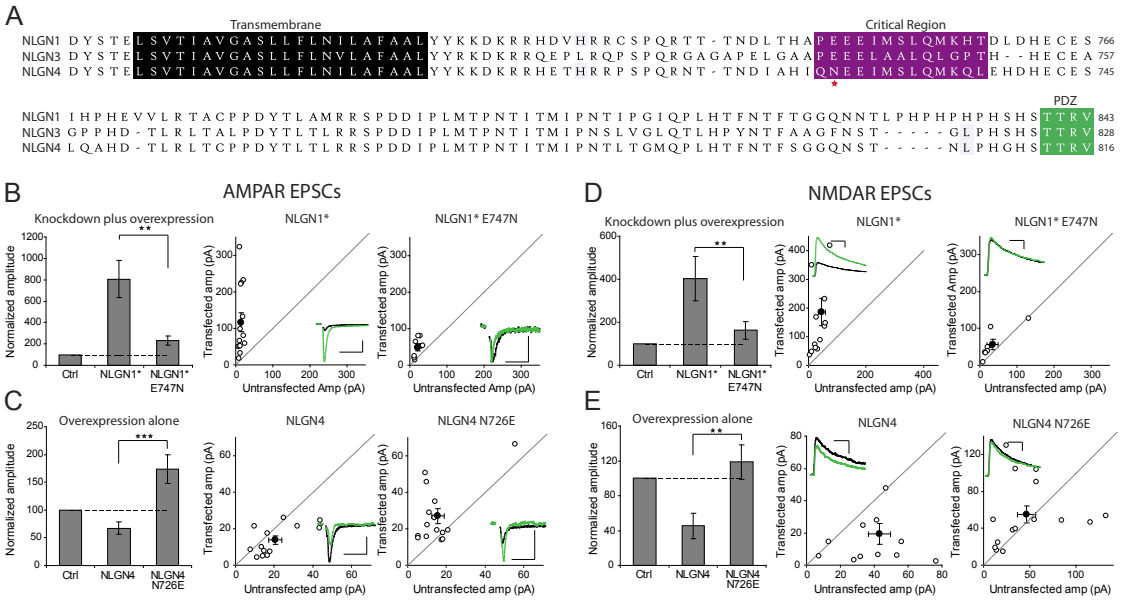

A
Transmembrane
Critical Region
NLGN1 D Y S T E L S V T I A V G A S L L F L N I L A F A A L Y Y K K D K R R H D V H R R C S P Q R T T - T N D L T H A P E E E I M S L Q M K H T D L D H E C E S 766
NLGN3 D Y S T E L S V T I A V G A S L L F L N V L A F A A L Y Y R K D K R R Q E P L R Q P S P Q R G A G A P E L G A A P E E E L A A L Q L G P T H - - H E C E A 757
NLGN4 D Y S T E L S V T I A V G A S L L F L N I L A F A A L Y Y K K D K R R H E T H R R P S P Q R N T - T N D I A H I Q N E E I M S L Q M K Q L E H D H E C E S 745
PDZ
NLGN1 I H P H E V V L R T A C P P D Y T L A M R R S P D D I P L M T P N T I T M I P N T I P G I Q P L H T F N T F T G G Q N N T L P H P H P H P H S H S T T R V 843
NLGN3 G P P H D - T L R L T A L P D Y T L T L R R S P D D I P L M T P N T I T M I P N S L V G L Q T L H P Y N T F A A G F N S T - - - - - G L P H S H S T T R V 828
NLGN4 L Q A H D - T L R L T C P P D Y T L T L R R S P D D I P L M T P N T I T M I P N T L T G M Q P L H T F N T F S G G Q N S T - - - - - N L P H G H S T T R V 816
B
AMPAR EPSCs
Knockdown plus overexpression
NLGN1*
NLGN1* E747N
Normalized amplitude
Transfected amp (pA)
Untransfected Amp (pA)
Ctrl
NLGN1*
NLGN1* E747N
C
Overexpression alone
NLGN4
NLGN4 N726E
Untransfected amp (pA)
D
NMDAR EPSCs
E

Figure 11. Dependence of neuroligin expression effects on the knockdown background.

(A) Evoked NMDAR EPSC amplitudes expressed as percent of control for NLGN3 overexpression alone ($p < 0.05$, n=10) or overexpression on the background of reduced endogenous neuroligin expression by the NLmiRs ($p > 0.05$, n=19). **(B)** Evoked AMPAR EPSC amplitudes expressed as percent of control for the expression of NLGN1* ($p < 0.01$, n=11) or NLGN1* E747N ($p < 0.005$, n=10) when expressed alone. No difference exists between the two conditions ($p > 0.05$). **(C)** Evoked AMPAR EPSC amplitudes expressed as percent of control for NLGN4 and NLGN4 N726E, each co-expressed with the NLmiRs, illustrating a significant difference ($p < 0.05$, n=6 NLGN4, n=13 NLGN4 N276E).

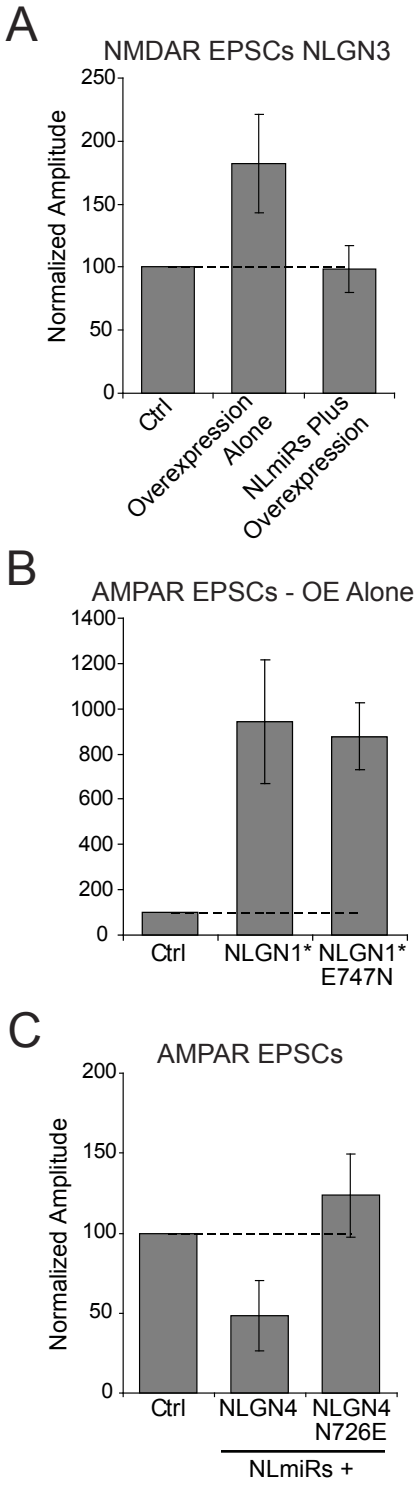

A
NMDAR EPSCs NLGN3
Normalized Amplitude
250
200
150
100
50
0
Ctrl
Overexpression Alone
NLmiRs Plus Overexpression
B
AMPAR EPSCs - OE Alone
1400
1200
1000
800
600
400
200
0
Ctrl
NLGN1*
NLGN1* E747N
C
AMPAR EPSCs
Normalized Amplitude
200
150
100
50
0
Ctrl
NLGN4
NLGN4 N726E
NLmiRs +

Figure 12. Mutation of the critical residue does not affect inhibitory synapses.

(A) IPSC amplitudes (recorded at 0mV) normalized to control ±SEM for neurons expressing NLmiRs ($p < 0.005$, n=10) or the combination of NLmiRs with NLGN3 ($p > 0.05$, n=10), NLGN3 E740N ($p > 0.05$, n=11), NLGN2* (RNAi-Proof) ($p < 0.0001$, n=17), and NLGN2* E740N ($p < 0.0001$, n=15). No significant difference exists between NLGN2* and NLGN2* E740N ($p > 0.05$). **(B)** Scatter plot of NLmiR expressing cells versus untransfected control cells demonstrating the reduction in IPSCs induced by the NLmiRs. **(C)** Scatter plot of cells expressing both NLmiRs and NLGN2* versus control demonstrating the enhancement of inhibitory currents induced by the expression of NLGN2*. **(D)** Scatter plot of cells expressing NLmiRs and NLGN2* with the glutamic acid at residue 740 mutated to asparagine versus control, which are not different than the NLGN2* without the point-mutation. Open circles are individual pairs, filled circles are mean ±SEM. Black sample traces are control, green are transfected (scale bar: 75pA, 30ms).

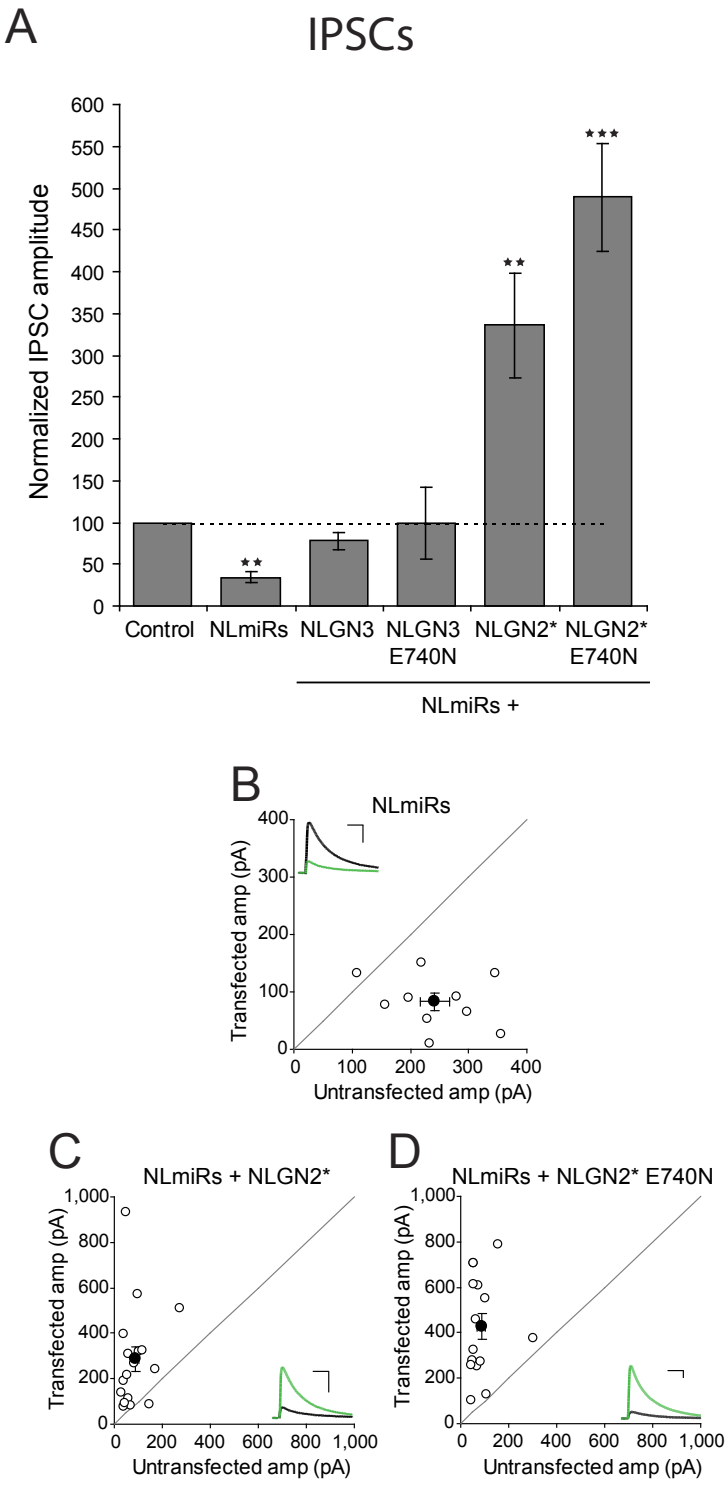

A
IPSCs
Normalized IPSC amplitude
600
550
500
450
400
350
300
250
200
150
100
50
0
Control
NLmiRs
NLGN3
NLGN3 E740N
NLGN2*
NLGN2* E740N
NLmiRs +
B
NLmiRs
Transfected amp (pA)
Untransfected amp (pA)
C
NLmiRs + NLGN2*
Transfected amp (pA)
Untransfected amp (pA)
D
NLmiRs + NLGN2* E740N
Transfected amp (pA)
Untransfected amp (pA)

Figure 13. Enhancement of inhibitory currents by NLGN3 is dependent on the presence of other neuroligins.

Evoked IPSC amplitudes (recorded at 0mV) normalized to control for neurons expressing NLGN3 alone, illustrating a large increase in inhibitory currents ($p < 0.005$, n=11). To the right is shown the scatter plot of paired currents recorded in NLGN3 expressing cells versus untransfected control cells. Open circles are individual pairs, filled circles are mean ±SEM.

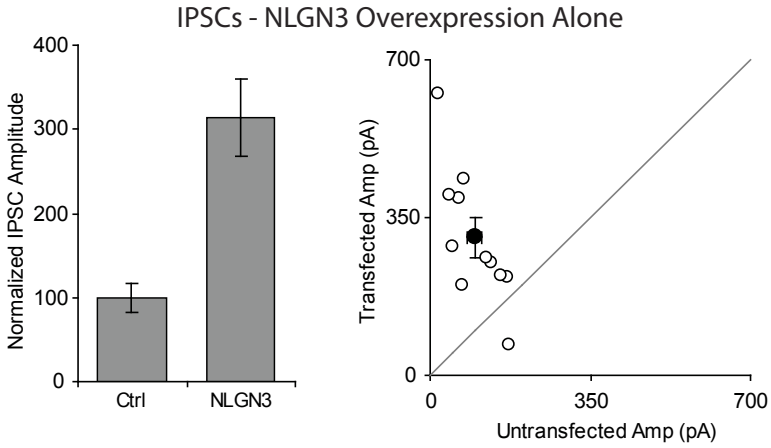

IPSCs - NLGN3 Overexpression Alone
Normalized IPSC Amplitude
400
300
200
100
0
Ctrl
NLGN3
Transfected Amp (pA)
700
350
0
0
350
700
Untransfected Amp (pA)

Figure 14. The effects of neuroligin on excitatory synapses are independent of excitatory synaptic activity.

(A) Schematic depicting the timecourse of these experiments. Days in vitro (DIV) is noted below the bar. **(B)** AMPAR- and NMDAR-mediated currents for cells expressing NLmiRs plus NLGN3 full-length in the presence of NBQX and APV. Scatter plots show transfected cells as compared to simultaneously recorded control cells. Open circles are individual pairs, filled circles are mean ±SEM. Black sample traces are control, green are transfected (scale bars AMPAR: 15pA, 50ms; NMDAR: 50pA, 100ms). Bar graphs plot experimental amplitudes normalized to control ±SEM. As was the case in the absence of drugs, NLGN3 induces an increase only in AMPAR mediated currents ($p < 0.005$, n=12) and not NMDAR mediated currents ($p > 0.05$, n=11). **(C)** AMPAR- and NMDAR-mediated currents for cells expressing NLmiRs plus NLGN1* (RNAi-Proof) in the presence of NBQX and APV. Scatter plots show transfected cells as compared to simultaneously recorded control cells. Open circles are individual pairs, filled circles are mean ±SEM. Black sample traces are control, green are transfected (scale bars AMPAR: 60pA, 50ms; NMDAR: 200pA, 100ms). Bar graphs plot experimental amplitudes normalized to control ±SEM. As in the absence of drug, NLGN1* expression results in increased AMPAR mediated ($p < 0.0005$, n=13) and NMDAR mediated ($p < 0.005$, n=14) currents.

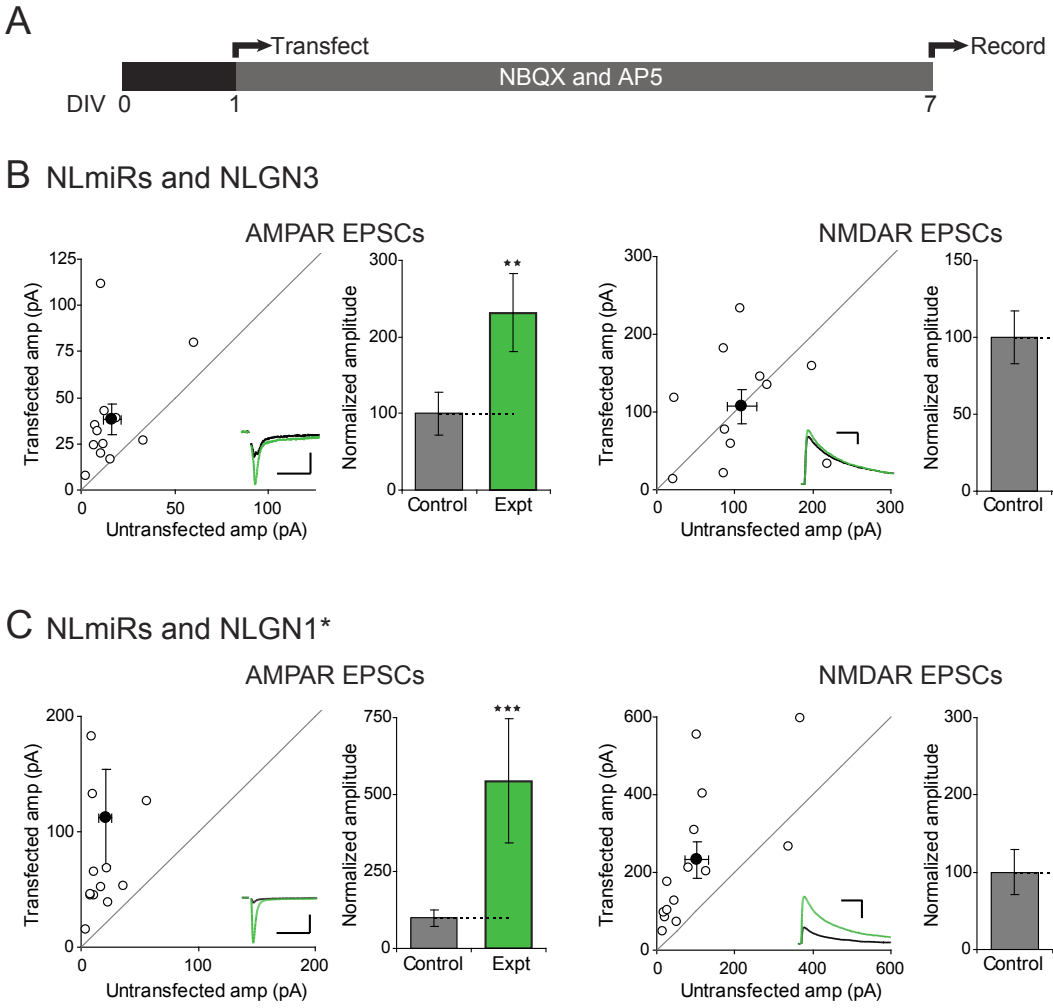

A
Transfect
Record
NBQX and AP5
DIV 0
1
7
B NLmiRs and NLGN3
AMPAR EPSCs
NMDAR EPSCs
Transfected amp (pA)
Untransfected amp (pA)
Normalized amplitude
Control
Expt
**
C NLmiRs and NLGN1*
AMPAR EPSCs
NMDAR EPSCs
***
**

Figure 15. Enhancement of excitatory currents by NLGN3 is not blocked by APV

(A) Schematic depicting the timecourse of these experiments. Days in vitro (DIV) is noted below the bar. **(B)** Evoked AMPAR EPSC amplitudes expressed as percent of control for the case of NLGN3 expression on the background of the NLmiRs, with the inclusion of APV in the media ($p < 0.005$, $n=10$).

A


Transfect
Record
APV
DIV 0
1
7

B

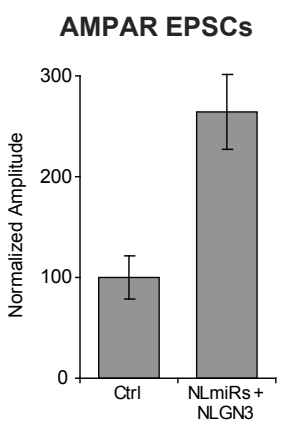

AMPAR EPSCs
Normalized Amplitude
300
200
100
0
Ctrl
NLmiRs + NLGN3

Figure 16. Mechanism of synaptic enhancement by neuroligins and specific deficits of the mutant.

(A) Spontaneous miniature EPSC amplitude in neurons expressing NLGN3 and NLGN3 E740N on triple NLGN knockdown background. Amplitudes expressed as percentage of control ±SEM; on knockdown background, amplitudes reduced by NLGN3 E740N compared with control ($p<0.05$, n=13) and NLGN3 full-length ($p<0.05$, n=10). Black sample traces: control; green: experimental (scale bars: 4pA, 10ms). **(B)** Spontaneous miniature EPSC frequencies with neuroligin replacements on triple knockdown background expressed as percentage of control ±SEM, showing increases by both NLGN3 ($p<0.005$, n=10) and NLGN3 E740N ($p<0.05$, n=13). Frequency increase significantly larger with full-length than with NLGN3 E740N ($p<0.05$) (scale bars: 20pA, 0.5s). **(C)** Spine density expressed as spines per micron ±SEM with expression of NLmiRs ($p<0.05$, n=12), or expression of NLmiRs in combination with NLGN3 ($p<0.0001$, n=11) or NLGN3 E740N ($p<0.05$, n=9). A significant difference exists between NLmiRs plus NLGN3 and NLmiRs plus NLGN3 E740N ($p<0.05$). Top four right-hand panels show representative images from each condition (scale bar: 5μm). Bottom two panels show localization of full-length and mutated neuroligin to spines. **(D)** Normalized VGLUT1 immunostaining intensity ±SEM onto neurons transfected with either GFP (n=16), NLmiRs, or neuroligin constructs with NLmiRs. VGLUT1 intensity decreased with NLmiRs expression ($p<0.001$, n=20); VGLUT1 intensity increased with all NLGN constructs on NLmiRs background (NLGN3, $p<0.01$, n=15; NLGN3 E740N, $p<0.01$, n=16; NLGN1*, $p<0.001$, n=18; NLGN1* E747N, $p<0.001$, n=14). Representative images show neurons immunolabeled with VGLUT1 (Left panel, red in merge) and GFP (green in merge). Scale bar 2μm.

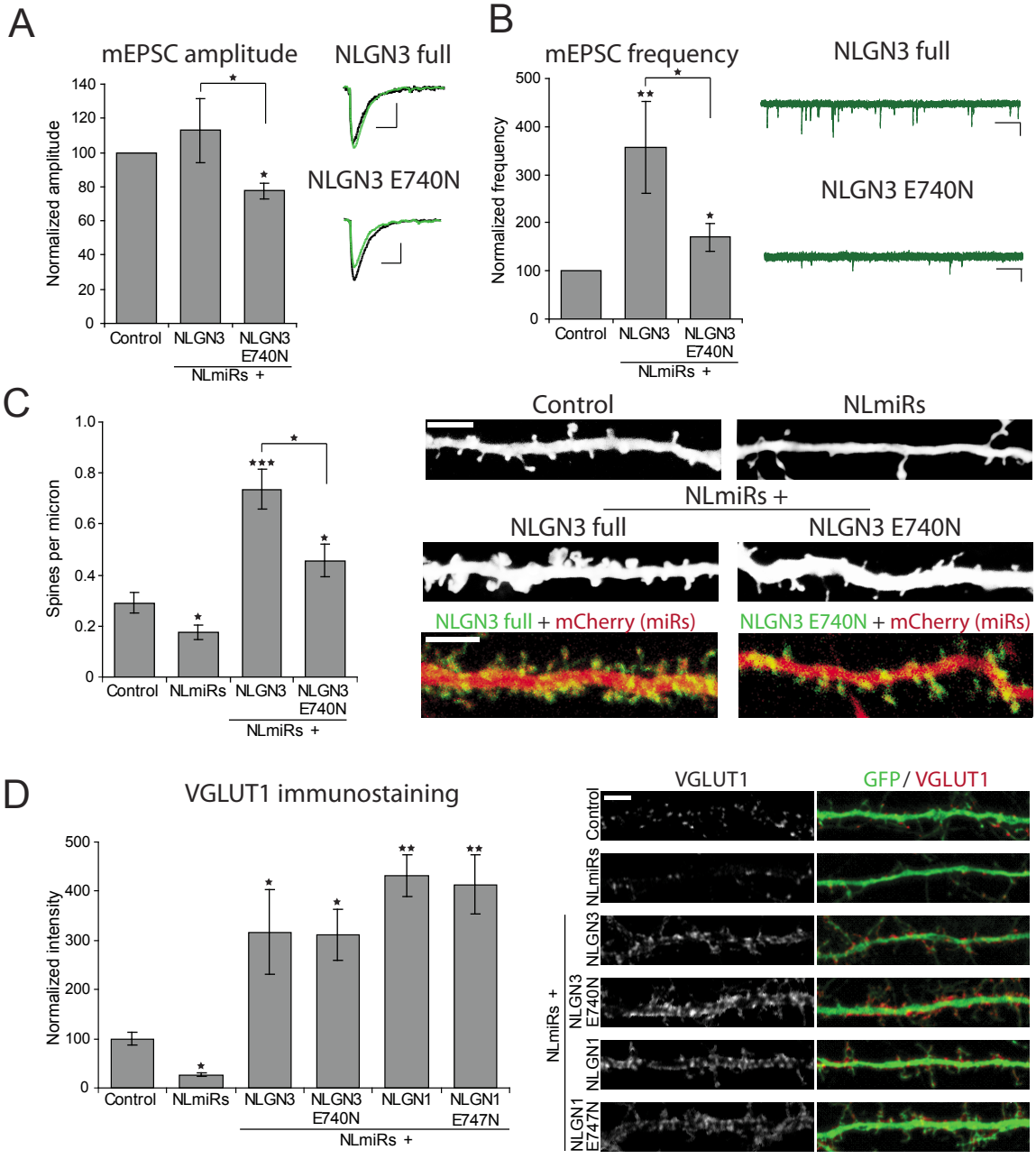
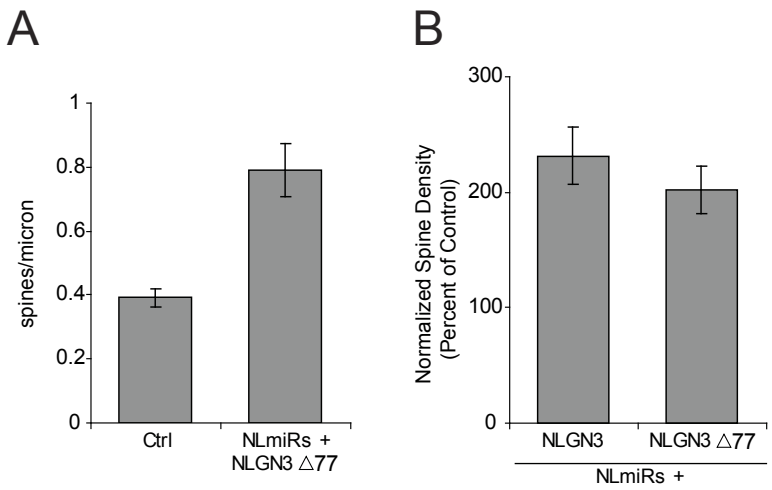

A
mEPSC amplitude
Normalized amplitude
140
120
100
80
60
40
20
0
Control
NLGN3
NLGN3 E740N
NLmiRs +
NLGN3 full
NLGN3 E740N
B
mEPSC frequency
Normalized frequency
500
400
300
200
100
0
Control
NLGN3
NLGN3 E740N
NLmiRs +
NLGN3 full
NLGN3 E740N
C
Spines per micron
1.0
0.8
0.6
0.4
0.2
0
Control
NLmiRs
NLGN3
NLGN3 E740N
NLmiRs +
Control
NLmiRs
NLmiRs +
NLGN3 full
NLGN3 E740N
NLGN3 full + mCherry (miRs)
NLGN3 E740N + mCherry (miRs)
D
VGLUT1 immunostaining
Normalized intensity
500
400
300
200
100
0
Control
NLmiRs
NLGN3
NLGN3 E740N
NLGN1
NLGN1 E747N
NLmiRs +
VGLUT1
GFP / VGLUT1
Control
NLmiRs
NLmiRs +
NLGN3
NLGN3 E740N
NLGN1
NLGN1 E747N

Figure 17. Enhancement of spine density by NLGN3 does not require a c-tail domain other than the critical region

(A) Spine density expressed as spines per micron for a stretch of primary apical dendrite between 100 and 200μm from the soma illustrating an increase in spine density in the case of NLGN3Δ77 on the background of the NLmiRs as compared to control ($p < 0.01$, n=7 ctrl, 11 expt). **(B)** Comparison of the change in spine density between expression of either NLGN3 full-length or Δ77 on the background of the NLmiRs, each normalized to their respective controls, showing no difference between these conditions ($p > 0.05$).


A
spines/micron
1
0.8
0.6
0.4
0.2
0
Ctrl
NLmiRs +
NLGN3 △77
B
Normalized Spine Density
(Percent of Control)
300
200
100
0
NLGN3
NLGN3 △77
NLmiRs +

CHAPTER 5:

A subtype specific function for the extracellular domain of neuroligin 1 in hippocampal LTP

Introduction

As a class of cells, neurons are unmatched in the variety of cellular processes that they display – from migration, dendrite and axon development, and targeting, to synaptogenesis, spiking, synaptic homeostasis and plasticity. Diversity within the proteome of a neuron is central to this wide range of abilities, with proteins specialized for each individual function. Yet, within the milieu of the proteome are families of related proteins, similar in sequence, but encoded by distinct genes. Determining redundancy and specialization within these families of proteins can be a challenge, as the presence of a shared function among a family of proteins under experimental constraints does not prove the lack of endogenous specialization *in vivo* any more than the presence of a unique response to an experimental constraint proves that specialization necessarily exists.

In humans, four major genes encode for a family of proteins termed neuroligins. These single-pass transmembrane proteins are found at postsynaptic sites, where they support the formation and maintenance of synapses through both intracellular, as well as trans-synaptic interactions (Washbourne et al., 2004). A cursory look at the neuroligins reveals high sequence and structural homology and a shared major binding partner in presynaptic neurexin (Ichtchenko et al., 1996). Indeed, this similarity is borne out functionally, as all of the neuroligins promote the formation and maintenance of synapses (Chih et al., 2005; Levinson et al., 2005). However, some notable differences have begun to emerge between the neuroligins, suggesting divergent roles for the individual members of this family.

Most dramatically, differences exist between neuroligin subtypes with regard to expression patterns at excitatory and inhibitory synapses, with neuroligin 1 (NLGN1) and neuroligin 3 (NLGN3) found at excitatory synapses and neuroligin 2 (NLGN2) and

NLGN3 found at inhibitory synapses (Budreck and Scheiffele, 2007; Song et al., 1999; Varoqueaux et al., 2004). However, beyond the broad excitatory/inhibitory divide, subtle differences exist specifically between the two major neuroligin subtypes found endogenously at excitatory synapses, NLGN1 and NLGN3. Notably, NLGN1 knockout animals have been shown to have deficits in memory (Blundell et al., 2010; Kim et al., 2008) while NLGN3 has been more strongly linked to autism and impairments in social behavior (Radyushkin et al., 2009). Yet, little has been done to directly compare the physiological roles of these two proteins.

In the present study, we explored for possible functional differences between NLGN1 and NLGN3. Using a variety of *in vivo* and *in vitro* techniques combining both knockdown and molecular replacement of the subtypes, we present novel differences in the physiological roles of these two proteins, most strikingly with respect to plasticity. Specifically, we find that NLGN1 has a clear role in the support of LTP in the hippocampus – in young CA1, but extending into adulthood in the dentate gyrus – a role that is not shared by NLGN3. We provide the first molecular dissection of the physiological differences between these neuroligin subtypes at excitatory synapses and find that the unique functions of NLGN1, both the potency of its synaptogenic phenotype and its role in LTP, depend on the inclusion of the B splice insertion site in its extracellular domain.

Results

NLGN1 is exclusively required for LTP in the adult dentate gyrus

We began this subtype comparison of the excitatory neuroligins by testing for a differential role in the support of adult plasticity. To do so, lentiviruses were produced to express previously validated microRNAs targeting NLGN1 (NLGN1 miR) or NLGN3 (NLGN3 miR) along with a fluorophore. In control experiments using dissociated hippocampal neurons, both constructs were shown to reduce their respective target transcripts by greater than 95% (Fig. 19A). These viruses were stereotaxically injected into the hippocampi of four-week-old rats. Ten to twelve days later, acute slices were taken and simultaneous recordings were made from virally transduced neurons and neighboring control cells in either area CA1 or the dentate gyrus (Fig. 18A**)**. A pairing protocol of 2 Hz stimulation for 90 seconds at a holding potential of 0 mV was used to simultaneously induce LTP in both the control and experimental cell.

In area CA1, knockdown of NLGN1 had no effect on LTP (Fig. 18B). However, a strikingly different phenotype was found in another region of the hippocampus, the dentate gyrus. Knockdown of NLGN1 in dentate granule cells resulted in a complete elimination of LTP (Fig. 18C) pointing to a requirement for NLGN1 in the expression of this plasticity. Knockdown of NLGN3, like that of NLGN1, had no effect on LTP in area CA1 (Fig. 18D). Yet unlike NLGN1, knockdown of NLGN3 also had no effect on LTP in the dentate gyrus (Fig. 18E). These results provide the first evidence in support of a requirement for NLGN1 in LTP in the dentate gyrus and establish a unique subtype difference between the two neuroligins.

To further examine the effect of single neuroligin subtype loss on excitatory synapses, we compared the amplitude of excitatory currents in transduced and control cells with each of the miRs in both hippocampal regions. Like LTP, neither AMPAR- nor

NMDAR-mediated currents were affected in area CA1 by the NLGN1 miR (Figs. 18B' and 19D). However, in dentate granule cells, NLGN1 knockdown did result in a substantial weakening of synaptic strength, with reductions in both AMPAR- and NMDAR-mediated currents upon knockdown of NLGN1 (Figs. 18C' and 19D). Knockdown of NLGN3 resulted in a phenotype with the same regional dependence – no effect on excitatory currents in area CA1, but reductions in both AMPAR- and NMDAR-mediated currents in the dentate gyrus – although the reductions were of a smaller magnitude than those following knockdown of NLGN1 (Figs. 18D'-E' and 19C-E). Interestingly, while knockdown of either neuroligin resulted in reductions of synaptic strength in the dentate gyrus, only knockdown of NLGN1 affected LTP. Thus, it would appear that there is a segregation of neuroligin function whereby loss of either NLGN1 or NLGN3 leads to reductions in synaptic currents, whereas only loss of NLGN1 prevents the induction of LTP.

Reduction of NMDA currents by NLGN1 knockdown is due to a loss of synapses

Because we observed a reduction in NMDAR-mediated current along with a loss of LTP in cells expressing the NLGN1 miR, we wanted to test whether the LTP deficit was due simply to a reduction in NMDAR signaling at individual synapses as a result of the knockdown. The induction of LTP using a pairing protocol is entirely dependent on Ca^{2+} influx through NMDARs (Gustafsson and Wigstrom, 1988; Nicoll et al., 1988; Nicoll and Malenka, 1995), therefore, a condition that reduces the number of NMDARs per synapse would be expected to display an LTP deficit. However, the induction of LTP using a pairing protocol operates on a synapse-by-synapse basis (Isaac et al., 1996; Matsuzaki et al., 2004). If the knockdown were to result in whole-synapse loss, LTP

would still be normal in the remaining synapses. The matched decreases in AMPAR- and NMDAR-mediated currents that we observe upon expression of the miRs in the dentate gyrus are consistent with an all-or-none loss of synapses (Fig. 19C) and previous manipulations from our own work and that of others have shown reductions in the frequency, but not amplitude of synaptic AMPAR currents as well as reductions in spine density following the knockdown of neuroligins (Aiga et al., 2011; Shipman et al., 2011), also consistent with an all-or-none loss of synapses rather than a loss of receptors per synapses. However, there have been reports of accompanying reductions in amplitude as well (Chen et al., 2010). A key issue, therefore, is whether the NMDAR content is altered at individual synapses. We first addressed this functionally, by collecting mixed spontaneous AMPAR- and NMDAR-mediated currents at -70 mV in the absence of external Mg^{2+}, then washing on APV and collecting the pure AMPAR-mediated currents. The pure AMPAR currents were then subtracted from the mixed currents to give a pure NMDAR-mediated spontaneous current. We performed these experiments using simultaneously recorded NLGN1 miR expressing neurons and neighboring control cells in the dentate gyrus, and collected both evoked and spontaneous currents, using the evoked currents to assess the validity of the technique.

We found that the stimulation-evoked, subtracted NMDAR-mediated currents in NLGN1 miR expressing cells were reduced, as expected, compared to control cells (Fig. 20A,B). Moreover, the magnitude of the reduction was identical to that found when NMDAR currents were measured at +40 mV in the previous experiment (as percent of control, +40 mV, 32.12 ± 5.26; subtracted 23.4 ± 4.92; $p > 0.05$), thus providing validation of the technique. Furthermore, neither the charge transfer of the NMDAR current as a percent of the total charge transfer of the mixed AMPAR/NMDAR current nor the kinetics of the NMDAR current were altered in the evoked response (Fig. 20C,D).

We next analyzed the spontaneous currents in these same cells (Fig. 20E) and found a dramatic reduction in the frequency of spontaneous events (Fig. 20F), but no change in amplitude of either the mixed current, the pure AMPAR current, or the pure, subtracted NMDAR current (Fig. 20G). Like the evoked current, the charge transfer of the spontaneous NMDAR currents as a percentage of the total charge transfer of the mixed currents did not differ between the transduced cells and control cells (Fig. 20H). We consequently conclude that the reduction in evoked NMDAR currents is functionally due to an all-or-none loss of synapses, while the remaining synapses must have normal numbers of NMDARs.

To further bolster the functional evidence for an all-or-none loss of synapses following neuroligin knockdown, we examined the structural component of an excitatory synapse, the dendritic spine. Following knockdown of NLGN1, we filled transduced dentate granule cells and neighboring control cells with fluorescent dye and imaged their dendrites to assess any changes in spine density (Fig. 20I). What we found was a reduction in spine density in those cells expressing the NLGN1 miR as compared to control (Fig. 20J). Moreover, this reduction was of a similar magnitude as the reduction we found in evoked currents. We also found a reduction in spine density in dentate granule cells following the knockdown of NLGN3, confirming that synaptic loss is a general response to neuroligin knockdown (Fig. 21A,B).

Finally, we performed a coefficient of variation analysis on the paired evoked recordings following neuroligin knockdown. This provides yet another test to discriminate changes in the quantal size, q (the magnitude of response to a quanta of transmitter or, physiologically, the number of receptors per synapse), from changes in quantal content, $N \times P_r$ (the number of release sites multiplied by the probability of release or, restated, the number of functional synapses on a given trial that contribute to the postsynaptic response). It has been shown both theoretically and experimentally that manipulations

which produce a change in synaptic strength due to a change in quantal content also lead to a reliable change in the coefficient of variation (CV), whereas changes in synaptic strength due to changes in *q* do not affect CV (Del Castillo and Katz, 1954; Malinow and Tsien, 1990; Manabe et al., 1993). More specifically, when the ratio of evoked synaptic current amplitudes for experimental and control cells is plotted against the ratio of CV^{-2} for the two conditions, changes in mean amplitude arising from changes in *q* vary along the horizontal line (y=1), whereas changes in amplitude arising from changes in quantal content vary along the 45º line (y=x).

In the case of NLGN1 knockdown, both the AMPAR- and NMDAR-mediated components of the EPSC yield points that vary along the 45º line, consistent with changes in the number of functional synapses rather than a change in the number of receptors per synapse (Fig. 20K). Again, the same analysis following knockdown of NLGN3 in the dentate gyrus found a similar dependence on quantal content (Fig. 21C). Thus, each of these converging lines of evidence points to an all-or-none loss of synapses rather than a within-synapse loss of receptors as the mechanism of the reduction in EPSC magnitude following knockdown of neuroligin. Therefore, the LTP deficit observed upon knockdown of NLGN1 is not due to a simple loss of NMDAR-mediated Ca^{2+} influx, but rather a more intrinsic effect of NLGN1 on the plasticity of a synapse.

Subtype specific synaptic phenotype of NLGN1 expression is dependent on a region in the extracellular domain

Given the clear segregation of function between NLGN1 and NLGN3 with respect to plasticity, we wished to determine the dependence of the phenotypic difference on sub-domains within the proteins. To do so, we constructed chimeric proteins of NLGN1

substituting in domains of NLGN3, given its close homology but lack of an effect of LTP, to identify a region of NLGN1 that gives rise to its unique properties. We screened these chimeras using overexpression in hippocampal organotypic slice cultures. Although this preparation is not amenable to tests of plasticity, we have previously found it useful for identifying the structural determinants of neuroligin function (Shipman et al., 2011). In this experimental system, we used biolistics to sparsely transfect hippocampal neurons with two constructs. One expresses the NLGN, wild-type or chimera, while the other expresses three chained microRNAs targeting NLGNs 1-3. The microRNAs will knock down endogenous neuroligin to provide a clean background on which to evaluate the effect of the expressed NLGN. This knockdown background was previously shown to be crucial for assessing effects of mutated neuroligin constructs (Shipman et al., 2011). As in the case of the recordings from acute slices, experimental cell currents are always compared to simultaneously recorded untransfected cells.

Since LTP in the dentate gyrus has been shown to have a postsynaptic mechanism (Colino and Malenka, 1993), one might expect these two neuroligins to differ with respect to the intracellular scaffolding of postsynaptic proteins. Therefore, we first constructed chimeric neuroligins of NLGN1 and NLGN3 with the extracellular domain of NLGN1 and the intracellular domain of NLGN3 and vice-versa to test the relative contribution of these two domains to the phenotypic differences between the neuroligin subtypes. Perfect protein homology in the transmembrane region permitted the construction of these chimeras without disrupting any protein structure at the cross-over point.

We used the magnitude of enhancement of NMDAR-mediated currents as our readout given that NLGN1 expression more potently enhances the NMDAR-mediated currents than NLGN3 (Fig. 22A,C). As both neuroligins enhance AMPAR-mediated currents, an enhancement of the AMPAR-mediated current was a requirement for all

chimeras included in this analysis. Surprisingly, we found that the phenotypic difference between NLGN1 and NLGN3 segregated with the extracellular rather than the intracellular domains. Specifically, a chimera containing the extracellular domain of NLGN1 with the intracellular domain of NLGN3 (NLGN1-TM-NLGN3) enhanced NMDAR-mediated current to the same degree as full-length NLGN1, while the reverse chimera (NLGN3-TM-NLGN1) exactly mimicked full-length NLGN3 (Fig. 22A,D). Thus it would appear that the extracellular domains of these neuroligins largely account for the subtype differences in phenotype, while the intracellular domains are exchangeable.

To narrow in on the specific region within the extracellular domain that might account for the unique properties of NLGN1, we constructed six additional chimeras with increasingly more of the NLGN3 extracellular domain and less of the NLGN1 extracellular domain. We found a clear molecular segregation of phenotype using these chimeras. Those chimeras that contained at least 326 amino acids from the extreme N-terminus of NLGN1 possessed the typical NLGN1 NMDAR enhancement, whereas chimeras that contained less than 254 amino acids of the NLGN1 N-terminus instead displayed NLGN3 type NMDAR enhancement (Fig. 24A,E). The difference between NLGN1 and NLGN3 in the region between amino acids 326 and 254 includes an alternatively spliced insertion in NLGN1 previously termed the site B (Ichtchenko et al., 1995) (Fig. 22B). Interestingly, inclusion of this B site has been shown to determine the specificity with which NLGN1 binds to specific splice variants of neurexin and subtly alter the spinogenic phenotype of NLGN1 overexpression (Boucard et al., 2005). We tested an additional mutant of NLGN1 with a deletion of eight amino acids in the B site and found that it indeed possessed a NLGN3-type NMDAR enhancement phenotype (Fig. 23).

In vivo molecular replacement demonstrates a dependence of LTP in young CA1 on the B site in the extracellular domain of NLGN1

We have, at this point, demonstrated that NLGN1, but not NLGN3, is required for LTP in the adult dentate gyrus, but not adult CA1, and that at least some aspects of the phenotypic difference between expression of NLGN1 and NLGN3 are due to the B site insertion in the extracellular domain of NLGN1. The remaining questions are: one, why is NLGN1 required for LTP in dentate gyrus and not CA1; and two, does the B site have ramifications for LTP as well as the baseline synaptogenic phenotype of NLGN1? With respect to the first question, might there be something about the dentate gyrus that renders it more susceptible to loss of a synaptic adhesion molecule in adulthood than area CA1? One possibility is that the dentate gyrus, one of two sites in the brain that incorporates substantial adult born neurons throughout life, may remain more plastic into adulthood, perhaps accounting for the susceptibility to loss of a synaptogenic molecule. This retained plasticity due to incorporation of adult-born neurons is an area of active research (reviewed: (Deng et al., 2010)), even to the extent that there have been previous reports that halting adult neurogenesis reduces the expression of LTP in the dentate gyrus (Massa et al., 2011; Singer et al., 2011). If this is the case, perhaps CA1 neurons would be susceptible to a knockdown of NLGN1 at an earlier developmental time point when the initial connections are still forming.

To test this hypothesis we switched to a different experimental setup, that of *in utero* electroporations. By introducing the NLGN1 miR construct *in utero* we can check the basal state of synaptic currents and LTP in cells with knocked-down NLGN1 at a very young age (Fig. 24A). The additional advantage of the *in utero* electroporations is that we can efficiently co-express a replacement neuroligin construct along with the NLGN1 miR, a situation that we could not reliably achieve in the adult due to the limited

packaging size of a lentivirus. Consistent with a developmental function for NLGN1 in the support of LTP, we found that LTP was abolished in NLGN1 miR expressing CA1 pyramidal neurons at this young time point (Fig. 24B). Moreover, like the adult dentate granule cells, but unlike adult CA1 cells, AMPAR- and NMDAR-mediated currents were reduced by the expression of the NLGN1 miR in young CA1 (Figs. 24C and 25A).

Given this susceptibility of LTP in young CA1 pyramidal neurons to knockdown of NLGN1 and the fact that *in utero* electroporations are amenable to molecular replacements, we next tested whether the extracellular site that we identified as responsible for the phenotypic difference between NLGN1 and NLGN3 in organotypic slice culture would also account for the differential roles in LTP. Specifically, we co-expressed the NLGN1 miR construct with two different neuroligin chimeras: NLGN1-326-NLGN3, which contains the B site insertion and is phenotypically similar to NLGN1; or NLGN1-254-NLGN3, which lacks the B site insertion and is phenotypically similar to NLGN3. We found that replacement with NLGN1-326-NLGN3 rescued LTP in these young CA1 pyramidal neurons, whereas replacement with NLGN1-254-NLGN3 did not rescue LTP (Fig. 24D,E). Each replacement construct rescued the reduction in AMPAR- and NMDAR-mediated synaptic currents that accompanied the knockdown of NLGN1 (Figs. 24C and 25B,C) and, again using coefficient of variation analysis, all changes in amplitude found with both the knockdown and replacements were consistent with changes in quantal content rather than alterations in the number of receptors per synapse (Figure 25D). Thus, it would appear that, at these synapses, the presence of the B site insertion in NLGN1 is a defining characteristic of an LTP-competent synapse.

Discussion

This study provides a detailed analysis of the subtype specific role of neuroligin in hippocampal LTP. We find that the presence of NLGN1 containing the alternatively spliced B site insertion is a requirement for the expression of LTP in young CA1 pyramidal cells at a time when initial synaptic connections are being made in abundance. Interestingly, this requirement for NLGN1 persists into adulthood in the dentate gyrus, where the incorporation of adult born neurons requires ongoing synaptic formation and remodeling. The other major neuroligin found at excitatory synapses, NLGN3, which lacks the B site insert, clearly has a function in the formation or maintenance of synapses, but is not required for the support of LTP.

The resistance of adult CA1 pyramidal neurons to knockdown by either neuroligin subtype is interesting. It may be that, in these more mature neurons, the diversity and expression level of other postsynaptic adhesion molecules is quite high, diminishing the response to the loss of any one subtype. A variety of other molecules occupy a similar niche to that of neuroligin and are expressed in the hippocampus including the LRRTM family (de Wit et al., 2009; Ko et al., 2009; Linhoff et al., 2009) and G-protein-coupled receptor CIRL1/Latrophilin-1 (Boucard et al., 2012). Yet information about the precise regional and developmental expression of each of these molecules is not yet available. While we were able to show that the lentiviral-expressed targeting sequences against each neuroligin were quite effective in a mixed hippocampal cell culture *in vitro*, there remains the technical possibility that knockdown efficiency would differ *in vivo,* which we were unable to assess directly. A final possibility is that stable adult CA1 synapses are less susceptible to the loss of neuroligin than the newly created or rapidly remodeling synapses that might be found in young CA1 or the dentate gyrus. Perhaps knocking down neuroligin in adult CA1 followed by a behavioral challenge intended to increase the

turnover rate of spines would result in a similar reduction in synapses in the adult as in the young CA1 neurons.

In the present study, we found that loss of neuroligin in adulthood led to a reduction in the number of synapses rather than a reduction in the number of AMPA or NMDA receptors per synapse. This is consistent with our previous finding, showing a loss of whole synapses upon knockdown of NLGNs 1-3 in organotypic hippocampal slice culture (Shipman et al., 2011). However, other studies have reported changes in the AMPA/NMDA ratio in the NLGN1 knockout (Chubykin et al., 2007; Soler-Llavina et al., 2011) or a lack of change in spine density (Soler-Llavina et al., 2011) which are at odds with the current results. These differences could be the result of differences in methodology, particularly the difference between whole brain germ-line knockouts and sparsely expressed RNAi. Developmental effects are unlikely given that we have seen evidence for whole-synapse loss in both developmentally immature slice cultures and young and adult brain. One explanation could be competitive effects whereby different phenotypes are seen when neuroligin is reduced in only a few cells versus the entirety of the cells. Alternatively, these differences could be purely technical. The paired recording setup measures changes in AMPAR- and NMDAR-mediated current more precisely than measurements of AMPA/NMDA ratios. Future studies utilizing conditionally floxed alleles of neuroligin should be able to settle these various possibilities.

This is not the first study to report an impairment of LTP following NLGN1 manipulations, although we believe it provides the most detail. Blundell et al. (2010) reported diminished, but still present, LTP in a NLGN1 knockout mouse using theta-burst stimulation while recording field potentials in CA1. Unlike the present study, however, these mice display altered AMPA/NMDA ratios, suggestive of an altered NMDA receptor content per synapse or NMDA receptor channel dysfunction, to which the authors ascribe the LTP deficit. Another group tested LTP in the amygdala following knockdown

of NLGN1 (Jung et al., 2010; Kim et al., 2008). Again the loss of LTP was accompanied by reductions in NMDA signaling with the likely explanation the loss of the NMDA-mediated inductive Ca^{2+} influx. Interestingly, the second of these studies found the loss of LTP in the amygdala to be pathway specific (Jung et al., 2010). Perhaps this pathway specificity could be mediated by a difference in expression of the specific molecular determinants identified here: postsynaptically, NLGN1 with the insertion at the B site or its presynaptic partner neurexin lacking the splice site 4 insertion.

It was quite unforeseen that the major difference in phenotype between overexpressed NLGN1 and NLGN3 would reside in the extracellular domain. This domain is known to mediate both cis- and trans- interactions. Specifically, homo- and heterodimerization have been described as well as binding to the presynaptic neurexins (Arac et al., 2007; Fabrichny et al., 2007). Based on our chimeric analysis and *in vivo* molecular replacement experiments, it is likely that the alternatively spliced insertion at site B in the extracellular domain of NLGN1 is responsible for its unique functions. Of the neuroligins, only the NLGN1 gene contains the possibility of an insertion at the B splice site, which has been shown to affect the specificity of neurexin binding. Specifically, NLGN1 containing the B insertion binds preferentially to β-neurexins lacking an insertion at splice site 4 and does not bind the longer form α-neurexins (Boucard et al., 2005). This splicing of neurexin at splice site 4 varies both developmentally and regionally throughout the brain while also being influenced by activity (Iijima et al., 2011). The presence of the B site in neuroligin likely has ramifications for the function of the protein, with a number of previous studies reporting different altered phenotypes of NLGN1 containing the B site that include a more potent synaptogenic phenotype (Boucard et al., 2005), a stronger bias toward excitatory synaptic formation (Chih et al., 2006), and differences in the rate of presynaptic induction (Lee et al., 2010). However, the role of the B site in normal physiological function remains unknown. Here we show, for the first

time, a physiological consequence of the B site insertion on synaptic plasticity. We propose that this effect is among the first hard evidence for the emerging model that neuroligin subtypes (along with other postsynaptic adhesion molecules) form a trans-synaptic code via their specific binding to the numerous alternatively spliced variants of neurexin – a code that specifies particular synaptic properties, in this case competence to undergo synaptic plasticity.

Figure 18. Role of neuroligin in the expression of adult hippocampal LTP.

(A) Schematic illustrating the timeline of the lentiviral injections and paired recordings from either area CA1 or dentate gyrus. **(B)** Knockdown of NLGN1 does not affect LTP in area CA1 (n = 6 ctrl, 6 expt), but does eliminate LTP in the dentate gyrus (n = 9 ctrl, 8 expt). For all LTP graphs, control, untransfected cells are shown as filled circles and experimental, transfected cells are shown as open circles. Traces show representative currents from control cells (in black) and experimental cells (in green) before and after LTP induction (scale bar: 50 pA/20 ms). **(B')** Bar graph (means ±SEM) shows no effect of the NLGN1miR on baseline AMPAR- ($p > 0.05$, n = 12) or NMDAR-mediated ($p > 0.05$, n = 10) currents based on paired recordings in CA1. **(C and C')** Knockdown of NLGN1 does eliminate LTP in the dentate gyrus (n = 9 ctrl, 8 expt) and also results in baseline reductions of both AMPAR- ($p < 0.001$, n = 16) and NMDAR-mediated ($p < 0.005$, n = 9) currents based on paired recordings. Graphs and sample traces are analogous to those in B. **(D and D')** Knockdown of NLGN3 does not affect LTP (n = 9 ctrl, 7 expt) or baseline currents (AMPAR: $p > 0.05$, n = 13; NMDAR: $p > 0.05$, n = 10) in area CA1 and also **(E and E')** does not affect LTP in the dentate gyrus (n = 7 ctrl, 7 expt), but does reduce both AMPAR- ($p < 0.001$, n = 15) and NMDAR-mediated ($p < 0.01$, n = 12) currents. As in B, traces show representative currents from control cells (in black) and experimental cells (in green) before and after LTP induction (scale bar: 100 pA/20 ms). Individual paired recordings used to generate baseline bar graphs are shown in Figure S1.

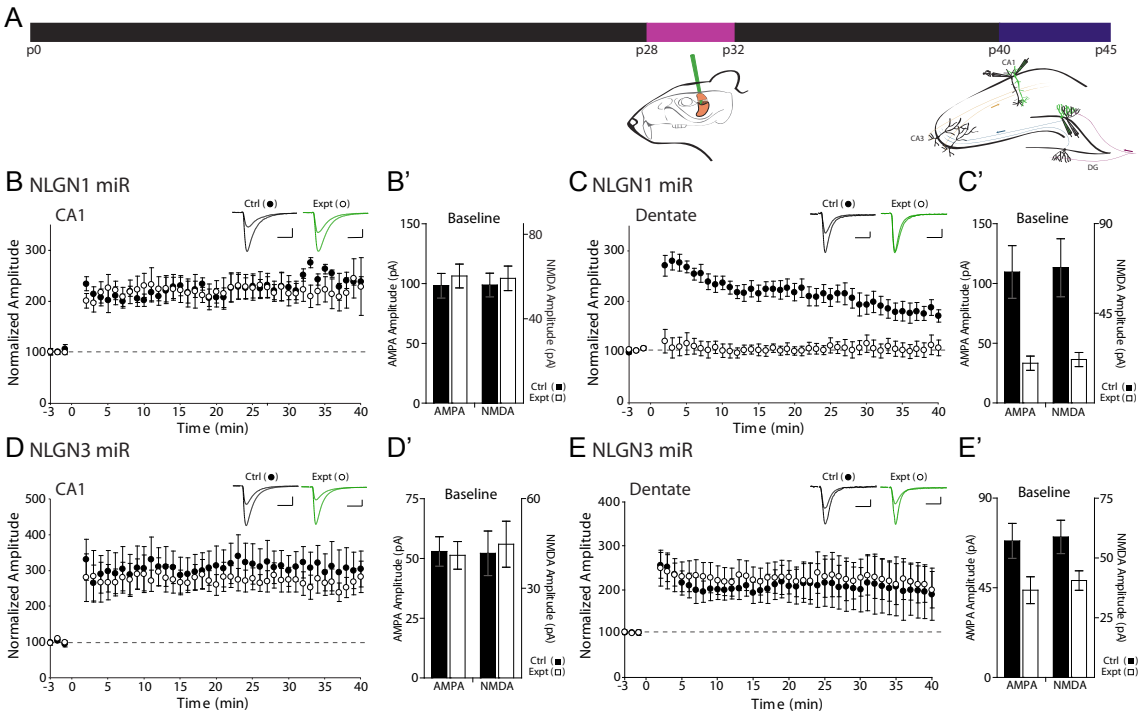

A
p0
p28
p32
p40
p45
CA1
CA3
DG
B NLGN1 miR
CA1
Ctrl (●)
Expt (○)
Normalized Amplitude
Time (min)
B'
Baseline
AMPA Amplitude (pA)
NMDA Amplitude (pA)
AMPA
NMDA
Ctrl (■)
Expt (□)
C NLGN1 miR
Dentate
C'
D NLGN3 miR
D'
E NLGN3 miR
E'

Figure 19. Quantification of knockdown efficiency by microRNA constructs and baseline effects of knockdown on excitatory currents in adult hippocampus.

(A) Reduction in NLGN1 mRNA following treatment with virus expressing NLGN1miR as assessed by real-time quantitative PCR, normalized to untransfected, control neurons. **(B)** Reduction in NLGN3 mRNA following treatment with virus expressing NLGN3miR as assessed by real-time quantitative PCR, normalized to untransfected, control neurons. **(C)** Knockdown of either NLGN1 or NLGN3 individually in the dentate gyrus results in matched decreases in AMPAR- and NMDAR-mediated currents, with NLGN1 knockdown more potently affecting current amplitudes. A two-way ANOVA test of knockdown condition (NLGN1miR, NLGN3miR) by receptor (AMPAR, NMDAR) showed a significant effect of condition ($F(1,48) = 12.38$, $p < 0.001$) with no effect of receptor ($F(1,48) = 0.6$, $p > 0.05$) or interaction ($F(1,48) = 0.08$, $p > 0.05$). Points represent individual pairs while bars represent mean ±SEM. **(D)** Lentiviral-mediated knockdown of NLGN1 in area CA1 does not affect synaptic AMPAR-mediated ($p > 0.05$, $n = 12$) or NMDAR-mediated ($p > 0.05$, $n = 10$) currents. However, in dentate gyrus, knockdown of NLGN1 results in reduced synaptic AMPAR-mediated ($p < 0.001$, $n = 16$) and NMDAR-mediated ($p < 0.005$, $n = 9$) currents. In scatter plots, open circles represent individual paired recordings, while filed circles represent means ±SEM. Traces show representative untransfected (in black) and transfected (in green) currents (scale bars: 20 pA/20 ms AMPA; 30 pA/100 ms NMDA). **(E)** Knockdown of NLGN3, like that of NLGN1, does not affect synaptic AMPAR-mediated ($p > 0.05$, $n = 13$) or NMDAR-mediated ($p > 0.05$, $n = 10$) currents in area CA1, but does result in reduced synaptic AMPAR-mediated ($p < 0.001$, $n = 15$) and NMDAR-mediated ($p < 0.01$, $n = 12$) currents in the dentate gyrus. As in A, open circles in scatter plots represent individual paired recordings, while filled circles represent means ±SEM. Traces show representative

untransfected (in black) and transfected (in green) currents (scale bars: 20 pA/20 ms AMPA; 30 pA/100 ms NMDA).

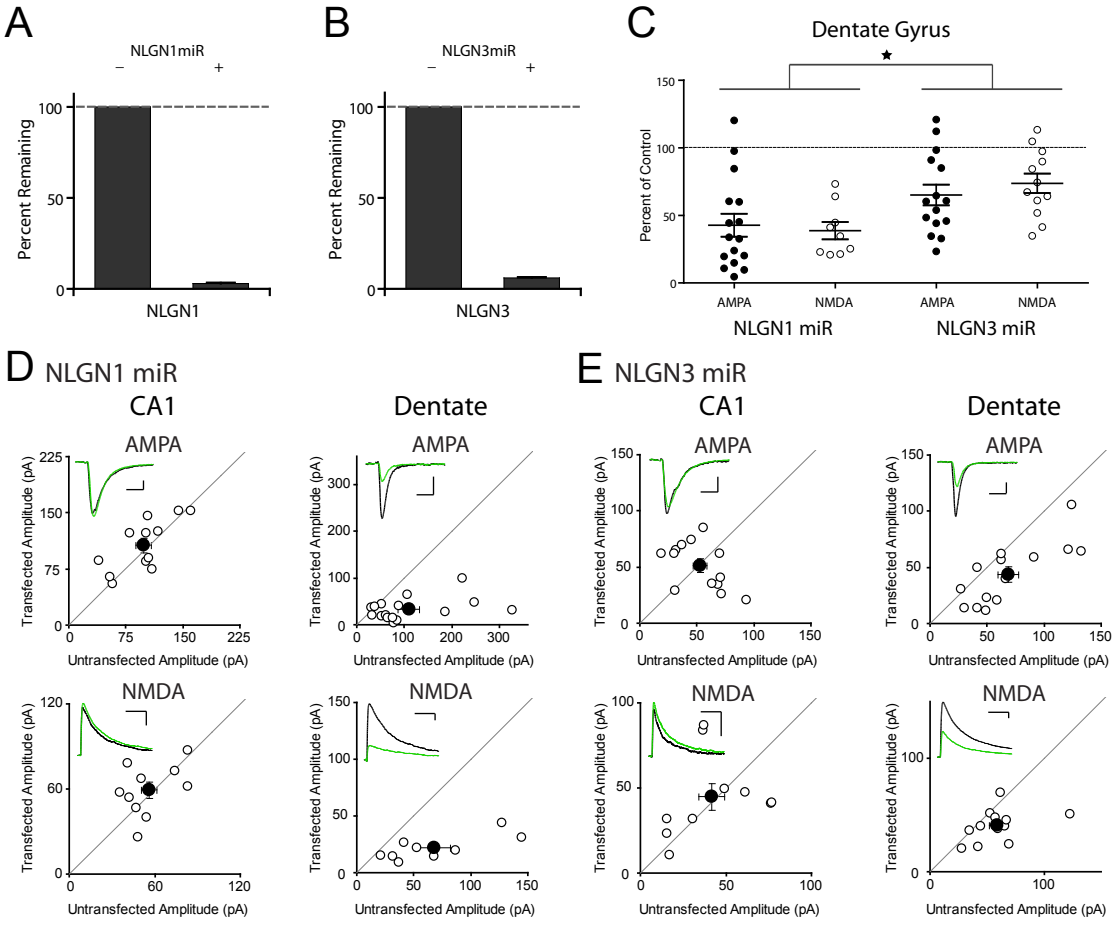

A
NLGN1miR
Percent Remaining
NLGN1
B
NLGN3miR
Percent Remaining
NLGN3
C
Dentate Gyrus
Percent of Control
AMPA
NMDA
NLGN1 miR
NLGN3 miR
D NLGN1 miR
CA1
Dentate
E NLGN3 miR
CA1
Dentate
Transfected Amplitude (pA)
Untransfected Amplitude (pA)

Figure 20. **Knockdown of NLGN1 results in a reduction in the number of functional synapses in the dentate gyrus.**

(A) Representative evoked currents recorded during this experiment, showing, to the left, mixed AMPAR/NMDAR-mediated currents from a control cell (in black) and a cell expressing the NLGN1 miR (in dark green) and pure AMPAR-mediated currents after the addition of APV from the same control cell (in grey) and experimental cell (in light green). To the right is shown the pure NMDAR-mediated, subtracted current from the control cell (in black) and experimental cell (in dark green). Scale bar: 20 pA/20 ms. **(B)** Knockdown of NLGN1 results in reductions in the evoked amplitude of the mixed current ($p < 0.05$, $n = 10$), a trend toward reductions in the pure AMPAR-mediated current ($p = 0.0547$, $n = 9$), and reductions in the subtracted, NMDAR-mediated current ($p < 0.05$, $n = 9$). Grey points with connecting lines indicate individual paired recordings, while black points indicate means ±SEM. **(C)** Evoked NMDAR-mediated charge transfer as a percentage of the total mixed charge transfer of the evoked response shown as mean ±SEM ($p > 0.05$, $n = 10$). **(D)** Weighted tau for the decay of the NMDAR-mediated component of the evoked current. Points with connecting lines indicate individual pairs ($p > 0.05$, $n = 9$). **(E)** Representative currents shown exactly as in A, except for spontaneous rather than evoked currents (scale bar: 4 pA/20 ms). **(F)** Knockdown of NLGN1 results in a reduction in the frequency of spontaneous currents ($p < 0.001$, $N = 12$). Grey points with connecting lines indicate individual paired recordings, while black points indicate means ±SEM. **(G)** Knockdown of NLGN1 does not alter the amplitude of spontaneous mixed currents ($p > 0.05$, $n = 15$ ctrl, 16 expt), pure AMPAR-mediated currents ($p > 0.05$, $n = 14$ ctrl, 15 expt), or subtracted, NMDAR-mediated currents ($p > 0.05$, $n = 12$ ctrl, 14 expt). Points indicate individual recordings, while bars indicate means ±SEM. **(H)** Spontaneous NMDAR-mediated charge transfer as a percentage of

the total mixed charge transfer of the spontaneous response shown as mean ±SEM ($p > 0.05$, $n = 9$). **(I)** Representative dye-filled dentate granule cells to use for spine density analysis from both control and NLGN1miR conditions. Scale bar: 5 μm. **(J)** Quantification of spine phenotype following knockdown of NLGN1 showing a reduction in the spine density as compared to control ($p < 0.005$, $n = 10$ ctrl, 11 expt). **(K)** Coefficient of variation analysis for paired recordings of NLGN1miR expressing cells and control cells in the dentate gyrus, consistent with changes in quantal content. Left graph plots individual pairs (AMPA $n = 16$; NMDA $n = 9$), right graph plots mean ±SEM. In each case, AMPAR responses are indicated by filled circles and NMDAR responses are indicated by open circles.

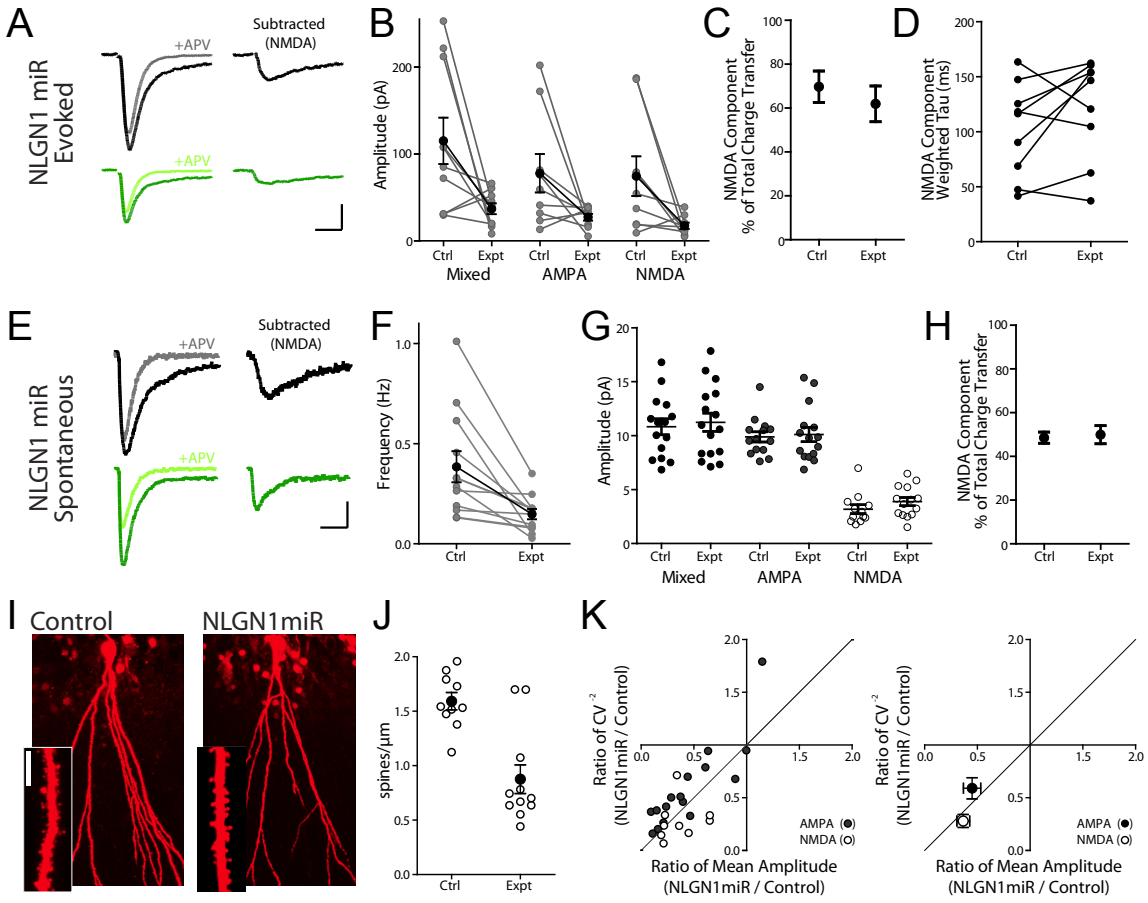

A
NLGN1 miR Evoked
+APV
Subtracted (NMDA)
+APV
B
Amplitude (pA)
Ctrl
Expt
Mixed
AMPA
NMDA
C
NMDA Component % of Total Charge Transfer
D
NMDA Component Weighted Tau (ms)
E
NLGN1 miR Spontaneous
F
Frequency (Hz)
G
H
I
Control
NLGN1miR
J
spines/µm
K
Ratio of CV -2 (NLGN1miR / Control)
AMPA (●)
NMDA (○)
Ratio of Mean Amplitude (NLGN1miR / Control)

Figure 21. Knockdown of NLGN3 in the dentate gyrus results in a reduction in the number of functional synapses.

(A) Representative dye-filled dentate granule cells to use for spine density analysis from both control and NLGN3miR conditions. Scale bar: 5 μm. **(B)** Quantification of spine phenotype following knockdown of NLGN3 showing a reduction in the spine density as compared to control ($p < 0.001$, n = 11 ctrl, 11 expt). **(C)** Coefficient of variation analysis for paired recordings of NLGN3miR expressing cells and control cells in the dentate gyrus. Values fall along the 45º line, interpreted as a change in quantal content (number of synapses x release probability), whereas values along the horizontal line would have indicated changes in quantal size (number of receptors per synapse). Left graph plots individual pairs (AMPA n = 11; NMDA n = 10), right graph plots mean ±SEM. AMPAR responses are indicated by filled circles and NMDAR responses are indicated by open circles.

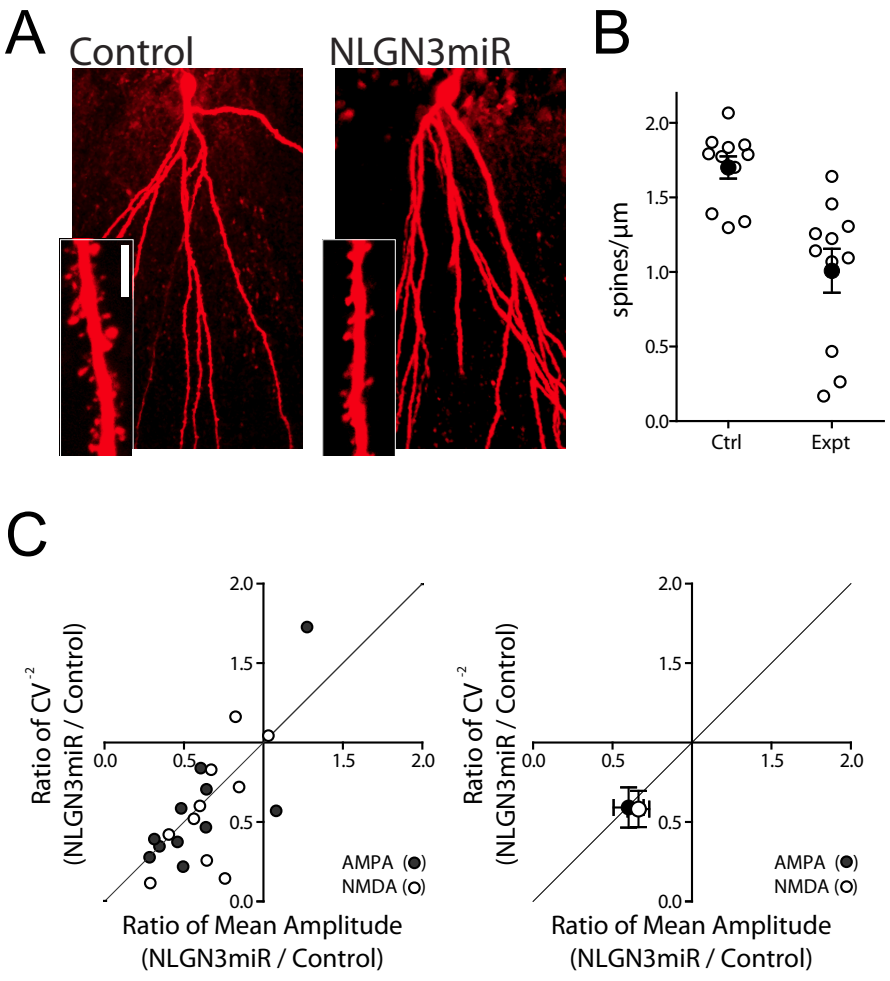

A
Control
NLGN3miR
B
spines/µm
2.0
1.5
1.0
0.5
0.0
Ctrl
Expt
C
Ratio of CV-2 (NLGN3miR / Control)
Ratio of Mean Amplitude (NLGN3miR / Control)
AMPA
NMDA
0.0
0.5
1.5
2.0

Figure 22. Differences in expression phenotype between NLGN1 and NLGN3 are due to a specific difference in the extracellular domain.

(A) Bar graph showing the effect of overexpression of NLGN1, NLGN3 or chimeras of the neuroligins on the background of a neuroligin knockdown (NLmiRs). Bar showing the NLmiR knockdown phenotype alone was previously published (Shipman et al., 2011) and is only repeated here for clarity. Increases in NMDAR-mediated currents as compared to control can be seen on this background with the expression of either full-length NLGN1 ($p < 0.001$, $n = 13$) or a chimera that contains the extracellular domain of NLGN1 and the intracellular domain of NLGN3 (NLGN1-TM-NLGN3, $p < 0.001$, $n = 14$). No increase above control is found upon expression of either full-length NLGN3 ($p > 0.05$, $n = 13$) or a chimera containing the extracellular domain of NLGN3 and the intracellular domain of NLGN1 (NLGN3-TM-NLGN1, $p > 0.05$, $n = 12$) on this background. Inclusion of at least 326 amino acids from the N-terminus of NLGN1 in the chimera confers an enhancement of NMDAR responses (NLGN1-418-NLGN3, $p < 0.005$, $n = 13$; NLGN1-390-NLGN3, $p < 0.05$, $n = 10$; NLGN1-326-NLGN3, $p < 0.005$, $n = 12$), whereas inclusion of 254 or fewer amino acids from the N-terminus of NLGN1 does not (NLGN1-254-NLGN3, $p > 0.05$, $n = 6$; NLGN1-211-NLGN3, $p > 0.05$, $n = 6$; NLGN1-166-NLGN3, $p > 0.05$, $n = 10$). Schematic below represents the gross domain structure of the neuroligins, with a short intracellular domain and long extracellular domain (TM: transmembrane). Blue is used to denote NLGN1, while red marks NLGN3. Two alternatively spliced sites (A, present in both NLGN1 and NLGN3, and B, present only in NLGN1) are marked in green. Amino acid numbers in the chimeras and to the left in the schematic are referenced to NLGN1 and indicate the first amino acid in the chimera that is unique to NLGN3. **(B)** Sequence comparison between NLGN1 and NLGN3 in the region of interest that differs between chimeras NLGN1-326-NLGN3 and

NLGN1-254-NLGN3 showing the B site insert in NLGN1. **(C)** Direct comparison of the full-length NLGN1 and NLGN3 expressed on the knockdown background showing a clear difference with respect to enhancement of NMDAR-mediated evoked currents ($p < 0.005$, n = 13 NLGN1, 13 NLGN3). Open circles represent individual paired recordings, while filled circles represent means ±SEM (NLGN1 in blue, NLGN3 in red). Traces show representative currents for each condition, with NLGN1 in blue and NLGN3 in red, each with a simultaneously recorded control cell (in black) (scale bar: 50 pA/100 ms). **(D)** Direct comparison of the two chimeras of neuroligin expressed on the knockdown background showing the same difference as in C for the NLGN1 extracellular domain-containing chimera (NLGN1-TM-NLGN3) as compared to the NLGN3 extracellular domain-containing chimera (NLGN3-TM-NLGN1) ($p < 0.001$, n = 14 NLGN1-TM-NLGN3, 12 NLGN3-TM-NLGN1). All other characteristics of the scatter plot are as in C, except that in this case blue marks NLGN1-TM-NLGN3 and red marks NLGN3-TM-NLGN1. **(E)** Direct comparison of chimeras NLGN1-326-NLGN3 and NLGN1-254-NLGN3 again illustrating the differential enhancement of the NMDAR-mediated evoked currents ($p < 0.05$, n = 12 NLGN1-326-NLGN3, 6 NLGN1-254-NLGN3). All other characteristics of the scatter plot are as in C, except that in this case blue marks NLGN1-326-NLGN3 and red marks NLGN3-254-NLGN1.

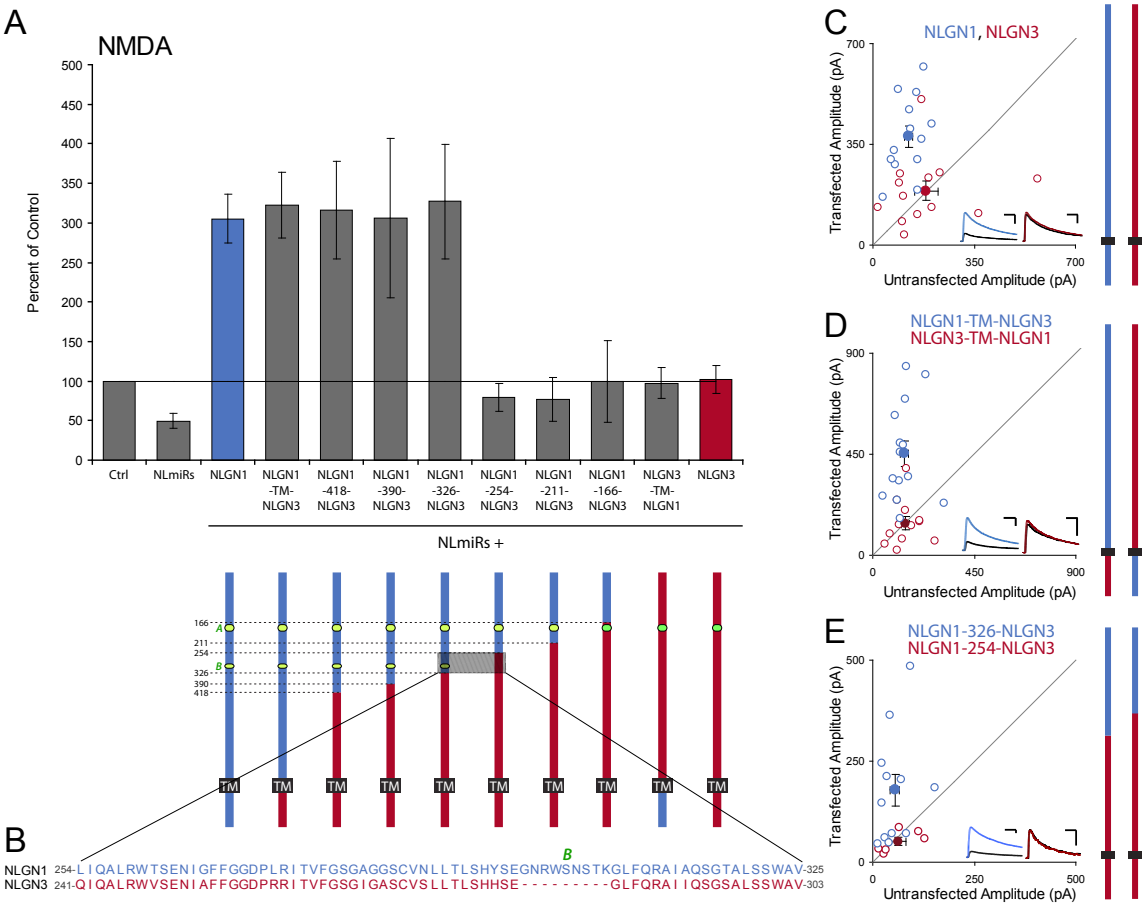

A
NMDA
Percent of Control
500
450
400
350
300
250
200
150
100
50
0
Ctrl
NLmiRs
NLGN1
NLGN1 -TM- NLGN3
NLGN1 -418- NLGN3
NLGN1 -390- NLGN3
NLGN1 -326- NLGN3
NLGN1 -254- NLGN3
NLGN1 -211- NLGN3
NLGN1 -166- NLGN3
NLGN3 -TM- NLGN1
NLGN3
NLmiRs +
166
A
211
254
B
326
390
418
TM
B
NLGN1 254-LIQALRWTSENIGFFGGDPLRITVFGSGAGGSCVNLLTLSHYSEGNRWSNSTKGLFQRAIAQSGTALSSWAV-325
NLGN3 241-QIQALRWVSENIAFFGGDPRRITVFGSGIGASCVSLLTLSHHSE---------GLFQRAIIQSGSALSSWAV-303
C
NLGN1, NLGN3
Transfected Amplitude (pA)
Untransfected Amplitude (pA)
700
350
0
D
NLGN1-TM-NLGN3
NLGN3-TM-NLGN1
900
450
E
NLGN1-326-NLGN3
NLGN1-254-NLGN3
500
250

Figure 23. Disruption of the B site insertion in NLGN1 impairs the enhancement of NMDAR-mediated currents.

Direct comparison of full-length NLGN1 and a mutant of NLGN1 with eight amino acids in the B site removed, each co-expressed with the NLmiRs, showing a lack of enhancement by the ΔB mutant ($p < 0.001$, n = 13 NLGN1, 11 NLGN1 ΔB). Full length NLGN1 data set, originally shown in Figure 3, is repeated here for clarity. Open circles represent individual paired recordings, while filled circles represent means ±SEM (NLGN1 in blue, NLGN1 ΔB in black). Traces show representative currents for each condition, with NLGN1 in blue and NLGN1 ΔB in black, each with a simultaneously recorded control cell (in grey) (scale bar: 30 pA/100 ms).

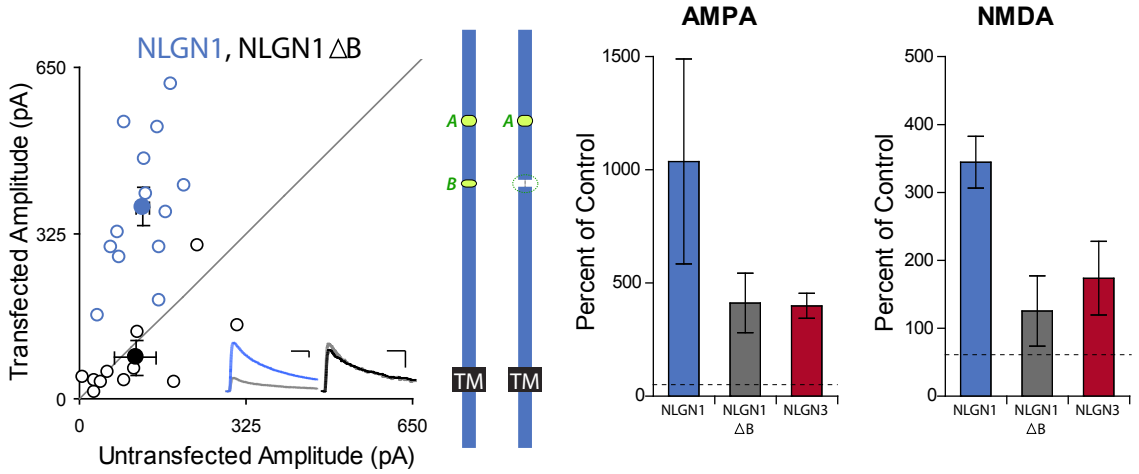

NLGN1, NLGN1 △B
Transfected Amplitude (pA)
Untransfected Amplitude (pA)
650
325
0
A
B
TM
AMPA
NMDA
Percent of Control
1500
1000
500
400
300
200
100
NLGN1
NLGN1 ΔB
NLGN3

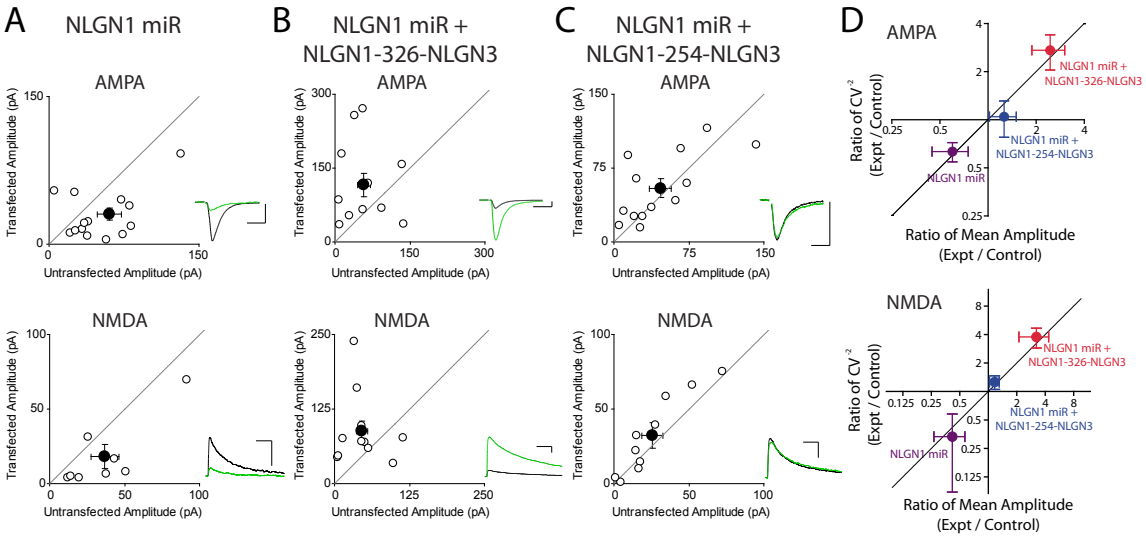
Figure 24. Role of NLGN1 and the B site insertion in its extracellular domain in young hippocampal LTP.

(A) Schematic illustrating the timeline of electroporations and paired recordings. **(B)** Knockdown of NLGN1 eliminates LTP in young CA1 (n = 9 ctrl, 7 expt). For all LTP graphs, control cells are shown as filled circles ±SEM and experimental cells are shown as open circles ±SEM. Traces show representative currents from control (in black) and experimental cells (in green) before and after LTP induction (scale bar: 40 pA/20 ms). **(B')** Bar graph (means ±SEM) shows a reduction in baseline AMPAR- ($p < 0.05$, n = 15) and NMDAR-mediated ($p < 0.05$, n = 8) EPSCs. **(C)** Knockdown of NLGN1 plus replacement by NLGN1-326-NLGN3 rescues the LTP deficit found with the knockdown alone (n = 6 ctrl, 6 expt) and **(C')** rescues the reduction in baseline currents (means ±SEM; AMPA, $p < 0.005$, n = 12; NMDA, $p < 0.005$, n = 12 versus NLGN1miR alone). **(D)** Knockdown of NLGN1 plus replacement by NLGN1-254-NLGN3 fails to rescue LTP (n = 10 ctrl, 7 expt) but **(D')** does rescue baseline currents (means ±SEM; AMPA, $p < 0.005$, n = 13; NMDA, $p < 0.005$, n = 10 versus NLGN1miR alone).


A
E16
p0
p11
p15
CA1
CA3
DG
B
NLGN1 miR
Ctrl (●)
Expt (○)
Normalized Amplitude
Time (min)
B′
Baseline
AMPA Amplitude (pA)
NMDA Amplitude (pA)
Ctrl (■)
Expt (□)
AMPA
NMDA
C
NLGN1 miR +
NLGN1- 326 -NLGN3
C′
D
NLGN1 miR +
NLGN1- 254 -NLGN3
D′

Figure 25. Baseline effects of NLGN1 knockdown and replacement by NLGN1-3 chimeras in young CA1 pyramidal neurons.

(A) *In utero* NLGN1miR expression results in reductions in AMPAR- ($p < 0.05$, $n = 15$) and NMDAR-mediated ($p < 0.05$, $n = 8$) EPSCs. For all scatter plots, open circles represent individual paired recordings, while filled circles represent means ±SEM. Traces show representative currents for each condition, with control in black and experimental in green (scale bar: 40 pA/20 ms). **(B)** *In utero* replacement of NLGN1 with NLGN1-326-NLGN3 chimera results in non-significant enhancements of AMPAR- ($p > 0.05$, $n = 12$) and NMDAR-mediated ($p > 0.05$, $n = 12$) responses. Scatter plots and traces are as in A. **(C)** *In utero* replacement of NLGN1 with NLGN1-254-NLGN3 chimera rescues AMPAR- ($p > 0.05$, $n = 13$) and NMDAR-mediated ($p > 0.05$, $n = 10$) currents to control levels. Scatter plots and traces are as in A. **(D)** Coefficient of variation analysis for paired recordings of NLGN1miR expressing cells and chimeric replacement cells in young CA1 pyramidal cells. For each data set, values fall along the 45º line, interpreted as changes in quantal content (number of synapses x release probability), whereas values along the horizontal line would have indicated changes in quantal size (number of receptors per synapse). Graph plots mean ±SEM.


A
NLGN1 miR
AMPA
Transfected Amplitude (pA)
Untransfected Amplitude (pA)
NMDA
B
NLGN1 miR +
NLGN1-326-NLGN3
C
NLGN1 miR +
NLGN1-254-NLGN3
D
Ratio of CV-2
(Expt / Control)
Ratio of Mean Amplitude
(Expt / Control)
NLGN1 miR +
NLGN1-326-NLGN3
NLGN1 miR +
NLGN1-254-NLGN3
NLGN1 miR

CHAPTER 6:

Distance dependent scaling of AMPARs is cell-autonomous and GluA2-dependent

Introduction

Information transfer between neurons, in the form of initiation or suppression of action potentials, occurs by the summing of many dendritic inputs in the soma. In this way, each individual neuron serves as a signal integrator, vastly increasing the information capacity of the system. However, as current travels along a dendrite, electrotonic filtering reduces the amplitude and slows the kinetics of electrical potentials. This represents a problem for the integration of signals in neurons with large, complex dendritic arbors whereby excitatory post-synaptic potentials (EPSPs) from distal synapses would contribute less than EPSPs from proximal synapses. Indeed, this critically affects our understanding of neural circuits, in which synaptic capacity across the dendrites of each individual neuron is assumed to be homogeneous. Yet, in functioning hippocampal pyramidal neurons, this problem appears to be solved by the cell, as the amplitude of somatic EPSPs has been shown to be independent of synapse distance from the soma (Magee and Cook, 2000).

Converging evidence has implicated up-regulation of synaptic AMPA receptors in distal synapses as the reason that somatic EPSPs appear similar despite differing amounts of filtering (Andrasfalvy and Magee, 2001; Smith et al., 2003), a phenomenon known as distance-dependent scaling. However, we know relatively little about how this scaling is achieved. Based on knockout animals, it has been proposed that the scaling is responsive to activity (Andrasfalvy et al., 2008) and may even share mechanistic similarities with long-term potentiation (LTP) based on a requirement for the AMPA receptor (AMPAR) subunit GluA1 (Andrasfalvy et al., 2003). The dependence on GluA1 differentiates LTP from another form of synaptic plasticity, homeostasis, which depends instead on GluA2 (Gainey et al., 2009; Goold and Nicoll, 2010). One might, then, pursue a model for distance-dependent scaling based on the molecules thought to be involved

in LTP. However, it is not known whether the requirement for GluA1 is specific, as has been shown to be the case in LTP (Hayashi et al., 2000; Shi et al., 2001), or might extend to other AMPAR subunits. Moreover, at the most basic level, it is not known whether distance-dependent scaling is generated by the network and greater architecture of the brain or, conversely, is generated on a cell-by-cell basis.

In this study, I set out to study the molecular properties of distance-dependent scaling. In doing so, I provide the first independent confirmation of an increase in synaptic AMPAR content as a function of distance in CA1 pyramidal cells. I am also able to show that the scaling is expressed, and may be manipulated, in a cell-autonomous manner and finally, that distance-dependent scaling requires both a reserve pool of AMPARs and specifically requires the subunit GluA2.

Results

Verification of a distance-dependent synaptic AMPAR gradient in CA1 pyramidal neurons

Distance-dependent scaling exemplifies the striking precision that exists in the realm of biology – neurons that perfectly counteract the passive electrical properties of their long dendritic lengths by increasing the strength of distal synapses. This normalization of input contribution over a swath of dendritic arbor has profound implications for the integration of synaptic signals and is consistently an important factor when modeling the activity of neurons *in silico* and interpreting the results of biological work. Yet despite the profound interpretive impact of distance-dependent scaling, the actual experimental evidence for its existence comes almost entirely from the work of a single laboratory. Without assailing the rigorous work done by the members of this laboratory, it remains a sad fact in science that much of what is published does not stand the test of time and the best evidence for any finding is reproducibility – that is, independent confirmation of a result by different experimenters. To this end, I set out to measure the strength of AMPAR-mediated synaptic responses as a function of distance from the soma in CA1 pyramidal neurons in an effort to independently confirm or deny the existence of a distance-dependent gradient.

Unfortunately, accurate measurements of the local synaptic currents cannot be made from the cell's soma where it is easy to record. Passive electrical filtering and the difficultly of achieving voltage-clamp over distance contribute too heavily to the recording of currents that originate far from the site of the patch pipette. For accurate estimations of AMPAR content at a synapse, one wants the recording pipette to be as physically close to the synapses of interest as possible. Therefore, I recorded miniature AMPAR excitatory postsynaptic currents (mEPSCs) by directly patching the primary apical

dendrite of hippocampal CA1 pyramidal neurons while locally stimulating the release of presynaptic vesicles of neurotransmitter by puffs of hyperosmotic solution (Fig. 26A). Because of the incredibly low rate of spontaneous mEPSCs in this preparation, these recordings contain a nearly pure population of mEPSCs arising from the area just around the recording pipette, the amplitude of which serves as a readout for synaptic AMPAR content. By varying the distance of my recordings from the cell body of the neuron, I was able to measure the amplitude of mEPSCs as a function of distance along the apical length of the dendrite.

I found that mEPSC amplitudes increase with distance from the soma (Fig. 26B), in perfect agreement with Magee et al. (2000). To be specific, the average amplitude of the most distal synapses in stratum radiatum was slightly more than double that of the most proximal synapses (Fig. 26C). By comparing the histogram of synaptic amplitudes of distal and proximal recordings, it becomes clear that the distal increase in amplitude is primarily due to an augmentation of large amplitude responses with a very slight change in the distribution of lower amplitude events (Fig. 26D). The original report of the scaling phenomenon found a similar perseverance of small amplitude events at distal locations (Magee and Cook, 2000), although this was not found to be the case in a subsequent study (Smith et al., 2003). This distinction has a profound implication on the interpretation of the phenomenon as the data presented here do not represent *scaling* of the response amplitude in a pure sense (Fig. 26D, inset).

Similar to the original characterization of distance-dependent scaling, I also recorded an increase in the kinetics of AMPAR mEPSCs along the proximo-distal axis (Fig. 26E). This speeding of distal currents may be largely accounted for by properties of the membrane (Magee and Cook, 2000) and voltage gated conductance that serve to normalize the temporal integration of synaptic inputs over the dendritic arbor (Magee, 1999). The result of my initial investigation of AMPAR-mediated synaptic currents as a

function of distance, then, is an unequivocal independent confirmation of the phenomenon of distance-dependent scaling.

Evidence for cell-autonomous scaling of AMPAR currents

In order to understand the molecular basis of distance-dependent scaling it would be beneficial to first know whether the gradient is regulated on a cell-by-cell basis or, rather, dependent on cell-extrinsic factors – those diffusible extracellular signals that underlie organization of the circuit in the first place. The stereotyped architecture of the hippocampus lends considerable ambiguity to this question: although the gradient of AMPARs is expressed as a function of distance from the cell body, the tight arrangement of the cell bodies of all CA1 pyramidal neurons into a single layer means that the gradient is also expressed within the coordinates of the larger structure of the hippocampus. So then, how can we know whether the AMPAR gradient is referenced to the cell body (and likely cell-autonomous) or, rather, the cell layer (and likely influenced by factors extrinsic to the pyramidal neuron)? To answer this question, I left behind the typical CA1 pyramidal neuron and turned to a relatively unstudied cell type of the hippocampus: the pyramidal-like principle neuron, or PLP cell. The gross morphology of a PLP cell is quite similar to that of an ordinary CA1 pyramidal neuron, but the location of the cell is perfectly suited to the question at hand. Rather than having their cell bodies tightly packed into a cell layer, PLP cells are scattered throughout stratum radiatum – this distribution, in fact, being their primary identifying feature (Fig. 27A, blue cells) (Bullis et al., 2007). The orientation of their apical dendrite runs parallel to that of the layer-based pyramidal neurons, but the location of individual PLP cell bodies varies within the larger architecture of the hippocampus. Assuming that these PLP cells also display distance-dependent scaling, there are two possible scenarios: one in which the

scaling will be referenced to the cell body; and another in which the scaling will be referenced to the architecture of the hippocampus – the cell layer in particular.

As I did for the CA1 pyramidal neurons, I recorded local mEPSCs via dendritic patches along the length of the primary apical dendrite of PLP cells. I then analyzed these currents as a function of both distance from the cell soma and as a function of distance from the cell layer. The mEPSC amplitudes recorded from PLP cells display a distance-dependent gradient that closely matches that of layer pyramidal neurons when referenced to the soma (Fig. 27B), but does not match when referenced to the cell layer (Fig. 27C). This soma-referenced gradient strongly suggests that distance-dependent scaling is a cell autonomous feature, rather than a consequence of the hippocampal architecture or diffusible molecular cues.

The gradient of AMPARs along the proximal-distal axis of pyramidal neurons does not exist alone. Rather, there are other distally-increasing gradients of ion channels. One such gradient is that of the I_h carrying channel HCN (Magee, 1998). In fact, HCN channels increase with distance from the soma of a CA1 pyramidal neuron by many times – much more severe of a gradient even than that of AMPARs. Interestingly, evidence has been presented for a reversed I_h gradient in PLP cells, having a high channel density near the soma but declining with distance (Bullis et al., 2007). Unfortunately, I was unable to replicate this reversed I_h gradient in my own recording, where I instead found increased sag currents at distal locations as compared to proximal locations in both layer pyramidal cells and PLP cells (Fig. 27D,E). Therefore, this topic was not further studied. Finally, I examined the rectification of synaptic AMPARs in PLP cells to check whether they express a similar subunit composition to that of layer-based CA1 pyramidal cells. GluA2 lacking AMPARs are blocked by intracellular spermine at positive potentials, leading to a rectifying current-voltage (IV) relationship, whereas GluA2 containing receptors are not blocked by intracellular spermine and, therefore,

pass current equally at both positive and negative potentials. In fact, I found quite similar rectification, signifying the presence of GluA2-containing AMPARs in PLP cells (Fig. 27F).

A sufficient supply of AMPARs is necessary for the expression of distance-dependent scaling

If the distance-dependent scaling of AMPARs is cell-autonomous, then I should be able to influence it using molecular manipulations of an individual cell. Previously it was shown that a mouse lacking the GluA1 subunit of an AMPAR – AMPARs in CA1 pyramidal neurons being heterotetramers containing GluA1, 2, or 3 (Wenthold et al., 1996) – does not express distance-dependent scaling (Andrasfalvy et al., 2003). AMPAR-mediated currents in this mouse were normal at proximal synapses, but failed to increase as a function of distance. The interpretation of this result was that distance-dependent scaling may share a molecular pathway with a form of synaptic plasticity – long-term potentiation (LTP) – that has also been shown to be dependent on GluA1. However, recent work has challenged the dependence of LTP on the GluA1 subunit, instead arguing that loss of GluA1 simply depletes a reserve pool of surface AMPARs that are necessary for the expression of LTP, independent of subunit composition (Granger et al., In Press).

Another method to deplete this reserve pool of AMPARs is to eliminate the AMPAR accessory subunit cornichon 2 (CNIH2), which is involved in the surface trafficking of AMPARs (Herring et al., In Revision; Schwenk et al., 2009; Shi et al., 2010). I therefore made use of an shRNA targeting CNIH2, which, like the deletion of GluA1, reduces the surface pool of AMPARs. I expressed this shRNA from a lentivirus, which I injected into the hippocampi of 4-week-old rats. This results in a very sparse distribution

of shRNA expressing pyramidal cells in CA1. Ten to twelve days later, I identified transduced cells via fluorescence and locally recorded sucrose-evoked mEPSCs from these cells as before. When the amplitudes of these currents are examined as a function of distance from the soma, it is clear that the knockdown of CNIH2 in individual cells results in a similar loss of distance-dependent scaling expression as was seen in the GluA1 knockout (Fig. 28A,B) – simultaneously confirming the cell-autonomous nature of the phenomenon and the dependence on a pool of reserve AMPARs.

CNIH2 has also been shown to influence the kinetics of the AMPAR response. Specifically, its presence has been shown to slow the kinetics of an AMPAR (Gill et al., 2011; Schwenk et al., 2009; Shi et al., 2010). We speculated that a theoretical gradient of CNIH2 could partially explain the faster kinetics of distal mEPSCs. Knockdown of CNIH2 did, as expected, speed mEPSC kinetics (Fig. 28C,D). However, both the proximal and distal mEPSCs became faster thus preserving the increase in mEPSC decay over the length of the dendrite (Fig. 28C,D). A theoretical CNIH2 gradient, therefore, does not explain the kinetic gradient.

Distance-dependent scaling additionally requires the GluA2 subunit

Loss of the reserve pool of AMPARs results in a loss of both LTP and distance-dependent scaling as evidenced by the GluA1 knockout and now a CNIH2 knockdown. Thus, there are some molecular similarities between distance-dependent scaling and a form of synaptic plasticity, but certainly not all plasticity is the same. Another form of synaptic plasticity, occurring over much longer timescales, is synaptic homeostasis – the alteration of synaptic strength in response to long-term changes in activity level of a neuron. This form of synaptic plasticity has been repeatedly shown to depend on a different AMPAR subunit: GluA2 (Gainey et al., 2009; Goold and Nicoll, 2010). Loss of GluA2 affects the neuron in a much different way than loss of GluA1. Whereas loss of

GluA1 greatly depletes both synaptic and extrasynaptic AMPARs, loss of GluA2 only depletes synaptic receptors (Lu et al., 2009). Thus, LTP is normal in GluA2 knockout cells (Meng et al., 2003) because the reserve pool of AMPARs is present. The dependence of synaptic homeostasis on GluA2, on the other hand, has been ascribed to something more intrinsic to the GluA2 subunit rather than simply a pool of receptors.

Might we be able to distinguish distance-dependent scaling from these divergent forms of plasticity based on its subunit dependence? To answer that question, I made an shRNA against GluA2, expressed via lentivirus and injected into the hippocampi of 4-week-old rats as before, to assess distance-dependent scaling in the absence of GluA2. This shRNA was validated by western (Fig. 29A) and, perhaps more importantly, via physiology in neurons (Fig. 29D). I compared rectification of evoked synaptic currents in control neurons to rectification in neurons expressing the shRNA against GluA2 and found that the control neurons had linear currents (GluA2 containing), while those expressing the shRNA displayed nearly complete rectification (GluA2 lacking) (Fig. 29D).

When I examined mEPSCs in cells expressing shGluA2 as a function of distance, I found that normal distance-dependent scaling was not maintained (Fig. 29B). Surprisingly, I actually found that knockdown of GluA2 lead to a slight reversal of the AMPAR gradient (Fig. 29B,C). Thus, distance-dependent scaling requires the GluA2 subunit and must share molecular pathway components with multiple forms of synaptic plasticity. Interestingly, the distance-dependent increase in the kinetics of synaptic response was unaffected by knockdown of GluA2 (Fig. 29E,F).

GluA2 is an organizer of synaptic location

The results thus far have dealt solely with the strength of individual excitatory synaptic inputs as a function of distance. What then about the anatomical organization of synapses along the proximal-distal axis? As it turns out, there is also a gradient of

synapse density along the length of the primary apical dendrite of a CA1 pyramidal neuron (Fig. 30A,B). Like synapse strength, synapse density also increases with distance from the soma. Remarkably, this synapse density changes with the loss of GluA2 in almost exactly the same manner as the change in distance-dependent scaling of AMPARs following loss of GluA2 – knockdown of GluA2 actually reverses the gradient of synapses, with the proximal dendrite having a greater density of synapses than the distal dendrite (Fig. 30A,C). It would seem then that, in addition to the role that GluA2 plays in organizing a gradient of synaptic strength along the length of a dendrite, it also plays a role in the organization of synapse location. Knockdown of GluA1, on the other hand, did not at all affect the organization of synapse density (Fig. 30D). An interpretation of this finding might be that, although this manipulation should reduce the amplitude of distal synaptic currents, it does so as a consequence of a lack of available receptors even though the mechanisms of scaling remain in place.

Maintenance of proper synapse density over long periods of time requires action potentials

What role does activity play in the organization of synaptic input location? Loss of GluA2 resulted in reversals of both the gradient of synapse strength and the gradient of synapse density. Perhaps the alteration in synapse location is actually downstream of a change in synaptic strength or signaling through the receptors. To test this, I first cultured organotypic hippocampal slices for two weeks in NBQX to block AMPARs, and then assessed synapse density. Long-term loss of AMPAR responses had no effect on synapse location or density (Fig. 31A) suggesting that a weakening of input strength is unlikely to explain the effects of the GluA2 knockdown. Maybe the effects could be due to a gain-of-function following the knockdown. GluA2 lacking receptors, unlike GluA2

containing receptors, are permeable to calcium (Geiger et al., 1995). Could calcium influx though AMPARs following the GluA2 knockdown explain the changes in spines? I cultured slices that contained shGluA2 expressing cells in NBQX for the duration of the expression and found no change in the spine phenotype as compared with shGluA2 in the absence of NBQX (Fig. 31B) suggesting that calcium influx though GluA2-lacking receptors is not contributing to this finding.

Finally, given that excitatory synaptic input had no discernable effect on spine maintenance, I checked whether output – spiking – of the neuron was of any influence. I cultured slices in the voltage-gated sodium channel blocker, TTX, for two weeks, after which time I found a substantial reduction in overall spine density (Fig. 31C). Of course, TTX will globally reduce activity of the slice with implications for both the spiking of a given neuron as well as network activity. To assess the influence of cell-autonomous spiking, I expressed a potassium channel (Kir2.1) in individual pyramidal neurons. Expression of this channel will hyperpolarize the cell and provide a potassium current that opposes any depolarization of the cell toward threshold (Burrone et al., 2002). I found that these neurons, like those cultured in TTX, had reductions in spine density as compared with control (Fig. 31D). Thus, spiking of an individual cell is necessary for the maintenance of proper synapse density.

Discussion

This study provides important insight into the molecular mechanisms of distance-dependent scaling. In it, I am able to show that distance-dependent scaling of synaptic AMPAR content is expressed cell-autonomously rather than being downstream of extracellular factors or network activity. Consistent with the cell-autonomous expression, distance-dependent scaling may be removed on a cell-by-cell basis with knockdown of either CNIH2 or GluA2. The dependence on CNIH2 suggests a reliance on a reserve pool of AMPARs, whereas the dependence on GluA2 suggests molecular similarity to homeostatic synaptic plasticity. Finally, like the gradient of AMPARs, a distally-increasing gradient of dendritic spines is also dependent on GluA2. Spine density does not depend on direct activation of AMPARs, but rather is maintained by the presence of action potentials.

It is debatable whether this distance-dependent increase in AMPAR content really represents a pure scaling of responses. The concept of synaptic scaling, as it has been applied to the homeostatic control of synaptic strength, has the defining principle of affecting all synapses in proportion to their initial strength (Turrigiano et al., 1998). Such scaling is therefore achieved by applying a multiplicative or divisive factor to all synapses equally, which is critical for maintaining the relationship of synapses to preserve information content of the system (Turrigiano, 2008). Based on the data presented here, the increase in distal mEPSC amplitudes is not the result of applying a multiplicative factor to across all proximal amplitudes (Fig. 26D). Rather, at distal locations, there is a selective increase in large amplitude events with very little change in the distribution of small amplitude events.

Given that the amplitude of somatic EPSPs has been empirically shown to be independent of synapse location (Magee and Cook, 2000), there are two possible

explanations for the skewing of mEPSC amplitude distributions that we observe at distal locations. First, it could be that the properties of the membrane and the presence of voltage-gated conductances affect the propagation of synaptic currents differently depending on their initial amplitude. Large amplitude responses may engage more voltage-gated channels than small amplitude responses, some of which actively oppose depolarization of the cell (I_A, I_h, and I_M for example). If, as a result, large amplitude currents are filtered more strongly than small amplitude currents as they travel along a dendrite, then large amplitude synapses would need to be increased in strength as a function of distance by a larger factor than that of small amplitude synapses to normalize the contribution to somatic depolarization.

On the other hand, this skewing of the distribution of mEPSC amplitudes at distal locations could reflect a fundamentally different integration model than the one that is currently accepted. Distal dendrites could, in fact, possess two separate populations of synapses: locally-acting, small amplitude synapses, and globally-acting, large amplitude synapses. Perhaps there is a population of distal synapses that do represent a pure multiplicative scaling of proximal synapse amplitudes, and those synapses are responsible for the somatic depolarizations whose amplitudes are independent of synapse location. There may then be an additional population of distal synapses that have small amplitudes which are not strong enough to contribute individually to depolarization of the soma, but do contribute to local depolarizations. These small amplitude synapses would sum in a way that is conceptually similar to the two-stage model of dendritic integration (Katz et al., 2009), whereas the large amplitude synapses would follow a global integration model.

The dependence of distance-dependent scaling on GluA2 suggests a molecular similarity to synaptic homeostasis. How might this guide future research into this phenomenon? Homeostasis has been shown to also act downstream of calcium

(Turrigiano, 2008), which functions as a signal of neural activity by binding calmodulin and activating CaM kinases (Wayman et al., 2008). Backpropagating action potentials may serve as an instructive signal for synapse distance by generating a calcium gradient though NMDARs and voltage-gated calcium channels (Sterratt et al., 2012). All of these are future molecular targets to define the molecular pathway of distance-dependent scaling.

Figure 26. Distance-dependent scaling of AMPARs.

(A) Schematic of the recording setup and example traces. CA1 pyramidal neurons are patched at varying distances along their primary apical dendrites and mEPSCs are recorded after being locally elicited by the application of hyperosmotic solution. Top, black trace shows the lack of spontaneous activity in the absence of hyperosmotic solution. Bottom traces show representative currents recorded from proximal (blue), mid (red), and distal (purple) locations (scale bar: 20pA/0.5s). **(B)** mEPSC amplitude increases as a function of distance from soma (n = 31; linear fit has non-zero slope, $p < 0.0001$, $R^2=0.7617$). Filled circles are individual recordings; line is a 2^{nd} order polynomial regression. **(C)** Average mEPSC amplitudes binned by location; proximal (50-120µm), mid (130-210µm), and distal (220-290µm). Compared with the amplitudes of proximal events (n = 8), both mid (n = 11; $p < 0.005$) and distal (n = 12; $p < 0.005$) mEPSCs are larger. Distal mEPSCs are additionally larger than mid ($p < 0.0005$). Bars show mean ±SEM. Traces to the right show average proximal (blue), mid (red), and distal (purple) mEPSCs (scale bar: 6pA/10ms). **(D)** Histogram of mEPSC amplitudes for all proximal and distal events showing an augmentation of large amplitude distal mEPSCs. Inset shows cumulative probability of mEPSC amplitudes (mean ±SEM). Black line shows proximal amplitudes scaled by 1.8. **(E)** Weighted tau for the decay of mEPSCs binned by location as in C. Compared with the decay of proximal events, both mid ($p < 0.05$) and distal ($p < 0.001$) mEPSCs are faster. Mid and distal decay times are not significantly different ($p > 0.05$). Bars show mean ±SEM. Traces to the right show average mEPSCs as in C, scaled and aligned to their peaks (scale bar: 10ms).

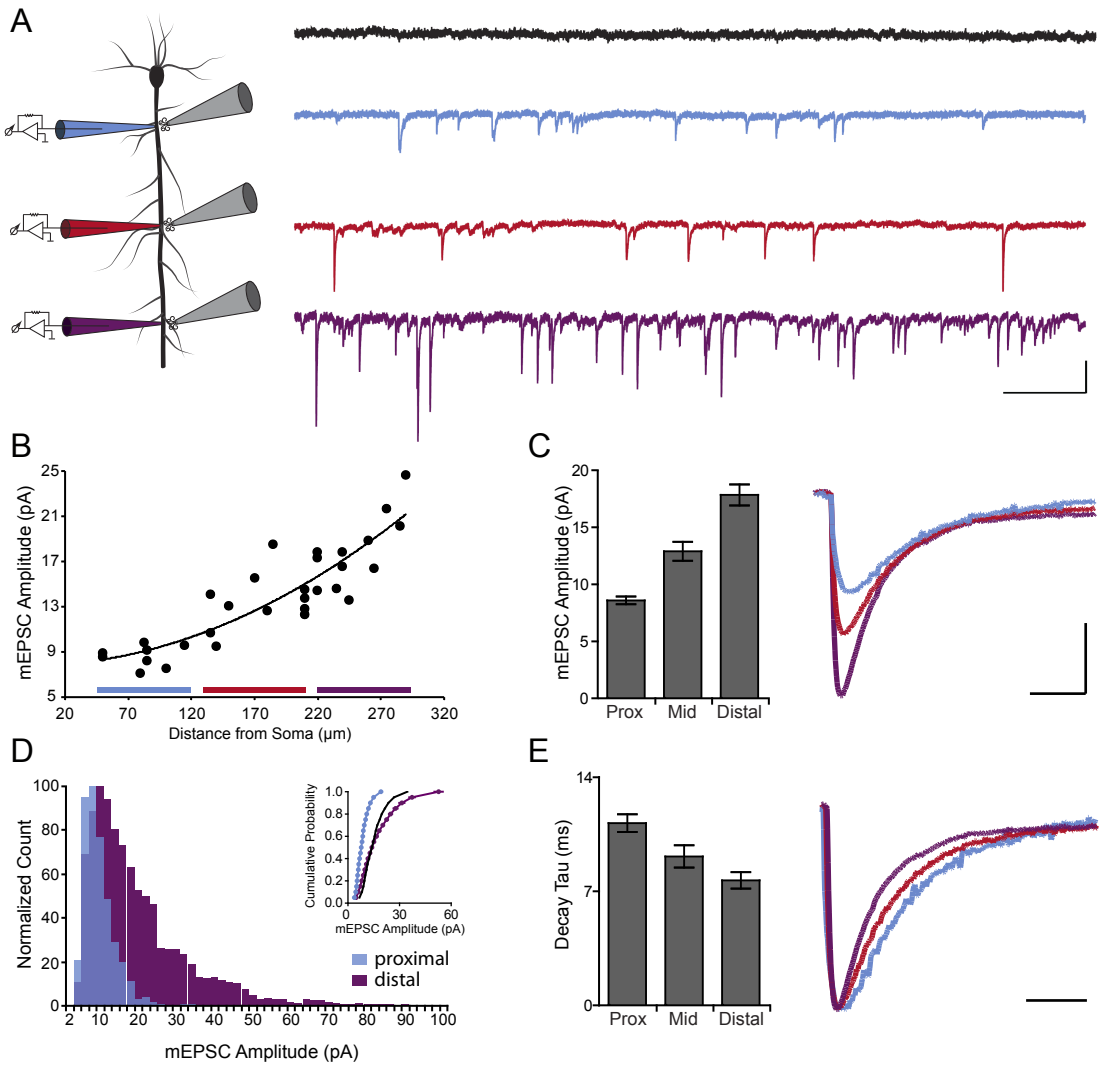

A
B
mEPSC Amplitude (pA)
Distance from Soma (μm)
C
mEPSC Amplitude (pA)
Prox
Mid
Distal
D
Normalized Count
mEPSC Amplitude (pA)
Cumulative Probability
proximal
distal
E
Decay Tau (ms)
Prox
Mid
Distal

Figure 27. AMPAR gradient is referenced to the soma in PLP cells.

(A) Organization of PLP cells. As opposed to CA1 pyramidal neurons (in grey) that have their cell bodies tightly packed in a layer, PLP cells (in blue) have their cell bodies scattered throughout stratum radiatum. **(B)** When referenced to the soma, AMPAR mEPSCs recorded from PLP cells increase with distance and match the scaling curve found in CA1 pyramidal neurons ($n = 19$; linear fit has non-zero slope, $p < 0.005$, $R^2=0.4184$). This linear fit of PLP amplitudes does not differ from that of CA1 pyramidal neuron amplitudes in either slope ($p > 0.05$) or elevation ($p > 0.05$). Blue filled circles show individual PLP recordings, gray filled circles show CA1 pyramidal recordings for comparison. **(C)** When referenced to the cell layer, PLP mEPSCs amplitudes do not match those recorded from CA1 pyramidal neurons (difference in elevation, $p < 0.0001$). Points are analogous to those in B. **(D)** Sag currents measured by a hyperpolarizing step at proximal (top) and distal (bottom) recording locations in CA1 pyramidal neurons. **(E)** As in D, but recorded in PLP cells. **(F)** Rectification of pyramidal and PLP cell AMPAR responses showing comparably linear currents. For both cell types, average evoked AMPAR response to extracellular stimulation at a holding potential of -70mV, 0mV, and +40mV are shown (scale bar: 50pA/25ms).

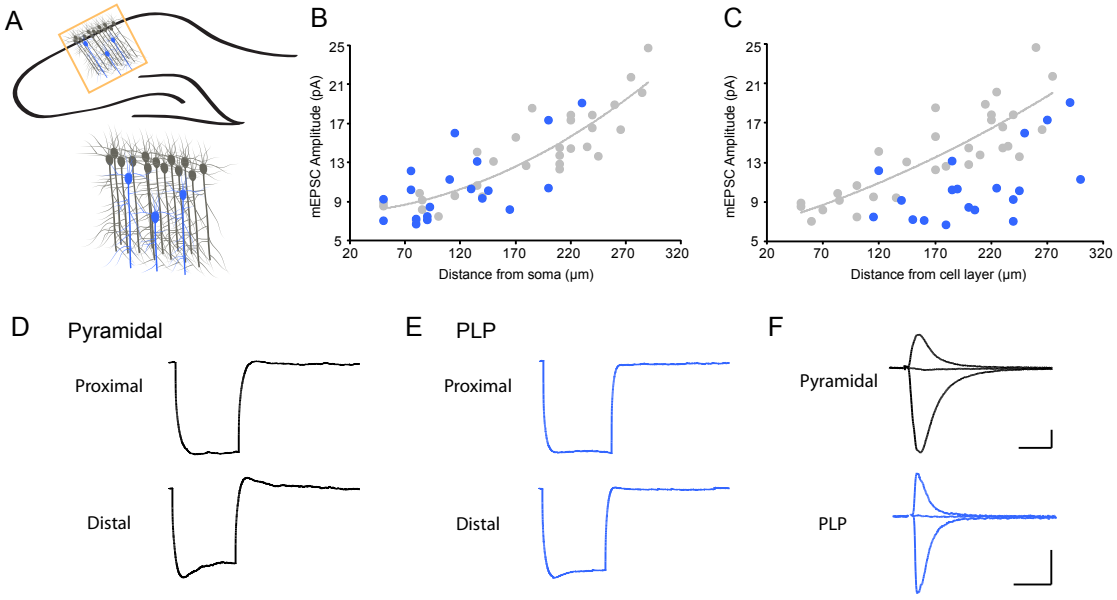

A
B
C
mEPSC Amplitude (pA)
25
21
17
13
9
5
20
70
120
170
220
270
320
Distance from soma (μm)
Distance from cell layer (μm)
D
Pyramidal
Proximal
Distal
E
PLP
Proximal
Distal
F
Pyramidal
PLP

Figure 28. Cornichon 2 knockdown selectively reduces distal EPSCs.

(A) Following knockdown of CNIH2, AMPAR mEPSCs do not increase as a function of distance from the soma (n = 12, slope of linear fit differs from control, $p < 0.0001$). Red filled circles show individual recordings from shCNIH2 expressing cells, gray filled circles show recordings from control cells for comparison. **(B)** Average mEPSC amplitudes binned by location: proximal (50-120µm) and distal (220-290µm). Proximal mEPSC amplitudes following knockdown (n = 8) do not differ from control proximal amplitudes ($p > 0.05$), whereas distal mEPSC amplitudes following knockdown (n = 4) are smaller than control distal amplitudes ($p < 0.005$). No difference exists between proximal and distal mEPSC amplitudes following knockdown ($p > 0.05$). Bars show mean ±SEM. Traces to the right show average proximal (light red) and distal (dark red) mEPSCs (scale bar: 2pA/10ms). **(C)** The decay kinetics of mEPSCs speed as a function of distance from the soma in control cells (n = 31; linear fit has non-zero slope, $p < 0.0005$, $R^2=0.3836$). This increase in kinetics as a function of distance remains after knockdown of CNIH2 (n = 12; slope of linear fit does not differ from control, $p > 0.05$), although there is a global speeding of decay (elevation of fit differs from control, $p < 0.0001$). Points are analogous to those in A. **(D)** Weighted tau for the decay of mEPSCs bined by location as in B. Compared with the decay of control mEPSCs, shCNIH2 expressing cells have faster proximal ($p < 0.01$) and distal ($p < 0.05$) events. Bars show mean ±SEM. Traces to the right show average mEPSCs as in B, scaled and aligned to their peaks (scale bar: 10ms).

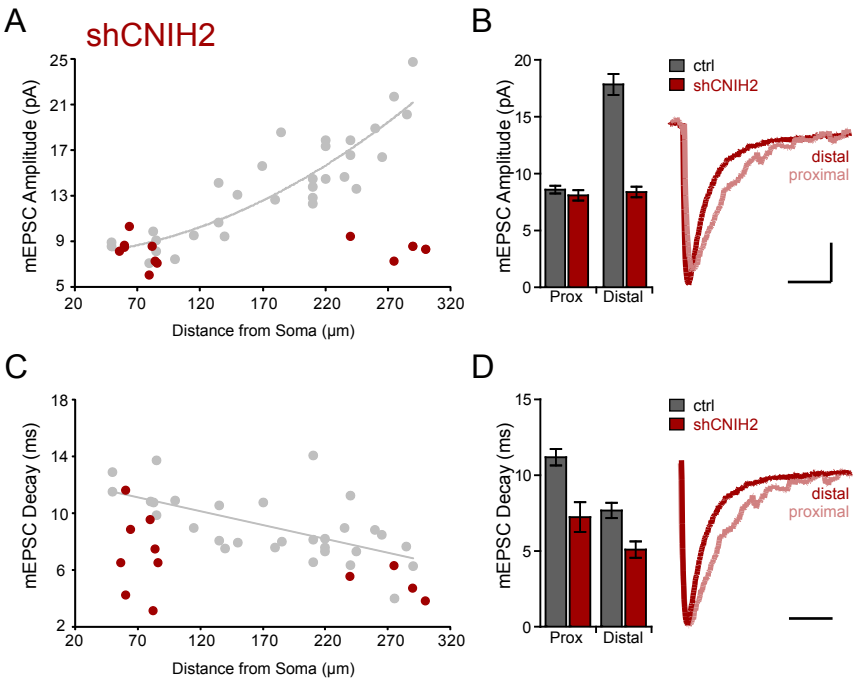

A
shCNIH2
mEPSC Amplitude (pA)
Distance from Soma (µm)
B
ctrl
shCNIH2
mEPSC Amplitude (pA)
Prox
Distal
distal
proximal
C
mEPSC Decay (ms)
Distance from Soma (µm)
D
ctrl
shCNIH2
mEPSC Decay (ms)
Prox
Distal
distal
proximal

Figure 29. GluA2 knockdown reverses the distance-dependent scaling of AMPARs.

(A) Lentiviral expression of an shRNA targeting GluA2 in dissociated neurons drastically reduces GluA2 protein without affecting the amount of other synaptic proteins. **(B)** Following knockdown of GluA2 in CA1 pyramidal neurons, AMPAR-mediated mEPSCs no longer increase, but rather decrease as a function of distance from the soma (n = 13; linear fit has non-zero, negative slope, $p < 0.05$, R^2=0.4264). Green filled circles show individual recordings from shGluA2 expressing cells, gray filled circles show recordings from control cells for comparison. **(C)** Average mEPSC amplitudes binned by location: proximal (50-120µm) and distal (220-290µm). Distal mEPSC amplitudes following knockdown are reduced as compared with control amplitudes (n = 5, $p < 0.005$), while there is a trend toward increased proximal amplitudes following knockdown (n = 5, p = 0.0932). Bars show mean ±SEM. Traces to the right show average proximal (light green) and distal (dark green) mEPSCs (scale bar: 2pA/10ms). **(D)** Expression of the shRNA in pyramidal neurons results in inwardly-rectifying AMPAR-mediated evoked currents consistent with a loss of GluA2 (n = 9 ctrl, 9 expt; $p < 0.0001$). Traces show representative currents at -70mV and +40mV for control (in black) and experimental (in green) cells (scale bar: 20ms). **(E)** Knockdown of GluA2 does not affect the speeding of AMPAR-mediated currents as a function of distance (n = 13; linear fit has non-zero slope, $p < 0.005$, R^2=0.5598) with no change in the slope ($p > 0.05$) or elevation ($p > 0.05$) as compared with control. Points are analogous to those in B. **(F)** Weighted tau for the decay of mEPSCs bined by location as in C. Following knockdown of GluA2, distal mEPSCs decay faster than proximal mEPSCs ($p < 0.05$) with no change in decay kinetics for proximal ($p > 0.05$) or distal ($p > 0.05$) events as compared with control. Bars show mean ±SEM. Traces to the right show average mEPSCs as in B, scaled and aligned to their peaks (scale bar: 10ms).

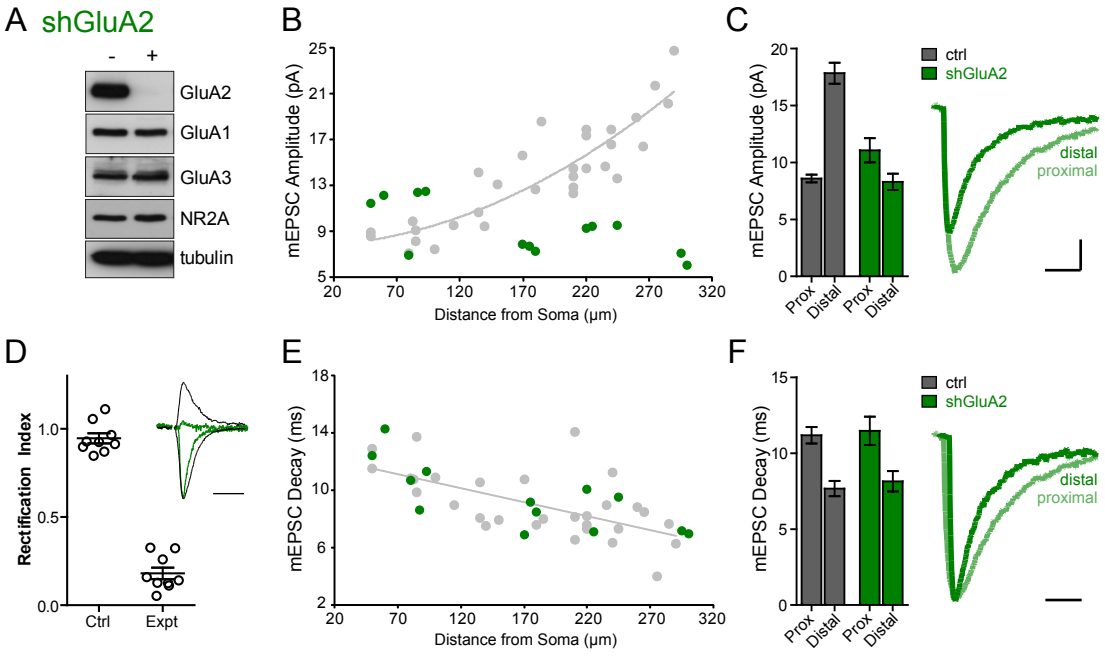

A shGluA2
-
+
GluA2
GluA1
GluA3
NR2A
tubulin
B
mEPSC Amplitude (pA)
Distance from Soma (µm)
C
mEPSC Amplitude (pA)
ctrl
shGluA2
distal
proximal
Prox
Distal
D
Rectification Index
Ctrl
Expt
E
mEPSC Decay (ms)
Distance from Soma (µm)
F
mEPSC Decay (ms)
ctrl
shGluA2
distal
proximal

Figure 30. GluA2 knockdown alters the organization of spine density.

(A) Images of control, GFP-expressing (in white) and shGluA2 expressing (in green) cells for spine analysis. **(B)** Spine density increases with distance from the soma in CA1 pyramidal neurons. Line plots the average number of spines per 30µm section of the primary apical dendrite (n = 20 cells). Shaded area: ±SEM. **(C)** Knockdown of GluA2 reverses the gradient of spine density. Green line plots the average (n = 7) ±SEM (shaded). Control is shown for comparison. **(D)** Knockdown of GluA1 does not affect spine density. Purple line plots the average (n = 5) ±SEM (shaded). Control is shown for comparison.

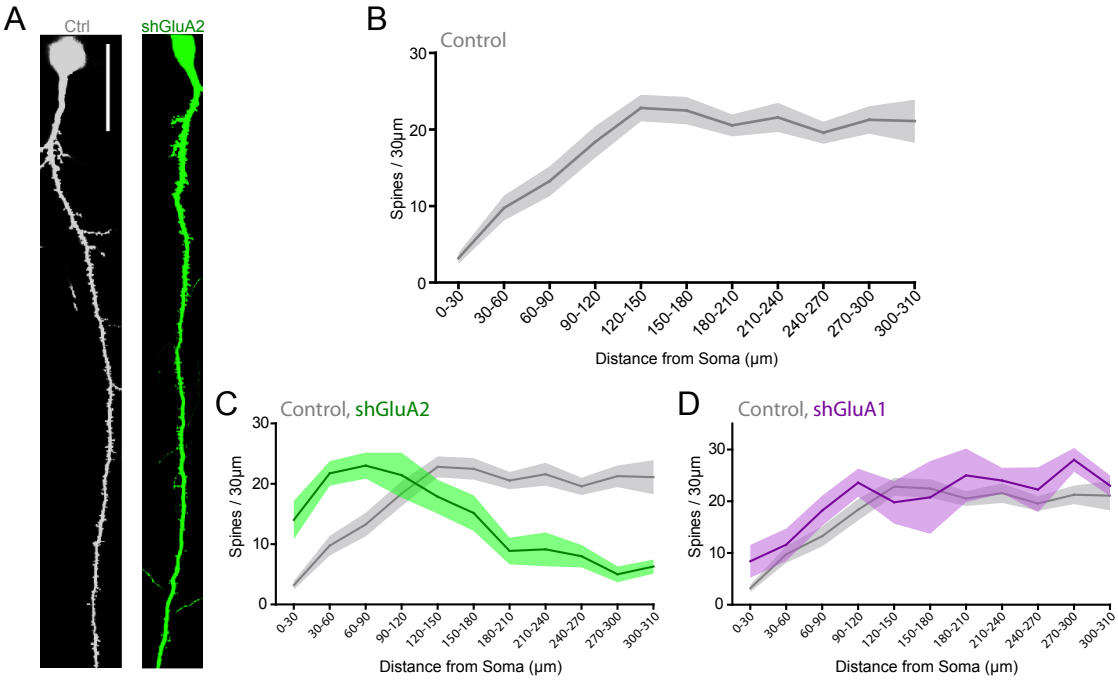
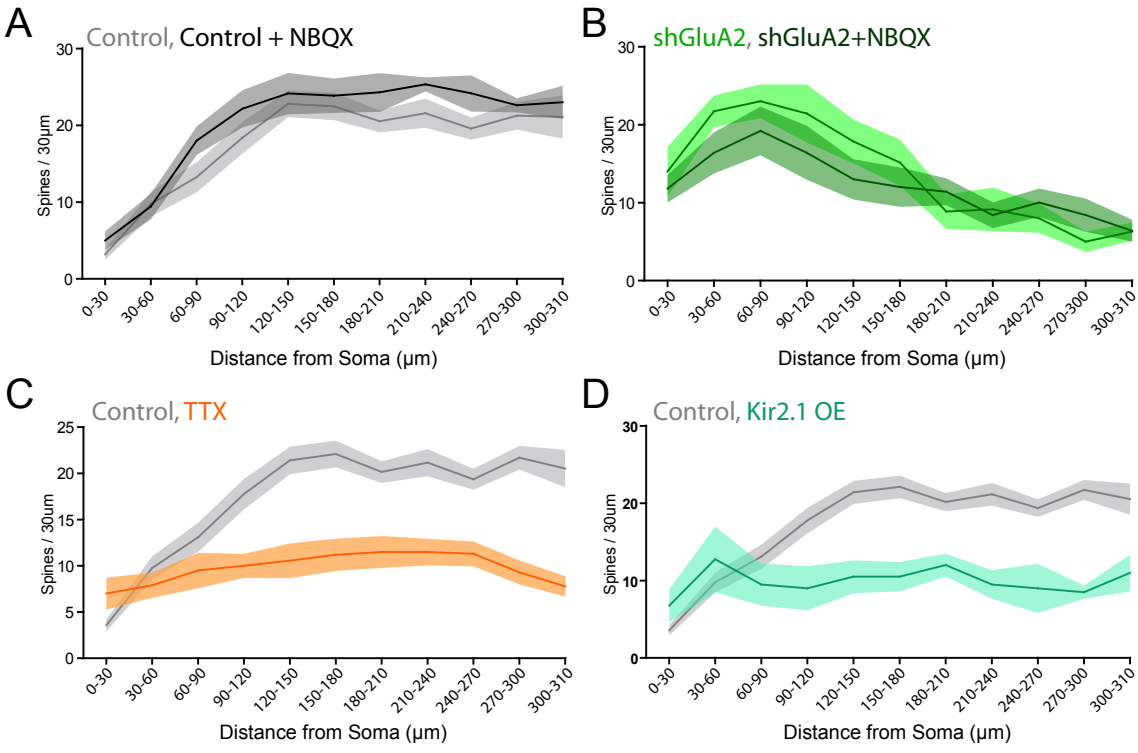

A
Ctrl
shGluA2
B
Control
Spines / 30µm
0
10
20
30
0-30
30-60
60-90
90-120
120-150
150-180
180-210
210-240
240-270
270-300
300-310
Distance from Soma (µm)
C
Control, shGluA2
Spines / 30µm
Distance from Soma (µm)
D
Control, shGluA1
Spines / 30µm
Distance from Soma (µm)

Figure 31. Spine density is affected by the presence of action potentials.

(A) Long-term pharmacological block of AMPARs does not affect spine density. Dark grey line plots the average number of spines per 30µm section of the primary apical dendrite (n = 7 cells). Shaded area: ±SEM. Control is shown for comparison. **(B)** Block of AMPARs does not affect spine density on the background of GluA2 knockdown. Dark green line plots the average (n = 5) ±SEM (shaded). shGluA2 alone (light green) is shown for comparison. **(C)** Long-term block of voltage-gated sodium channels reduces spine density. Orange line plots the average (n = 10) ±SEM (shaded). Control is shown for comparison. **(D)** Overexpression of a potassium channel to limit excitability results in a reduction in spine density. Blue line plots the average (n = 4) ±SEM (shaded). Control is shown for comparison.


A
Control, Control + NBQX
Spines / 30µm
Distance from Soma (µm)
B
shGluA2, shGluA2+NBQX
Spines / 30um
Distance from Soma (µm)
C
Control, TTX
Spines / 30um
Distance from Soma (µm)
D
Control, Kir2.1 OE
Spines / 30um
Distance from Soma (µm)
0-30
30-60
60-90
90-120
120-150
150-180
180-210
210-240
240-270
270-300
300-310

CHAPTER 7:
General Conclusions

Neuroligins are distinctly synaptogenic

Based on the bulk of evidence presented in this thesis that the expression level of neuroligin controls the number of anatomical and functional synapses, with increases in neuroligin consistently resulting in greater numbers of synapses and decreases in neuroligin consistently resulting in fewer synapses, it seems almost absurd to need to argue the point that neuroligins are synaptogenic molecules. However, there are those who continue to deny any role for neuroligin in the formation or assembly of synapses, instead arguing for a role in synaptic validation: a theoretical choice point that occurs after a synapse has been made where, as a function of neuroligin and synaptic activity, the synapse is either maintained, altered, or destroyed (Chubykin et al., 2007; Ko et al., 2009). Two pieces of evidence have been used to bolster this validation hypothesis (Sudhof, 2008). The first is that neurons taken from the triple knockout of mouse of neuroligins 1-3 can still form synapses at a normal density (Varoqueaux et al., 2006). However, knowing what we know now about the diversity of other synaptic adhesion molecules that are present (Siddiqui and Craig, 2011) it is entirely reasonable that functional redundancy could explain the lack of an obvious effect. It should be pointed out that these animals die due to a synaptic deficit in the brainstem, which would seem to argue for necessity (Varoqueaux et al., 2006). Perhaps brainstem neurons lack a particular compensatory molecule that is present in other neurons. In any case, I would argue that definitive statements about the necessity of neuroligin in normal synaptic formation cannot be made based on the triple knockout, due to the potential influence of other molecules in the absence of neuroligin.

The second line of evidence in support of the validation hypothesis is the fact that the effects of neuroligin overexpression have been shown to be activity dependent (Chubykin et al., 2007). Here, the concept is that if the effect of neuroligin is responsive to synaptic activity and synaptic activity can only occur after a synapse has formed, then

any role for neuroligin must occur after synapse assembly. I initially had a hard time touching base with this finding, but was finally able to show some activity dependence of neuroligin 1 expression when I drastically reduced the expression level of the construct (Fig. 32). I believe that there is a flaw in the logic, however, that leads to an assumption that this proves that neuroligin cannot have a role in the formation of synapses. In all cases, manipulations of activity are not occurring at an isolated synapse or set of synapses that are being studied, but rather globally affecting the whole cell. It has been shown that neuronal activity can result in increased surface expression of neuroligin (Thyagarajan and Ting, 2010). Moreover, in my hands, activity dependence of neuroligin is absent when neuroligin is strongly overexpressed, suggesting that any regulatory effect activity has on neuroligin can be overcome by simply increasing the amount of neuroligin in the cell. Thus, a more parsimonious explanation would be that the surface expression of neuroligin may be regulated by neuronal activity, but that once the neuroligin is on the surface it leads to the formation of new synapses in an activity-independent manner.

In the most conservative view, I can only say that the expression level of neuroligin in the postsynaptic cell is tightly correlated with the number of synapses onto that cell. It is conceivable that there are necessary steps in the genesis of a synapse that occur either prior to or subsequent to the interaction between neuroligin and neurexin. However, in order to explain the bidirectional control of synapse density by neuroligin, these steps would either need to be purely permissive or dependent on neuroligin. To say that neuroligin is synaptogenic, therefore, is the most reasonable interpretation of all evidence and anything beyond that is purely a semantic argument.

Overexpression or knockdown of neuroligin results in all-or-none changes in the number of synapses

Throughout all my studies of neuroligin, one common finding was that manipulations of the expression level of neuroligin exerted changes in synaptic strength via all-or-none gains (in the case of overexpression) or losses (in the case of knockdown) of excitatory synapses. Overexpression of excitatory neuroligins (1 or 3) leads to increases in both AMPAR- and NMDAR-mediated responses, increases in the density of dendritic spines, increases in CV^{-2} of the postsynaptic response, increases in the presence of opposing presynaptic markers, and increases in the frequency of spontaneous mEPSCs without a change in mEPSC amplitude. The convergence of all these individual findings is nearly incontrovertible evidence that an increase in postsynaptic neuroligin leads to an increase in the number, and not strength, of functional synapses.

Manipulations of neuroligin expression in the opposite direction, knockdown, lead to reductions in both AMPAR- and NMDAR-mediated responses, reductions in the density of dendritic spines, reductions CV^{-2} of the postsynaptic response, reductions in the presence of opposing presynaptic markers, and reductions in sEPSC and mEPSC frequency without a change in sEPSC amplitude. As in the case of overexpression, the sum of all these findings is very strong evidence that reducing the expression of postsynaptic neuroligin leads to a loss, rather than a weakening, of functional synapses.

Again, the reason to belabor this point is that there is evidence to the contrary to be found in the literature. Increases in the AMPA/NMDA ratio have been reported in the neuroligin 1 knockout (Chubykin et al., 2007; Kim et al., 2008; Soler-Llavina et al., 2011) as have a lack of change in spine density (Soler-Llavina et al., 2011), while overexpression of neuroligin has been reported to decrease the AMPA/NMDA ratio

(Chubykin et al., 2007). The one point of agreement I have with these findings is that upon overexpression of neuroligin 1 or neuroligin 3 in organotypic slice cultures, I did record larger increases in AMPAR-mediated than NMDAR-mediated responses. However, this was not what I found when I moved to *in vivo* expression (see below). As for the rest of the discrepancies following loss of neuroligin, for the time being I must put my findings above those of the rest of the field due simply to the increased precision of the technique that I applied. Many of the previous findings used germ-line knockouts which will affect the circuit as well as individual cellular properties and all of them used AMPA/NMDA ratios, which are an imprecise manner of measuring changes in synaptic strength. My application of the dual-whole cell recording technique combined with single-cell genetic manipulations will yield accurate independent measurements of both the AMPAR- and NMDAR-mediated synaptic currents with tight internal control provided by a neighboring wild-type cell. Until such time that conditional knockouts of neuroligin are available to be assayed with single-cell knockdown and dual-whole cell recordings, the synaptic losses that I report following knockdown of neuroligin must be held as the standard of the field.

From structure to function of neuroligin

Here I have reported three basic functions of neuroligin, each dependent on a separate structural domain of the protein. Dimerization of neuroligin, occurring via a four-helix bundle in the extracellular domain, is necessary for the clustering of presynaptic neurexin, which seems to be required to generate a functional presynaptic site (see Chapter 3). A yet unknown molecular interaction in the cytoplasmic tail is required for assembly of the postsynaptic site (see Chapter 4). Finally, a specific trans-synaptic interaction between neuroligin and neurexin, mediated by the alternative splicing of the extracellular domain determines synaptic properties (see Chapter 5).

In the time since my initial observations of each of these findings, other similar and complementary reports have been published. Concerning dimerization, it was shown that clustering of neuroligin may be important for vesicular release even outside the nervous system. Clustered, but not diffuse neuroligin in pancreatic β cells can stimulate trans-cellular insulin release (Suckow et al., 2012). Moreover, the requirement for clustering of neurexin in the formation of synapses may be a general mechanism that regulates the trans-synaptic action by adhesion molecules as GluRδ2 must assemble into a tetramer before inducing synapse formation through cerebellin and neurexin (Lee et al., 2012).

Soon after the publication of my finding that postsynaptic assembly via neuroligin requires a critical region in the cytoplasmic domain, another group reported that an autism-associated mutation in the cytoplasmic domain of neuroligin 3 selectively impairs AMPAR-mediated transmission without affecting the trans-synaptic effects of neuroligin (Etherton et al., 2011). The similarity in phenotype of these two mutations as well as the fact that they are both found in a small region of the intracellular domain may suggest a common mechanism that relies on a membrane-proximal region of the cytoplasmic tail.

I report here that alternative splicing of both neuroligin and neurexin determines particular synaptic properties of the synapse resulting from the interaction of these two proteins. In particular, there is a developmental requirement for splice site B containing neuroligin 1, which binds preferentially to splice site 4 lacking neurexin. Interestingly, Iijima et al. (2011) report that splicing of neurexin at site 4 is dependent on activity and regulated both spatially and developmentally in the brain.

The post- and trans-synaptic effects of neuroligin are largely separable

One interesting outcome of the various results presented here is that, although neuroligin has potentiating effects on both the post- and presynaptic cell, these two

functions of neuroligin do not appear to be reliant on one another and, indeed, may be manipulated independently. Specifically, mutations to the extracellular dimerization domain of neuroligin, which result in a loss of the trans-synaptic effect of neuroligin, do not affect its ability to increase postsynaptic spine density or the accumulation of PSD-95. Conversely, mutations to the cytoplasmic tail that reduce the ability of neuroligin to assemble the postsynaptic site have no effect the trans-synaptic phenotype of neuroligin expression. This independence of function might provide insight into the manner in which different neuroligins create different synapses. Indeed, the difference in overxpression phenotype between neuroligin 1 and neuroligin 3 was entirely transferred by a swap of their extracellular domains.

The effect of experimental preparation on neuroligin phenotypes

Throughout these studies, I used multiple different experimental preperations: dissociated neuronal culture, organotypic slice culture, and acute hippocampal slices. While neuroligin effects were grossly similar between each of these preparations, there were some subtle differences between slice culture and acute slices. The first relates to knockdown of individual neuroligins. In area CA1, I found no effect in slice culture of knocking down neuroligin 1 with biolistic expression of the miR (Fig. 33), whereas I found reductions in synaptic currents in acute slices when I similarly knocked down neuroligin 1 using *in utero* electroporations. Interestingly, these effects were dependent on age as lentiviral mediated knockdown in adult CA1 had no effect. Perhaps developmental stage explains these discrepencies as the correlation of development between cultured neurons and *in vivo* neurons is notoriously difficult.

I also found a strange difference between slice culture and acute slices with respect to the relative enhancement of AMPAR- and NMDAR-mediated currents by overexpression of neuroligin. In slice culture, overexpression of neuroligin 1 or neuroligin

3 consistently resulted in larger increases in the AMPAR-mediated currents than NMDAR-mediated currents. Overexpression *in vivo* using *in utero* electroporations, however, yielded perfectly matched increases in AMPAR- and NMDAR-mediated responses in acute slice recordings. Perhaps there could be a difference in the propensity to form silent synapses in these two preparations that accounts for the different overexpression phenotypes. Regardless of the explanation, clearly some caution is warranted when interpreting subtleties of overexpression phenotypes in slice culture.

Future directions for the study of neuroligin

There are many possibilities for future experiments based on the results presented in this thesis that would advance our understanding of neuroligin and its function at synapses. An obvious complement to the findings presented in Chapter four would be the identification of the molecular interaction mediated by the region of the intracellular domain that I found to be critically involved in the assembly of an excitatory postsynaptic site. This would almost certainly need to proceed initially with a biochemical investigation to identify possible protein interactions that occur at or near the critical cytoplasmic region of neuroligin, and could be followed-up with subsequent physiological confirmation in neurons. We have long thought of this hypothetical interaction as performing a scaffolding role at the postsynaptic site, which may be true. However, we have no evidence to rule out the possibility for catalysis of an enzymatic signaling reaction mediated by this site.

Another straightforward direction for future research, based on the fact that different neuroligin subtypes create synapses with different properties as shown in Chapter five, would be to examine the localization of these different subtypes at

synapses throughout the brain. This could proceed initially by the analysis of different cell types of the brain using *in situ* hybridization or microdissections followed by qRT-PCR to examine mRNA expression of neuroligin subtypes and splice variants as well as the complement of other postsynaptic adhesion molecules present. At some point, a more detailed analysis might prove useful, to look at subcellular localization of different postsynaptic adhesion molecules. In this analysis, the presynaptic side should not be ignored as the final synaptic properties may well be determined through the interplay of post- and presynaptic adhesion molecules.

A more subtle finding that emerged from these studies and could be the target of future research is that the function of neuroligin 2 at inhibitory synapses did not depend on the same intracellular critical region as did the function of neuroligins at excitatory synapses. This might be expected given that excitatory and inhibitory postsynaptic sites are quite molecularly distinct and might thus require divergent functions of the cytoplasmic tail of neuroligin. However, I also found no effect of a neuroligin 2 mutation that should eliminate binding to gephyrin (Fig. 34), which has been proposed as the mechanism by which neuroligin 2 assembles the inhibitory synaptic site (Poulopoulos et al., 2009). Given the power of the triple knockdown and replacement system that I have developed for the study of excitatory neuroligins, the application of this system to interrogate the function of subdomains of neuroligin 2 may well prove highly informative.

Continuing on the thread of inhibitory synapses, I also found an interesting dependence of neuroligin 3 function at inhibitory synapses on the presence of other neuroligins. Specifically, I found that on a wild-type background, expression of neuroligin 3 substantially enhances inhibitory synaptic currents (Fig. 35). However, when expressed on the background of the triple neuroligin knockdown, neuroligin 3 had a minimal effect on inhibitory currents, a differential of almost three fold when compared to the effect of neuroligin 3 expression on a wild-type background (Fig. 35). Given the

evidence that neuroligin 3 is co-localized with neuroligin 2 at inhibitory synapses (Budreck and Scheiffele, 2007) and that neuroligin 2 and neuroligin 3 form heterodimers (Dean et al., 2003), it could be that the trafficking of neuroligin 3 to inhibitory synapses, and thus its effect on inhibitory synapses, is dependent on neuroligin 2. One would want to begin by comparing the enhancement of inhibitory currents by neuroligin 3 on a wild-type background to its enhancement when combined with knockdown of neuroligin 2 to initiate an investigation into this phenomenon.

Is distance-dependent scaling conceptually or mechanistically similar to homeostasis?

In Chapter six, I present evidence that the increase in AMPARs as a function of distance from the soma in hippocampal pyramidal neurons is dependent on GluA2, in much the same way that homeostasis has been reported to be (Goold and Nicoll, 2010; Turrigiano et al., 1998). Does this suggest a general mechanistic similarity between the two phenomena? In order to convincingly demonstrate that distance-dependent scaling is or is not mechanistically similar to synaptic homeostasis one would want to assess its dependence on the activity of a neuron – particularly the presence of action potentials. I have been, thus far, unable to do so, but am hopeful that I or someone else will eventually be able to test this relationship.

There is a further question as to whether the distance-dependent increase in AMPARs is similar in its expression to synaptic homeostasis, given that it is not a multiplicative scaling of synaptic strengths from proximal to distal inputs, but rather an augmentation of large amplitude synaptic responses at distal locations. It would be interesting to explore the way that this augmentation of large amplitude synapses and

preservation of small amplitude synapses onto distal dendrites affects the integration of inputs, perhaps using *in silico* models.

Figure 32. Activity dependence of neuroligin 1 phenotype at a reduced expression level

(A) Expression level dependence of neuroligin 3 effect in organotypic slice culture. On the background of the NLmiRs, reduced expression of neuroligin 3 (achieved by expression following an IRES rather than preceding an IRES) results in dramatically less of an enhancement of AMPAR-mediated responses than high expression (NLmiRs plus NLGN3, n = 40, versus NLmiRs plus IRES NLGN3 with a Kozak sequence, n = 12, or without a Kozak sequence, n = 9, $p < 0.001$). No difference was observed based on the inclusion of the Kozak sequence ($p > 0.05$). Bars show mean ±SEM. Scatter plot to the right shows individual pairs (open circles) and means ±SEM (filled circles) of the paired recordings for three conditions: NLmiRs plus NLGN3 (in black), NLmiRs plus IRES NLGN3 containing a Kozak sequence (in red), and NLmiRs plus IRES NLGN3 lacking a Kozak sequence (in blue). **(B)** Expression dependence of the NMDAR-mediated enhancement by neuroligin 3, showing no obvious correlation with expression level ($p > 0.05$). Bar graph and scatter plot is analogous to that in A. **(C)** When expressed at a reduced level, NLGN1 enhancement of AMPAR-mediated responses is responsive to activity. On the background of the NLmiRs, maintaining cultures in APV and NBQX for the duration of expression reduces the enhancing effect of NLGN1 compared with a no-drug condition (control, n = 17; drug, n = 15; $p < 0.05$). Bars show mean ±SEM. Scatter plots to the right show individual paired recordings (open circles) and means ±SEM (filled circles) for both cases. Sample traces show representative currents from untransfected (in black) and transfected (in green) cells (scale bar: 30pA/20ms). **(D)** A similar reduction in NLGN1 enhancement of the NMDAR-mediated response was seen when slices were cultured in APV and NBQX (control, n = 17; drug, n = 15; $p < 0.05$). Bar graph and scatter plots are analogous to those in C. Sample traces show

representative currents from untransfected (in black) and transfected (in green) cells (scale bar: 60pA/100ms).

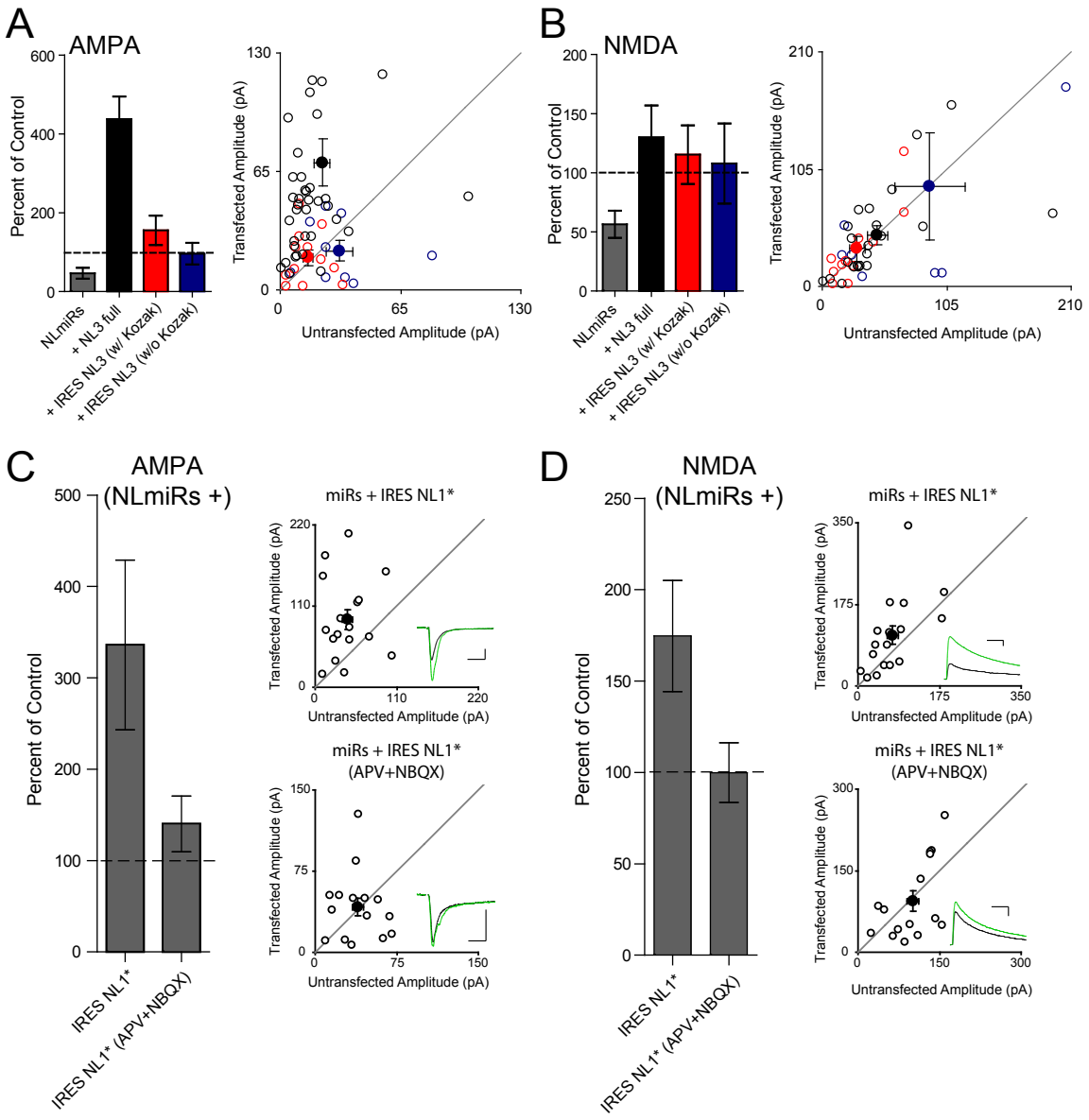

A
AMPA
Percent of Control
600
400
200
0
NLmiRs
+ NL3 full
+ IRES NL3 (w/ Kozak)
+ IRES NL3 (w/o Kozak)
Transfected Amplitude (pA)
130
65
0
0
65
130
Untransfected Amplitude (pA)
B
NMDA
Percent of Control
200
150
100
50
0
NLmiRs
+ NL3 full
+ IRES NL3 (w/ Kozak)
+ IRES NL3 (w/o Kozak)
Transfected Amplitude (pA)
210
105
0
0
105
210
Untransfected Amplitude (pA)
C
AMPA
(NLmiRs +)
Percent of Control
500
400
300
200
100
0
IRES NL1*
IRES NL1* (APV+NBQX)
miRs + IRES NL1*
Transfected Amplitude (pA)
220
110
0
0
110
220
Untransfected Amplitude (pA)
miRs + IRES NL1*
(APV+NBQX)
Transfected Amplitude (pA)
150
75
0
0
75
150
Untransfected Amplitude (pA)
D
NMDA
(NLmiRs +)
Percent of Control
250
200
150
100
50
0
IRES NL1*
IRES NL1* (APV+NBQX)
miRs + IRES NL1*
Transfected Amplitude (pA)
350
175
0
0
175
350
Untransfected Amplitude (pA)
miRs + IRES NL1*
(APV+NBQX)
Transfected Amplitude (pA)
300
150
0
0
150
300
Untransfected Amplitude (pA)

Figure 33. Differential phenotype of neuroligin 1 knockdown in culture versus acute slices

(A) Single knockdown of neuroligin 1 has no effect on AMPAR-mediated synaptic currents in organotypic slice culture when expressed using biolistics ($n = 10$, $p > 0.05$), but reduces AMPAR-mediated synaptic currents in acute slices when expressed via *in utero* electroporation ($n = 15$, $p < 0.05$). **(B)** Scatter plot of individual paired recordings (open circles) and mean ±SEM (filled circle) in slice culture. **(C)** As in B, but for acute slice recordings.

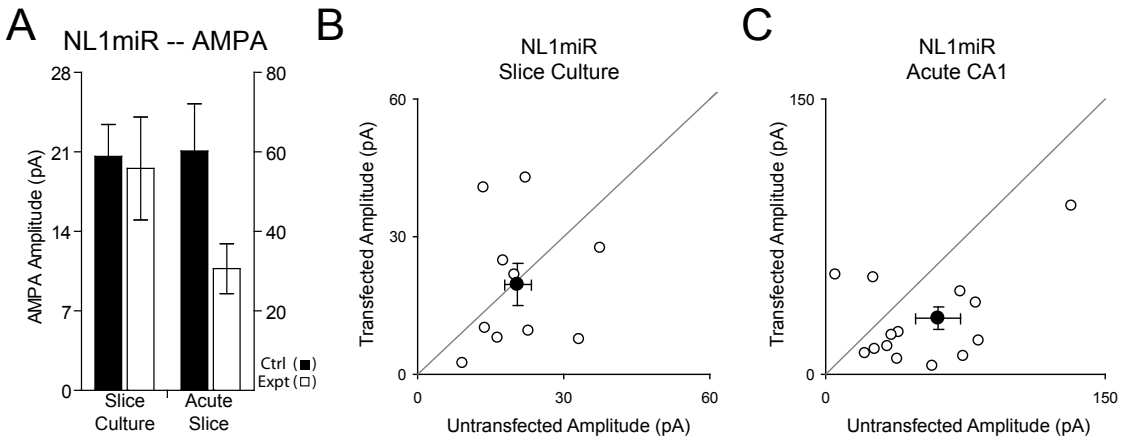

A
NL1miR -- AMPA
AMPA Amplitude (pA)
28
21
14
7
0
80
60
40
20
Ctrl (■)
Expt (□)
Slice Culture
Acute Slice
B
NL1miR
Slice Culture
Transfected Amplitude (pA)
60
30
0
0
30
60
Untransfected Amplitude (pA)
C
NL1miR
Acute CA1
Transfected Amplitude (pA)
150
0
0
150
Untransfected Amplitude (pA)

Figure 34. Mutation of gephyrin-binding site does not alter enhancement of inhibitory currents by neuroligin 2

(A) Expression of neuroligin 2 on the background of the triple knockdown (n = 17) enhances inhibitory synaptic currents compared with expression of the NLmiRs alone (n = 10, $p < 0.0001$), as does expression of a mutant that should block gephyrin binding (Y770A, n = 10, $p < 0.0001$). No difference exists between the enhancements induced by wild-type or mutant neuroligin 2 ($p > 0.05$). Bar graph shows means ±SEM. **(B)** Scatter plot showing individual paired recordings (open circles) and means ±SEM (filled circles) for expression of wild-type (in black) and Y770A mutant (in red) neuroligin 2, each on the background of the NLmiRs.

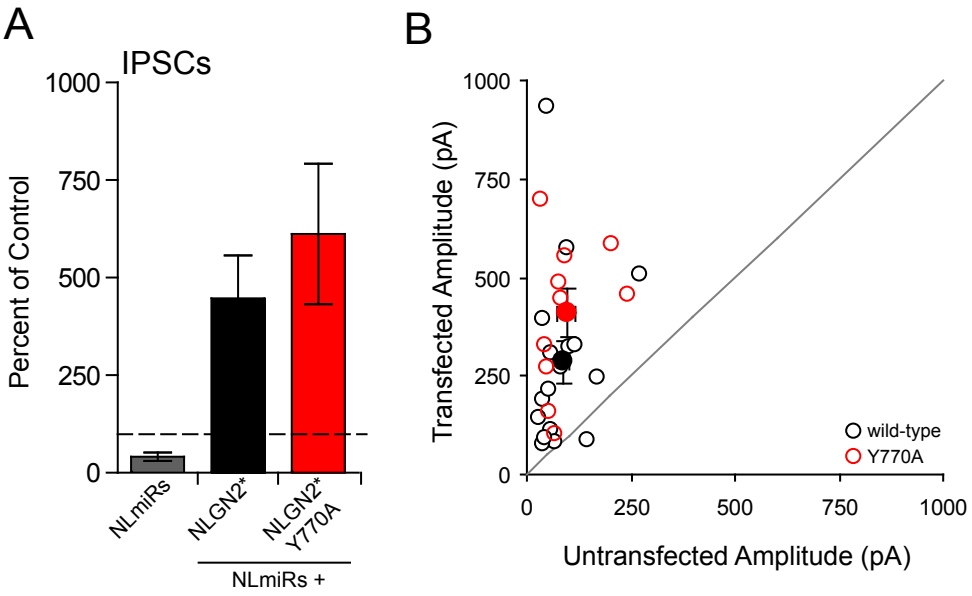
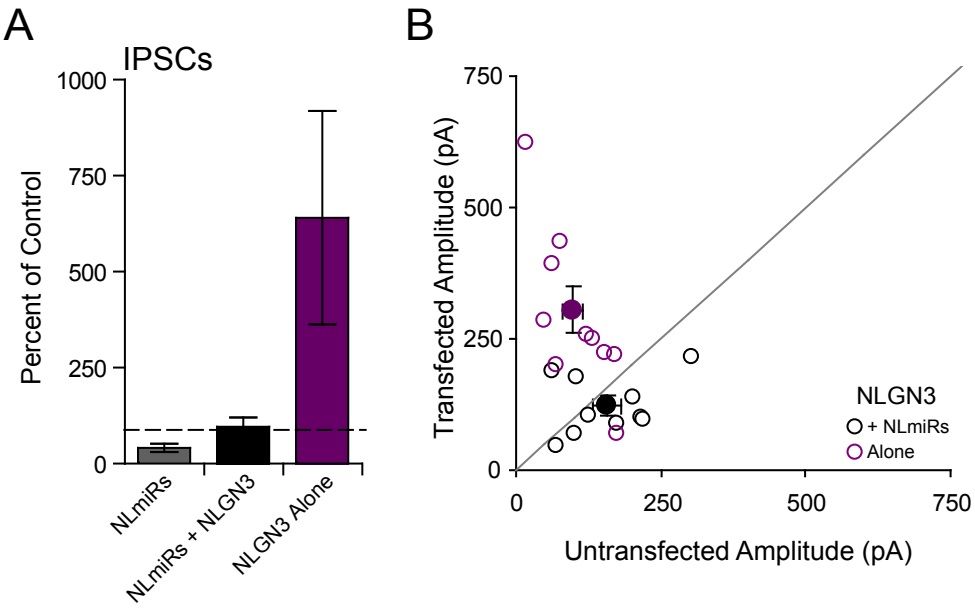

A
IPSCs
Percent of Control
1000
750
500
250
0
NLmiRs
NLGN2*
NLGN2*
Y770A
NLmiRs +
B
Transfected Amplitude (pA)
Untransfected Amplitude (pA)
1000
750
500
250
0
0
250
500
750
1000
wild-type
Y770A

Figure 35. Enhancement of inhibitory currents by neuroligin 3 is dependent on the presence of other neuroligins.

(A) On the background of the triple knockdown of neuroligins, overexpression of neuroligin 3 results in a small, but significant enhancement of inhibitory synaptic currents (NLmiRs, n = 10; NLmiRs plus NLGN3, n = 10; $p < 0.01$). The enhancement of inhibitory currents by neuroligin 3 alone is, however, much larger (n = 11, $p < 0.01$ versus NLmiRs plus NLGN3). **(B)** Scatter plot showing individual paired recordings (open circles) and means ±SEM (filled circles) for expression of NLmiRs plus NLGN3 (in black) and NLGN3 alone (in purple).


A
IPSCs
Percent of Control
1000
750
500
250
0
NLmiRs
NLmiRs + NLGN3
NLGN3 Alone
B
Transfected Amplitude (pA)
750
500
250
0
0
250
500
750
Untransfected Amplitude (pA)
NLGN3
+ NLmiRs
Alone

CHAPTER 8:

References

Ahmed, O. J., and Mehta, M. R. (2009). The hippocampal rate code: anatomy, physiology and theory. Trends Neurosci *32*, 329-338.

Aiga, M., Levinson, J. N., and Bamji, S. X. (2011). N-cadherin and neuroligins cooperate to regulate synapse formation in hippocampal cultures. J Biol Chem *286*, 851-858.

Andrasfalvy, B. K., and Magee, J. C. (2001). Distance-dependent increase in AMPA receptor number in the dendrites of adult hippocampal CA1 pyramidal neurons. J Neurosci *21*, 9151-9159.

Andrasfalvy, B. K., Makara, J. K., Johnston, D., and Magee, J. C. (2008). Altered synaptic and non-synaptic properties of CA1 pyramidal neurons in Kv4.2 knockout mice. J Physiol *586*, 3881-3892.

Andrasfalvy, B. K., Smith, M. A., Borchardt, T., Sprengel, R., and Magee, J. C. (2003). Impaired regulation of synaptic strength in hippocampal neurons from GluR1-deficient mice. J Physiol *552*, 35-45.

Arac, D., Boucard, A. A., Ozkan, E., Strop, P., Newell, E., Sudhof, T. C., and Brunger, A. T. (2007). Structures of neuroligin-1 and the neuroligin-1/neurexin-1 beta complex reveal specific protein-protein and protein-Ca2+ interactions. Neuron *56*, 992-1003.

Arikkath, J., and Reichardt, L. F. (2008). Cadherins and catenins at synapses: roles in synaptogenesis and synaptic plasticity. Trends Neurosci *31*, 487-494.

Ascher, P., and Nowak, L. (1988). The role of divalent cations in the N-methyl-D-aspartate responses of mouse central neurones in culture. J Physiol *399*, 247-266.

Barrow, S. L., Constable, J. R., Clark, E., El-Sabeawy, F., McAllister, A. K., and Washbourne, P. (2009). Neuroligin1: a cell adhesion molecule that recruits PSD-95 and NMDA receptors by distinct mechanisms during synaptogenesis. Neural Dev *4*, 17.

Bekkers, J. M., and Stevens, C. F. (1990). Presynaptic mechanism for long-term potentiation in the hippocampus. Nature *346*, 724-729.

Biederer, T., Sara, Y., Mozhayeva, M., Atasoy, D., Liu, X., Kavalali, E. T., and Sudhof, T. C. (2002). SynCAM, a synaptic adhesion molecule that drives synapse assembly. Science *297*, 1525-1531.

Bliss, T. V., and Collingridge, G. L. (1993). A synaptic model of memory: long-term potentiation in the hippocampus. Nature *361*, 31-39.

Bliss, T. V., and Lomo, T. (1973). Long-lasting potentiation of synaptic transmission in the dentate area of the anaesthetized rabbit following stimulation of the perforant path. J Physiol *232*, 331-356.

Blundell, J., Blaiss, C. A., Etherton, M. R., Espinosa, F., Tabuchi, K., Walz, C., Bolliger, M. F., Sudhof, T. C., and Powell, C. M. (2010). Neuroligin-1 deletion results in impaired spatial memory and increased repetitive behavior. J Neurosci *30*, 2115-2129.

Bolliger, M. F., Pei, J., Maxeiner, S., Boucard, A. A., Grishin, N. V., and Sudhof, T. C. (2008). Unusually rapid evolution of Neuroligin-4 in mice. Proc Natl Acad Sci U S A *105*, 6421-6426.

Boucard, A. A., Chubykin, A. A., Comoletti, D., Taylor, P., and Sudhof, T. C. (2005). A splice code for trans-synaptic cell adhesion mediated by binding of neuroligin 1 to alpha- and beta-neurexins. Neuron *48*, 229-236.

Boucard, A. A., Ko, J., and Sudhof, T. C. (2012). High Affinity Neurexin Binding to Cell Adhesion G-protein-coupled Receptor CIRL1/Latrophilin-1 Produces an Intercellular Adhesion Complex. J Biol Chem *287*, 9399-9413.

Bredt, D. S., and Nicoll, R. A. (2003). AMPA receptor trafficking at excitatory synapses. Neuron *40*, 361-379.

Budreck, E. C., and Scheiffele, P. (2007). Neuroligin-3 is a neuronal adhesion protein at GABAergic and glutamatergic synapses. Eur J Neurosci *26*, 1738-1748.

Bullis, J. B., Jones, T. D., and Poolos, N. P. (2007). Reversed somatodendritic I(h) gradient in a class of rat hippocampal neurons with pyramidal morphology. J Physiol *579*, 431-443.

Burrone, J., O'Byrne, M., and Murthy, V. N. (2002). Multiple forms of synaptic plasticity triggered by selective suppression of activity in individual neurons. Nature *420*, 414-418.

Butz, S., Okamoto, M., and Sudhof, T. C. (1998). A tripartite protein complex with the potential to couple synaptic vesicle exocytosis to cell adhesion in brain. Cell *94*, 773-782.

Chen, S. X., Tari, P. K., She, K., and Haas, K. (2010). Neurexin-neuroligin cell adhesion complexes contribute to synaptotropic dendritogenesis via growth stabilization mechanisms in vivo. Neuron *67*, 967-983.

Chih, B., Engelman, H., and Scheiffele, P. (2005). Control of excitatory and inhibitory synapse formation by neuroligins. Science *307*, 1324-1328.

Chih, B., Gollan, L., and Scheiffele, P. (2006). Alternative splicing controls selective trans-synaptic interactions of the neuroligin-neurexin complex. Neuron *51*, 171-178.

Ching, M. S., Shen, Y., Tan, W. H., Jeste, S. S., Morrow, E. M., Chen, X., Mukaddes, N. M., Yoo, S. Y., Hanson, E., Hundley, R.*, et al.* (2010). Deletions of NRXN1 (neurexin-1) predispose to a wide spectrum of developmental disorders. Am J Med Genet B Neuropsychiatr Genet *153B*, 937-947.

Chubykin, A. A., Atasoy, D., Etherton, M. R., Brose, N., Kavalali, E. T., Gibson, J. R., and Sudhof, T. C. (2007). Activity-dependent validation of excitatory versus inhibitory synapses by neuroligin-1 versus neuroligin-2. Neuron *54*, 919-931.

Clackson, T., Yang, W., Rozamus, L. W., Hatada, M., Amara, J. F., Rollins, C. T., Stevenson, L. F., Magari, S. R., Wood, S. A., Courage, N. L.*, et al.* (1998).

Redesigning an FKBP-ligand interface to generate chemical dimerizers with novel specificity. Proc Natl Acad Sci U S A *95*, 10437-10442.

Colino, A., and Malenka, R. C. (1993). Mechanisms underlying induction of long-term potentiation in rat medial and lateral perforant paths in vitro. J Neurophysiol *69*, 1150-1159.

Comoletti, D., De Jaco, A., Jennings, L. L., Flynn, R. E., Gaietta, G., Tsigelny, I., Ellisman, M. H., and Taylor, P. (2004). The Arg451Cys-neuroligin-3 mutation associated with autism reveals a defect in protein processing. J Neurosci *24*, 4889-4893.

Comoletti, D., Grishaev, A., Whitten, A. E., Tsigelny, I., Taylor, P., and Trewhella, J. (2007). Synaptic arrangement of the neuroligin/beta-neurexin complex revealed by X-ray and neutron scattering. Structure *15*, 693-705.

Craig, A. M., and Kang, Y. (2007). Neurexin-neuroligin signaling in synapse development. Curr Opin Neurobiol *17*, 43-52.

Daoud, H., Bonnet-Brilhault, F., Vedrine, S., Demattei, M. V., Vourc'h, P., Bayou, N., Andres, C. R., Barthelemy, C., Laumonnier, F., and Briault, S. (2009). Autism and nonsyndromic mental retardation associated with a de novo mutation in the NLGN4X gene promoter causing an increased expression level. Biol Psychiatry *66*, 906-910.

de Wit, J., Sylwestrak, E., O'Sullivan, M. L., Otto, S., Tiglio, K., Savas, J. N., Yates, J. R., 3rd, Comoletti, D., Taylor, P., and Ghosh, A. (2009). LRRTM2 interacts with Neurexin1 and regulates excitatory synapse formation. Neuron *64*, 799-806.

Dean, C., and Dresbach, T. (2006). Neuroligins and neurexins: linking cell adhesion, synapse formation and cognitive function. Trends Neurosci *29*, 21-29.

Dean, C., Scholl, F. G., Choih, J., DeMaria, S., Berger, J., Isacoff, E., and Scheiffele, P. (2003). Neurexin mediates the assembly of presynaptic terminals. Nat Neurosci *6*, 708-716.

Del Castillo, J., and Katz, B. (1954). Quantal components of the end-plate potential. J Physiol *124*, 560-573.

Deng, W., Aimone, J. B., and Gage, F. H. (2010). New neurons and new memories: how does adult hippocampal neurogenesis affect learning and memory? Nat Rev Neurosci *11*, 339-350.

Dresbach, T., Neeb, A., Meyer, G., Gundelfinger, E. D., and Brose, N. (2004). Synaptic targeting of neuroligin is independent of neurexin and SAP90/PSD95 binding. Mol Cell Neurosci *27*, 227-235.

Etherton, M. R., Tabuchi, K., Sharma, M., Ko, J., and Sudhof, T. C. (2011). An autism-associated point mutation in the neuroligin cytoplasmic tail selectively impairs AMPA receptor-mediated synaptic transmission in hippocampus. EMBO J *30*, 2908-2919.

Fabrichny, I. P., Leone, P., Sulzenbacher, G., Comoletti, D., Miller, M. T., Taylor, P., Bourne, Y., and Marchot, P. (2007). Structural analysis of the synaptic protein neuroligin and its beta-neurexin complex: determinants for folding and cell adhesion. Neuron *56*, 979-991.

Fu, Z., Washbourne, P., Ortinski, P., and Vicini, S. (2003). Functional excitatory synapses in HEK293 cells expressing neuroligin and glutamate receptors. J Neurophysiol *90*, 3950-3957.

Futai, K., Kim, M. J., Hashikawa, T., Scheiffele, P., Sheng, M., and Hayashi, Y. (2007). Retrograde modulation of presynaptic release probability through signaling mediated by PSD-95-neuroligin. Nat Neurosci *10*, 186-195.

Gainey, M. A., Hurvitz-Wolff, J. R., Lambo, M. E., and Turrigiano, G. G. (2009). Synaptic scaling requires the GluR2 subunit of the AMPA receptor. J Neurosci *29*, 6479-6489.

Gauthier, J., Siddiqui, T. J., Huashan, P., Yokomaku, D., Hamdan, F. F., Champagne, N., Lapointe, M., Spiegelman, D., Noreau, A., Lafreniere, R. G.*, et al.* (2011). Truncating mutations in NRXN2 and NRXN1 in autism spectrum disorders and schizophrenia. Hum Genet *130*, 563-573.

Geiger, J. R., Melcher, T., Koh, D. S., Sakmann, B., Seeburg, P. H., Jonas, P., and Monyer, H. (1995). Relative abundance of subunit mRNAs determines gating and Ca2+ permeability of AMPA receptors in principal neurons and interneurons in rat CNS. Neuron *15*, 193-204.

Gill, M. B., Kato, A. S., Roberts, M. F., Yu, H., Wang, H., Tomita, S., and Bredt, D. S. (2011). Cornichon-2 modulates AMPA receptor-transmembrane AMPA receptor regulatory protein assembly to dictate gating and pharmacology. J Neurosci *31*, 6928-6938.

Goold, C. P., and Nicoll, R. A. (2010). Single-cell optogenetic excitation drives homeostatic synaptic depression. Neuron *68*, 512-528.

Graf, E. R., Zhang, X., Jin, S. X., Linhoff, M. W., and Craig, A. M. (2004). Neurexins induce differentiation of GABA and glutamate postsynaptic specializations via neuroligins. Cell *119*, 1013-1026.

Granger, A. J., Shi, Y., Lu, W., Cerpas, M., and Nicoll, R. A. (In Press). LTP requires a reserve pool of glutamate receptors independent of subunit type. Nature.

Gustafsson, B., and Wigstrom, H. (1988). Physiological mechanisms underlying long-term potentiation. Trends Neurosci *11*, 156-162.

Gutierrez, R. C., Hung, J., Zhang, Y., Kertesz, A. C., Espina, F. J., and Colicos, M. A. (2009). Altered synchrony and connectivity in neuronal networks expressing an autism-related mutation of neuroligin 3. Neuroscience *162*, 208-221.

Hata, Y., Butz, S., and Sudhof, T. C. (1996). CASK: a novel dlg/PSD95 homolog with an N-terminal calmodulin-dependent protein kinase domain identified by interaction with neurexins. J Neurosci *16*, 2488-2494.

Hayashi, Y., Shi, S. H., Esteban, J. A., Piccini, A., Poncer, J. C., and Malinow, R. (2000). Driving AMPA receptors into synapses by LTP and CaMKII: requirement for GluR1 and PDZ domain interaction. Science *287*, 2262-2267.

Hebb, D. O. (1949). Organization of Behavior: a Neuropsychological Theory (New York, John Wiley).

Heine, M., Thoumine, O., Mondin, M., Tessier, B., Giannone, G., and Choquet, D. (2008). Activity-independent and subunit-specific recruitment of functional AMPA receptors at neurexin/neuroligin contacts. Proc Natl Acad Sci U S A *105*, 20947-20952.

Herring, B. E., Shi, Y., Suh, Y. H., Zheng, C. Y., Blankenship, S. M., Roche, K. W., and Nicoll, R. A. (In Revision). Cornichon proteins determine the subunit composition of synaptic AMPA receptors.

Hjelmstad, G. O., Nicoll, R. A., and Malenka, R. C. (1997). Synaptic refractory period provides a measure of probability of release in the hippocampus. Neuron *19*, 1309-1318.

Hoon, M., Soykan, T., Falkenburger, B., Hammer, M., Patrizi, A., Schmidt, K. F., Sassoe-Pognetto, M., Lowel, S., Moser, T., Taschenberger, H.*, et al.* (2011). Neuroligin-4 is localized to glycinergic postsynapses and regulates inhibition in the retina. Proc Natl Acad Sci U S A *108*, 3053-3058.

Ichtchenko, K., Hata, Y., Nguyen, T., Ullrich, B., Missler, M., Moomaw, C., and Sudhof, T. C. (1995). Neuroligin 1: a splice site-specific ligand for beta-neurexins. Cell *81*, 435-443.

Ichtchenko, K., Nguyen, T., and Sudhof, T. C. (1996). Structures, alternative splicing, and neurexin binding of multiple neuroligins. J Biol Chem *271*, 2676-2682.

Iida, J., Hirabayashi, S., Sato, Y., and Hata, Y. (2004). Synaptic scaffolding molecule is involved in the synaptic clustering of neuroligin. Mol Cell Neurosci *27*, 497-508.

Iijima, T., Wu, K., Witte, H., Hanno-Iijima, Y., Glatter, T., Richard, S., and Scheiffele, P. (2011). SAM68 regulates neuronal activity-dependent alternative splicing of neurexin-1. Cell *147*, 1601-1614.

Ikeda, M., Aleksic, B., Kirov, G., Kinoshita, Y., Yamanouchi, Y., Kitajima, T., Kawashima, K., Okochi, T., Kishi, T., Zaharieva, I.*, et al.* (2010). Copy number variation in schizophrenia in the Japanese population. Biol Psychiatry *67*, 283-286.

Irie, M., Hata, Y., Takeuchi, M., Ichtchenko, K., Toyoda, A., Hirao, K., Takai, Y., Rosahl, T. W., and Sudhof, T. C. (1997). Binding of neuroligins to PSD-95. Science *277*, 1511-1515.

Isaac, J. T., Hjelmstad, G. O., Nicoll, R. A., and Malenka, R. C. (1996). Long-term potentiation at single fiber inputs to hippocampal CA1 pyramidal cells. Proc Natl Acad Sci U S A *93*, 8710-8715.

Jamain, S., Quach, H., Betancur, C., Rastam, M., Colineaux, C., Gillberg, I. C., Soderstrom, H., Giros, B., Leboyer, M., Gillberg, C., and Bourgeron, T. (2003).

Mutations of the X-linked genes encoding neuroligins NLGN3 and NLGN4 are associated with autism. Nat Genet *34*, 27-29.

Jung, S. Y., Kim, J., Kwon, O. B., Jung, J. H., An, K., Jeong, A. Y., Lee, C. J., Choi, Y. B., Bailey, C. H., Kandel, E. R., and Kim, J. H. (2010). Input-specific synaptic plasticity in the amygdala is regulated by neuroligin-1 via postsynaptic NMDA receptors. Proc Natl Acad Sci U S A *107*, 4710-4715.

Katz, Y., Menon, V., Nicholson, D. A., Geinisman, Y., Kath, W. L., and Spruston, N. (2009). Synapse distribution suggests a two-stage model of dendritic integration in CA1 pyramidal neurons. Neuron *63*, 171-177.

Kerchner, G. A., and Nicoll, R. A. (2008). Silent synapses and the emergence of a postsynaptic mechanism for LTP. Nat Rev Neurosci *9*, 813-825.

Kim, J., Jung, S. Y., Lee, Y. K., Park, S., Choi, J. S., Lee, C. J., Kim, H. S., Choi, Y. B., Scheiffele, P., Bailey, C. H.*, et al.* (2008). Neuroligin-1 is required for normal expression of LTP and associative fear memory in the amygdala of adult animals. Proc Natl Acad Sci U S A *105*, 9087-9092.

Ko, J., Fuccillo, M. V., Malenka, R. C., and Sudhof, T. C. (2009a). LRRTM2 functions as a neurexin ligand in promoting excitatory synapse formation. Neuron *64*, 791-798.

Ko, J., Zhang, C., Arac, D., Boucard, A. A., Brunger, A. T., and Sudhof, T. C. (2009b). Neuroligin-1 performs neurexin-dependent and neurexin-independent functions in synapse validation. EMBO J *28*, 3244-3255.

Kwon, S. K., Woo, J., Kim, S. Y., Kim, H., and Kim, E. (2010). Trans-synaptic adhesions between netrin-G ligand-3 (NGL-3) and receptor tyrosine phosphatases LAR, protein-tyrosine phosphatase delta (PTPdelta), and PTPsigma via specific domains regulate excitatory synapse formation. J Biol Chem *285*, 13966-13978.

Lawson-Yuen, A., Saldivar, J. S., Sommer, S., and Picker, J. (2008). Familial deletion within NLGN4 associated with autism and Tourette syndrome. Eur J Hum Genet *16*, 614-618.

Lee, H., Dean, C., and Isacoff, E. (2010). Alternative Splicing of Neuroligin Regulates the Rate of Presynaptic Differentiation. J Neurosci *30*, 11435-11446.

Lee, S. J., Uemura, T., Yoshida, T., and Mishina, M. (2012). GluRdelta2 assembles four neurexins into trans-synaptic triad to trigger synapse formation. J Neurosci *32*, 4688-4701.

Levinson, J. N., Chery, N., Huang, K., Wong, T. P., Gerrow, K., Kang, R., Prange, O., Wang, Y. T., and El-Husseini, A. (2005). Neuroligins mediate excitatory and inhibitory synapse formation: involvement of PSD-95 and neurexin-1beta in neuroligin-induced synaptic specificity. J Biol Chem *280*, 17312-17319.

Levinson, J. N., and El-Husseini, A. (2005). Building excitatory and inhibitory synapses: balancing neuroligin partnerships. Neuron *48*, 171-174.

Linhoff, M. W., Lauren, J., Cassidy, R. M., Dobie, F. A., Takahashi, H., Nygaard, H. B., Airaksinen, M. S., Strittmatter, S. M., and Craig, A. M. (2009). An unbiased

expression screen for synaptogenic proteins identifies the LRRTM protein family as synaptic organizers. Neuron *61*, 734-749.

Lise, M. F., and El-Husseini, A. (2006). The neuroligin and neurexin families: from structure to function at the synapse. Cell Mol Life Sci *63*, 1833-1849.

Lu, W., Shi, Y., Jackson, A. C., Bjorgan, K., During, M. J., Sprengel, R., Seeburg, P. H., and Nicoll, R. A. (2009). Subunit composition of synaptic AMPA receptors revealed by a single-cell genetic approach. Neuron *62*, 254-268.

Magee, J. C. (1998). Dendritic hyperpolarization-activated currents modify the integrative properties of hippocampal CA1 pyramidal neurons. J Neurosci *18*, 7613-7624.

Magee, J. C. (1999). Dendritic Ih normalizes temporal summation in hippocampal CA1 neurons. Nat Neurosci *2*, 848.

Magee, J. C., and Cook, E. P. (2000). Somatic EPSP amplitude is independent of synapse location in hippocampal pyramidal neurons. Nat Neurosci *3*, 895-903.

Malenka, R. C., and Nicoll, R. A. (1993). NMDA-receptor-dependent synaptic plasticity: multiple forms and mechanisms. Trends Neurosci *16*, 521-527.

Malinow, R., and Tsien, R. W. (1990). Presynaptic enhancement shown by whole-cell recordings of long-term potentiation in hippocampal slices. Nature *346*, 177-180.

Manabe, T., Wyllie, D. J., Perkel, D. J., and Nicoll, R. A. (1993). Modulation of synaptic transmission and long-term potentiation: effects on paired pulse facilitation and

EPSC variance in the CA1 region of the hippocampus. J Neurophysiol *70*, 1451-1459.

Massa, F., Koehl, M., Wiesner, T., Grosjean, N., Revest, J. M., Piazza, P. V., Abrous, D. N., and Oliet, S. H. (2011). Conditional reduction of adult neurogenesis impairs bidirectional hippocampal synaptic plasticity. Proc Natl Acad Sci U S A *108*, 6644-6649.

Matsuzaki, M., Honkura, N., Ellis-Davies, G. C., and Kasai, H. (2004). Structural basis of long-term potentiation in single dendritic spines. Nature *429*, 761-766.

Meng, Y., Zhang, Y., and Jia, Z. (2003). Synaptic transmission and plasticity in the absence of AMPA glutamate receptor GluR2 and GluR3. Neuron *39*, 163-176.

Missler, M., Zhang, W., Rohlmann, A., Kattenstroth, G., Hammer, R. E., Gottmann, K., and Sudhof, T. C. (2003). Alpha-neurexins couple Ca2+ channels to synaptic vesicle exocytosis. Nature *423*, 939-948.

Mitchell, S. J., and Silver, R. A. (2003). Shunting inhibition modulates neuronal gain during synaptic excitation. Neuron *38*, 433-445.

Mosca, T. J., Hong, W., Dani, V. S., Favaloro, V., and Luo, L. (2012a). Trans-synaptic Teneurin signalling in neuromuscular synapse organization and target choice. Nature.

Mosca, T. J., Hong, W., Dani, V. S., Favaloro, V., and Luo, L. (2012b). Trans-synaptic Teneurin signalling in neuromuscular synapse organization and target choice. Nature *484*, 237-241.

Nam, C. I., and Chen, L. (2005). Postsynaptic assembly induced by neurexin-neuroligin interaction and neurotransmitter. Proc Natl Acad Sci U S A *102*, 6137-6142.

Nicoll, R. A., Kauer, J. A., and Malenka, R. C. (1988). The current excitement in long-term potentiation. Neuron *1*, 97-103.

Nicoll, R. A., and Malenka, R. C. (1995). Contrasting properties of two forms of long-term potentiation in the hippocampus. Nature *377*, 115-118.

Petralia, R. S., Esteban, J. A., Wang, Y. X., Partridge, J. G., Zhao, H. M., Wenthold, R. J., and Malinow, R. (1999). Selective acquisition of AMPA receptors over postnatal development suggests a molecular basis for silent synapses. Nat Neurosci *2*, 31-36.

Pettersen, E. F., Goddard, T. D., Huang, C. C., Couch, G. S., Greenblatt, D. M., Meng, E. C., and Ferrin, T. E. (2004). UCSF Chimera--a visualization system for exploratory research and analysis. J Comput Chem *25*, 1605-1612.

Poulopoulos, A., Aramuni, G., Meyer, G., Soykan, T., Hoon, M., Papadopoulos, T., Zhang, M., Paarmann, I., Fuchs, C., Harvey, K.*, et al.* (2009). Neuroligin 2 drives postsynaptic assembly at perisomatic inhibitory synapses through gephyrin and collybistin. Neuron *63*, 628-642.

Poulopoulos, A., Soykan, T., Tuffy, L. P., Hammer, M., Varoqueaux, F., and Brose, N. (2012). Homodimerization and isoform-specific heterodimerization of neuroligins. Biochem J *446*, 321-330.

Prange, O., Wong, T. P., Gerrow, K., Wang, Y. T., and El-Husseini, A. (2004). A balance between excitatory and inhibitory synapses is controlled by PSD-95 and neuroligin. Proc Natl Acad Sci U S A *101*, 13915-13920.

Radyushkin, K., Hammerschmidt, K., Boretius, S., Varoqueaux, F., El-Kordi, A., Ronnenberg, A., Winter, D., Frahm, J., Fischer, J., Brose, N., and Ehrenreich, H. (2009). Neuroligin-3-deficient mice: model of a monogenic heritable form of autism with an olfactory deficit. Genes Brain Behav *8*, 416-425.

Redies, C., Hertel, N., and Hubner, C. A. (2012). Cadherins and neuropsychiatric disorders. Brain Res *1470*, 130-144.

Rowen, L., Young, J., Birditt, B., Kaur, A., Madan, A., Philipps, D. L., Qin, S., Minx, P., Wilson, R. K., Hood, L., and Graveley, B. R. (2002). Analysis of the human neurexin genes: alternative splicing and the generation of protein diversity. Genomics *79*, 587-597.

Rujescu, D., Ingason, A., Cichon, S., Pietilainen, O. P., Barnes, M. R., Toulopoulou, T., Picchioni, M., Vassos, E., Ettinger, U., Bramon, E.*, et al.* (2009). Disruption of the neurexin 1 gene is associated with schizophrenia. Hum Mol Genet *18*, 988-996.

Scheiffele, P., Fan, J., Choih, J., Fetter, R., and Serafini, T. (2000). Neuroligin expressed in nonneuronal cells triggers presynaptic development in contacting axons. Cell *101*, 657-669.

Schwenk, J., Harmel, N., Zolles, G., Bildl, W., Kulik, A., Heimrich, B., Chisaka, O., Jonas, P., Schulte, U., Fakler, B., and Klocker, N. (2009). Functional proteomics

identify cornichon proteins as auxiliary subunits of AMPA receptors. Science *323*, 1313-1319.

Shi, S., Hayashi, Y., Esteban, J. A., and Malinow, R. (2001). Subunit-specific rules governing AMPA receptor trafficking to synapses in hippocampal pyramidal neurons. Cell *105*, 331-343.

Shi, Y., Suh, Y. H., Milstein, A. D., Isozaki, K., Schmid, S. M., Roche, K. W., and Nicoll, R. A. (2010). Functional comparison of the effects of TARPs and cornichons on AMPA receptor trafficking and gating. Proc Natl Acad Sci U S A *107*, 16315-16319.

Shipman, S. L., Schnell, E., Hirai, T., Chen, B. S., Roche, K. W., and Nicoll, R. A. (2011). Functional dependence of neuroligin on a new non-PDZ intracellular domain. Nat Neurosci *14*, 718-726.

Siddiqui, T. J., and Craig, A. M. (2011). Synaptic organizing complexes. Curr Opin Neurobiol *21*, 132-143.

Silva, A. J., Stevens, C. F., Tonegawa, S., and Wang, Y. (1992). Deficient hippocampal long-term potentiation in alpha-calcium-calmodulin kinase II mutant mice. Science *257*, 201-206.

Singer, B. H., Gamelli, A. E., Fuller, C. L., Temme, S. J., Parent, J. M., and Murphy, G. G. (2011). Compensatory network changes in the dentate gyrus restore long-term potentiation following ablation of neurogenesis in young-adult mice. Proc Natl Acad Sci U S A *108*, 5437-5442.

Smith, M. A., Ellis-Davies, G. C., and Magee, J. C. (2003). Mechanism of the distance-dependent scaling of Schaffer collateral synapses in rat CA1 pyramidal neurons. J Physiol *548*, 245-258.

Soler-Llavina, G. J., Fuccillo, M. V., Ko, J., Sudhof, T. C., and Malenka, R. C. (2011). The neurexin ligands, neuroligins and leucine-rich repeat transmembrane proteins, perform convergent and divergent synaptic functions in vivo. Proc Natl Acad Sci U S A *108*, 16502-16509.

Song, J. Y., Ichtchenko, K., Sudhof, T. C., and Brose, N. (1999). Neuroligin 1 is a postsynaptic cell-adhesion molecule of excitatory synapses. Proc Natl Acad Sci U S A *96*, 1100-1105.

Sousa, I., Clark, T. G., Holt, R., Pagnamenta, A. T., Mulder, E. J., Minderaa, R. B., Bailey, A. J., Battaglia, A., Klauck, S. M., Poustka, F., and Monaco, A. P. (2010). Polymorphisms in leucine-rich repeat genes are associated with autism spectrum disorder susceptibility in populations of European ancestry. Mol Autism *1*, 7.

Spencer, D. M., Wandless, T. J., Schreiber, S. L., and Crabtree, G. R. (1993). Controlling signal transduction with synthetic ligands. Science *262*, 1019-1024.

Stan, A., Pielarski, K. N., Brigadski, T., Wittenmayer, N., Fedorchenko, O., Gohla, A., Lessmann, V., Dresbach, T., and Gottmann, K. (2010). Essential cooperation of N-cadherin and neuroligin-1 in the transsynaptic control of vesicle accumulation. Proc Natl Acad Sci U S A.

Stell, W. K., Ishida, A. T., and Lightfoot, D. O. (1977). Structural basis for on-and off-center responses in retinal bipolar cells. Science *198*, 1269-1271.

Sterratt, D. C., Groen, M. R., Meredith, R. M., and van Ooyen, A. (2012). Spine calcium transients induced by synaptically-evoked action potentials can predict synapse location and establish synaptic democracy. PLoS Comput Biol *8*, e1002545.

Stoppini, L., Buchs, P. A., and Muller, D. (1991). A simple method for organotypic cultures of nervous tissue. J Neurosci Methods *37*, 173-182.

Suckow, A. T., Zhang, C., Egodage, S., Comoletti, D., Taylor, P., Miller, M. T., Sweet, I. R., and Chessler, S. D. (2012). Transcellular neuroligin-2 interactions enhance insulin secretion and are integral to pancreatic beta-cell function. J Biol Chem, (Epub ahead of print).

Sudhof, T. C. (2008). Neuroligins and neurexins link synaptic function to cognitive disease. Nature *455*, 903-911.

Tabuchi, K., Blundell, J., Etherton, M. R., Hammer, R. E., Liu, X., Powell, C. M., and Sudhof, T. C. (2007). A neuroligin-3 mutation implicated in autism increases inhibitory synaptic transmission in mice. Science *318*, 71-76.

Tabuchi, K., and Sudhof, T. C. (2002). Structure and evolution of neurexin genes: insight into the mechanism of alternative splicing. Genomics *79*, 849-859.

Tallafuss, A., Constable, J. R., and Washbourne, P. (2010). Organization of central synapses by adhesion molecules. Eur J Neurosci *32*, 198-206.

Tanaka, H., Miyazaki, N., Matoba, K., Nogi, T., Iwasaki, K., and Takagi, J. (2012). Higher-order architecture of cell adhesion mediated by polymorphic synaptic adhesion molecules neurexin and neuroligin. Cell Rep *2*, 101-110.

Thyagarajan, A., and Ting, A. Y. (2010). Imaging activity-dependent regulation of neurexin-neuroligin interactions using trans-synaptic enzymatic biotinylation. Cell *143*, 456-469.

Trussell, L. O. (1999). Synaptic mechanisms for coding timing in auditory neurons. Annu Rev Physiol *61*, 477-496.

Turrigiano, G. G. (2008). The self-tuning neuron: synaptic scaling of excitatory synapses. Cell *135*, 422-435.

Turrigiano, G. G., Leslie, K. R., Desai, N. S., Rutherford, L. C., and Nelson, S. B. (1998). Activity-dependent scaling of quantal amplitude in neocortical neurons. Nature *391*, 892-896.

Uemura, T., Lee, S. J., Yasumura, M., Takeuchi, T., Yoshida, T., Ra, M., Taguchi, R., Sakimura, K., and Mishina, M. (2010). Trans-synaptic interaction of GluRdelta2 and Neurexin through Cbln1 mediates synapse formation in the cerebellum. Cell *141*, 1068-1079.

Ullrich, B., Ushkaryov, Y. A., and Sudhof, T. C. (1995). Cartography of neurexins: more than 1000 isoforms generated by alternative splicing and expressed in distinct subsets of neurons. Neuron *14*, 497-507.

Ushkaryov, Y. A., Petrenko, A. G., Geppert, M., and Sudhof, T. C. (1992). Neurexins: synaptic cell surface proteins related to the alpha-latrotoxin receptor and laminin. Science *257*, 50-56.

Vaags, A. K., Lionel, A. C., Sato, D., Goodenberger, M., Stein, Q. P., Curran, S., Ogilvie, C., Ahn, J. W., Drmic, I., Senman, L.*, et al.* (2012). Rare deletions at the neurexin 3 locus in autism spectrum disorder. Am J Hum Genet *90*, 133-141.

Varoqueaux, F., Aramuni, G., Rawson, R. L., Mohrmann, R., Missler, M., Gottmann, K., Zhang, W., Sudhof, T. C., and Brose, N. (2006). Neuroligins determine synapse maturation and function. Neuron *51*, 741-754.

Varoqueaux, F., Jamain, S., and Brose, N. (2004). Neuroligin 2 is exclusively localized to inhibitory synapses. Eur J Cell Biol *83*, 449-456.

Walantus, W., Elias, L., and Kriegstein, A. (2007). In utero intraventricular injection and electroporation of E16 rat embryos. J Vis Exp, 236.

Wang, K., Zhang, H., Ma, D., Bucan, M., Glessner, J. T., Abrahams, B. S., Salyakina, D., Imielinski, M., Bradfield, J. P., Sleiman, P. M.*, et al.* (2009). Common genetic variants on 5p14.1 associate with autism spectrum disorders. Nature *459*, 528-533.

Washbourne, P., Dityatev, A., Scheiffele, P., Biederer, T., Weiner, J. A., Christopherson, K. S., and El-Husseini, A. (2004). Cell adhesion molecules in synapse formation. J Neurosci *24*, 9244-9249.

Wayman, G. A., Lee, Y. S., Tokumitsu, H., Silva, A. J., and Soderling, T. R. (2008). Calmodulin-kinases: modulators of neuronal development and plasticity. Neuron *59*, 914-931.

Wenthold, R. J., Petralia, R. S., Blahos, J., II, and Niedzielski, A. S. (1996). Evidence for multiple AMPA receptor complexes in hippocampal CA1/CA2 neurons. J Neurosci *16*, 1982-1989.

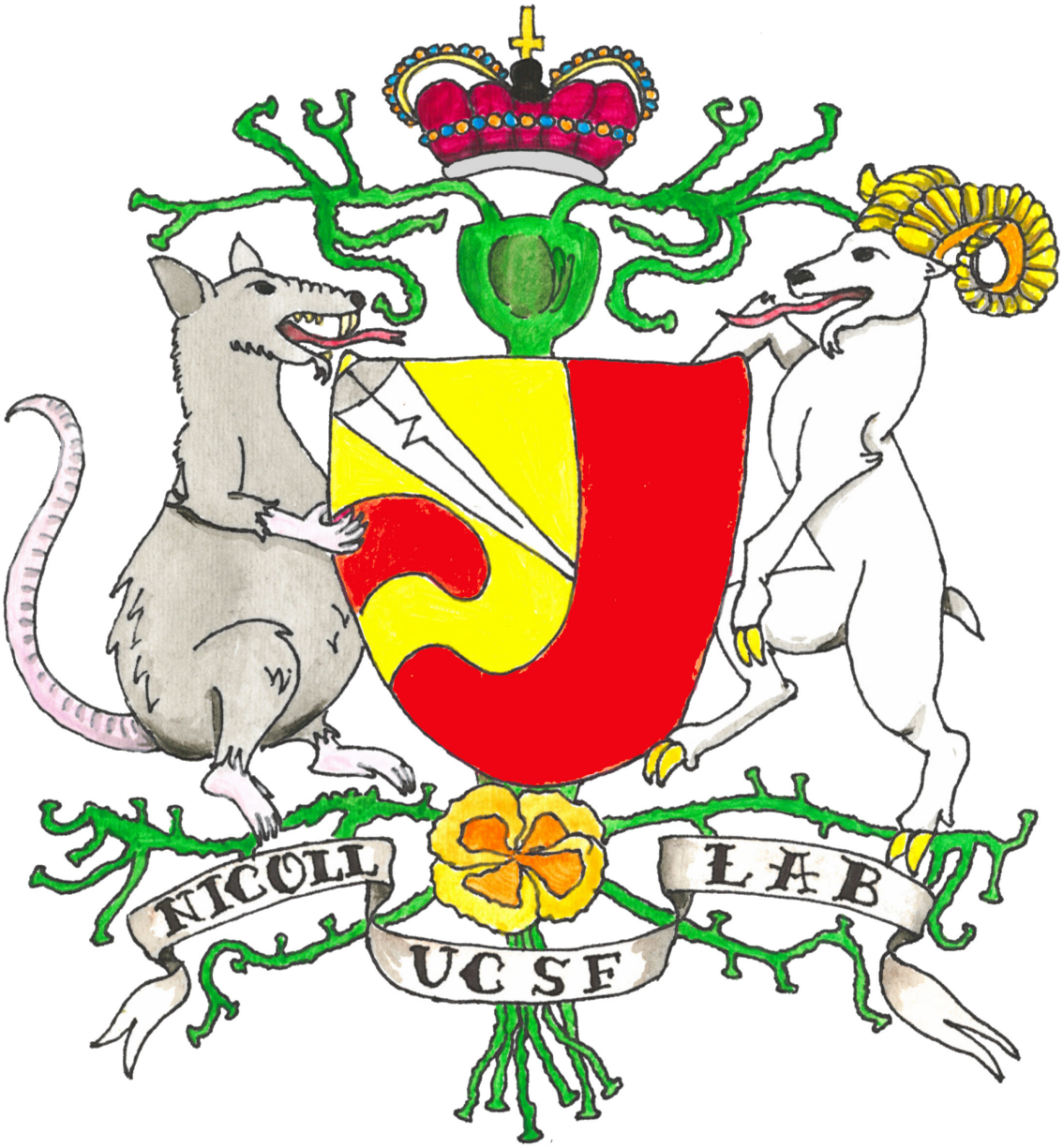
Wittenmayer, N., Korber, C., Liu, H., Kremer, T., Varoqueaux, F., Chapman, E. R., Brose, N., Kuner, T., and Dresbach, T. (2009). Postsynaptic Neuroligin1 regulates presynaptic maturation. Proc Natl Acad Sci U S A *106*, 13564-13569.

Woo, J., Kwon, S. K., Choi, S., Kim, S., Lee, J. R., Dunah, A. W., Sheng, M., and Kim, E. (2009). Trans-synaptic adhesion between NGL-3 and LAR regulates the formation of excitatory synapses. Nat Neurosci *12*, 428-437.

Yamagata, M., Sanes, J. R., and Weiner, J. A. (2003). Synaptic adhesion molecules. Curr Opin Cell Biol *15*, 621-632.

Yan, J., Oliveira, G., Coutinho, A., Yang, C., Feng, J., Katz, C., Sram, J., Bockholt, A., Jones, I. R., Craddock, N.*, et al.* (2005). Analysis of the neuroligin 3 and 4 genes in autism and other neuropsychiatric patients. Mol Psychiatry *10*, 329-332.

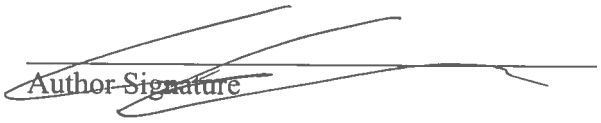
Zhang, C., Milunsky, J. M., Newton, S., Ko, J., Zhao, G., Maher, T. A., Tager-Flusberg, H., Bolliger, M. F., Carter, A. S., Boucard, A. A.*, et al.* (2009). A neuroligin-4 missense mutation associated with autism impairs neuroligin-4 folding and endoplasmic reticulum export. J Neurosci *29*, 10843-10854.


NICOLL
LAB
UCSF

Publishing Agreement

It is the policy of the University to encourage the distribution of all these, dissertations, and manuscripts. Copies of all UCSF theses, dissertations, and manuscripts will be routed to the library via the Graduate Division. The library will make all theses, dissertations, and manuscripts accessible to the public and will preserve these to the best of their abilities, in perpetuity.

I hereby grant permission to the Graduate Division of the University of California, San Francisco to release copies of my thesis, dissertation, or manuscript to the Campus Library to provide access and preservation, in whole or in part, in perpetuity.



Author Signature

10/23/12

Date